# Origin of the Late Jurassic to Early Cretaceous peraluminous granitoids in the northeastern Hunan province (middle Yangtze region), South China: Geodynamic implications for the Paleo-Pacific subduction

Wenbin Ji, Wei Lin, Michel Faure, Yan Chen, Yang Chu, Zhenhua Xue

# Origin of the Late Jurassic to Early Cretaceous peraluminous granitoids in the northeastern Hunan province (middle Yangtze region), South China: Geodynamic implications for the Paleo-Pacific subduction

Wenbin Ji [a,b], Wei Lin [a,*], Michel Faure [b], Yan Chen [b], Yang Chu [a], Zhenhua Xue [a]

[a] State Key Laboratory of Lithospheric Evolution, Institute of Geology and Geophysics, Chinese Academy of Sciences, Beijing 100029, China

[b] Institut des Sciences de la Terre d'Orléans, UMR 7327, Université d'Orléans-CNRS, 45071 Orléans, France

First author: Wenbin Ji, E-mail: jiwenbin@mail.iggcas.ac.cn

Corresponding author: Wei Lin, E-mail: linwei@mail.iggcas.ac.cn

## Abstract

The Late Mesozoic granitic belt in the northeastern Hunan province (situated in the south of the middle Yangtze region) represents the western front of the large magmatic province of SE China. In order to determine their ages and petrogenesis, we carried out zircon U–Pb dating, Hf isotope and whole-rock geochemical analyses for four granitic plutons, namely Taohuashan, Dayunshan-Mufushan, Wangxiang and Lianyunshan. Our SIMS zircon U–Pb ages, together with previously published data, reveal that the magmatic activities in this area can be roughly subdivided into three phases at 151–146 Ma, 132–127 Ma and ca. 117 Ma, and the Dayunshan-Mufushan batholith therein is a composite pluton. These four plutons are mainly composed of weakly to strongly peraluminous biotite or two-mica monzogranites, with a minor amount of biotite granodiorites. Their geochemical features are similar to S-type as well as fractionated S-type granites, with enrichment in LREEs and negative Ba, Sr, Nb, P and Ti anomalies. All samples show negative zircon εHf(t) values ranging from -12.5 to -3.6, corresponding to crustal Hf model ($T_{DM}^{C}$) ages of 1.4–2.0 Ga. It is inferred that these granitoids were derived from partial melting of metasedimentary rocks analogous to the Neoproterozoic Lengjiaxi Group, predominantly with psammitic component. Fractional crystallization probably played an important role in the magma evolution, while input of mantle-derived magma was insignificant. Combined with other geological evidence, our new data allow us to propose that the Cretaceous (132–127 Ma and ca. 117 Ma) magmatism might be response to episodic slab rollback of the

Paleo-Pacific plate, while the early-stage (151–146 Ma) magmatism that overlapped the epilogue of Jurassic magmatic flare-up and subsequent magmatic quiescence probably foreshadowed the transformation from foundering of a subducted flat-slab to slab rollback. Alternatively, slab foundering after a SE-directed intracontinental subduction in the central SCB cannot be ruled out for geodynamic interpretation of the Jurassic magmatism in SE China.

**Keywords:** South China; Late Mesozoic tectono-magmatism; Peraluminous granitoids; Geochronology and petrogenesis; Paleo-Pacific subduction

## 1. Introduction

Southeast China is an important part of the circum-Pacific magmatic and metallogenic belt (e.g., Zhou and Li, 2000; Zhou et al., 2006). Jurassic-Cretaceous (referred to as the "Yanshanian" period in Chinese literature) intrusive and volcanic rocks occupy a vast area of SE China (mostly in Anhui, Zhejiang, Jiangxi, Fujian and Guangdong provinces), forming a ca. 600 km wide magmatic belt parallel to the present coastline (Fig. 1). Despite intensive research in the past decades, origin and evolution of this large magmatic province are still hotly debated. For instance, its temporal-spatial configuration and geodynamic setting have not been well understood yet. The Jurassic (ca. 195–150 Ma) igneous rocks are widespread in the hinterland (e.g., the Nanling Range), while the Cretaceous (ca. 140–90 Ma) intrusive rocks coeval with voluminous volcanic rocks are mainly distributed in the coastal area and the middle-lower reaches of the Yangtze River. An oceanward younging trend for the Late Mesozoic magmatism resulted from northwestward subduction of the Paleo-Pacific plate with an increasing subduction angle had been proposed (Zhou and Li, 2000). Instead, Wang et al. (2011) recently suggested that the 180 to 125 Ma igneous rocks experienced a northeastward migration due to southwestward Paleo-Pacific subduction and corresponding slab rollback. Furthermore, it is noteworthy that more Jurassic granites have been identified in the coastal area in recent years (Cui et al., 2012; Liu et al., 2012; Zhang et al., 2015). Thus temporal-spatial distribution of the Jurassic-Cretaceous magmatic rocks deserves a reappraisal. Geodynamic trigger of the Mesozoic tectono-magmatism in eastern China has been generally ascribed to the subduction of the Paleo-Pacific plate beneath the Eurasian continent. However, the subduction pattern is still an open question,

diverse models have been proposed for SE China, such as shallow subduction and subsequent slab rollback (Zhou and Li, 2000; Jiang et al., 2009, 2011), break-up and foundering of a subducted flat-slab (Li and Li, 2007; X.H. Li et al., 2007, 2013b; Z.X. Li et al., 2012), ridge subduction (Ling et al., 2009, Sun et al., 2010; H. Li et al., 2012) and repeated slab advance-retreat (Jiang et al., 2015; Wang et al., 2016). Particularly, the Paleo-Pacific subduction beneath SE China was supposed to initiate during the Permian (Li and Li, 2007), Late Triassic (Jiang et al., 2015), Early Jurassic (Zhou et al., 2006) or Early Cretaceous (Chen et al., 2008). Other outdated or minority models include Alpine-type continental collision (Hsü et al., 1990), wrench faulting (Xu, 1993), strike-slip faulting plus concomitant rifting (Gilder et al., 1996), and lithospheric extension maybe unrelated to the Paleo-Pacific subduction (Li, 2000).

More importantly, numerous polymetallic deposits in SE China have been inferred to be closely related to the Mesozoic granitoids (Wang et al., 2011; Mao et al., 2013 and references therein). In addition to the geodynamic setting, controversial issues on the granitoids themselves involve their petrogenetic types (such as I-type, S-type or A-type granites, as well as fractionated granites) and the nature of source rocks, especially the degree of mantle contribution to the magma generation (e.g., X.H. Li et al., 2007; Wong et al., 2009; Jiang et al., 2009, 2011; Huang et al., 2013, 2015; Huang and Jiang, 2014; Zhang et al., 2015; Wang et al., 2016). Several Late Mesozoic granitic plutons crop out in the northeastern part of Hunan province, situated in the south of the middle Yangtze region (middle reach of the Yangtze River; Figs. 1 and 2). These granitic plutons represent the western front of the large magmatic province of SE China. However, due to the lack of detailed investigations, the geochronology and petrogenesis of these granitic rocks remain in dispute (Wang and Deng, 2004; Li et al., 2005; L.X. Wang et al., 2008, 2014; Xu et al., 2009). In this paper, we present zircon U–Pb ages and Hf isotopic data, major and trace element geochemical data for four granitic plutons (namely Taohuashan, Dayunshan-Mufushan, Wangxiang and Lianyunshan) in this area. This provides us an opportunity to decipher their origin and tectonic implications for the Late Mesozoic tectono-magmatic history of SE China.

## 2. Geological setting

### 2.1. Tectonic framework

Southeast China belongs to the eastern South China block (SCB) that consists of the Yangtze craton in the northwest and the Cathaysia block in the southeast (Fig. 1). It is generally accepted that the amalgamation of the Yangtze and Cathaysia blocks formed the Neoproterozoic Jiangnan orogen, with subduction-collision process before ca. 820 Ma (e.g., Charvet et al., 1996; Li et al., 2009a; Zhao et al., 2011; X.L. Wang et al., 2014; Zhao, 2015 and references therein). Subsequently, the SCB underwent continental rifting after ca. 820 Ma, with development of the Nanhua failed rift basin followed by platform sedimentation (Wang and Li, 2003). During the Phanerozoic, the SCB experienced three main tectono-thermal events (for a review, see Y.J. Wang et al., 2013 and references therein), including: (1) Early Paleozoic intracontinental orogeny mainly in the Wuyi-Yunkai domain of the Cathaysia block (e.g., Lin et al., 2008; Faure et al., 2009; Charvet et al., 2010; Z.X. Li et al., 2010; Shu et al., 2014, 2015); (2) Triassic orogeny around the SCB such as the northward continental deep-subduction along the Dabie-Sulu belt to the north and the South China-Indochina collision to the south, as well as in interior of the SCB (i.e., the intracontinental Jiuling-Xuefengshan belt superposed upon the pre-existing Jiangnan orogen) (e.g., Chu et al., 2012a, 2012b; Chu and Lin, 2014; Faure et al., 2008, 2014, 2016); (3) Late Mesozoic intracontinental deformation and magmatism, especially the development of the so-called “Southeast China basin and range tectonics” under an overall extensional regime (e.g., Gilder et al., 1996; Li, 2000; Lin et al., 2000; Shu et al., 2009; Ji et al., 2014; J.H. Li et al., 2014).

The Jurassic-Cretaceous magmatic rocks are mostly distributed in the Cathaysia block, whereas a small amount of contemporaneous plutons croup out in the Yangtze craton. In the northeastern part of Hunan province, Late Mesozoic granitoids intruded into the middle segment of the Jiuling-Xuefengshan belt (Figs. 1 and 2). To the northwest, the Cretaceous-Cenozoic Jianghan basin covers most area of the middle Yangtze craton. The Precambrian basement exposed in the study area is a pile of weakly metamorphosed (greenschist facies) flysch sequences, i.e., the Lengjiaxi Group, mainly consisting of metasandstone, metasiltstone and slate (BGMRHN, 1988; Gu et al., 2002; Xu et al., 2007). As in other regions, the Lengjiaxi Group and its equivalents were intruded by ca. 820 Ma strongly peraluminous (S-type) granitoids (such as the largest Jiuling batholith to the southeast, northwestern Jiangxi province), and then unconformably covered by rifting-related clastic sedimentary rocks represented by the Neoproterozoic (Nanhuan period) Banxi Group and its equivalents (W. Wang et al., 2010, 2012, 2013; Gao et al., 2011; Meng et al., 2013; Zhao et al., 2011, 2013; X.L.

Wang et al., 2013, 2014; Yan et al., 2015). This angular unconformity is widely considered to be the response to final amalgamation of the Yangtze and Cathaysia blocks. The late Neoproterozoic (Sinian period) to Middle Triassic strata mostly distributed in the northeastern part of the study area are roughly continuous, except for a distinct hiatus between the Silurian and Devonian (BGMRHN, 1988). They mainly consist of carbonate and siliciclastic rocks in a shallow-marine environment. Two regional unconformities, respectively below the Middle Devonian conglomerate and the sporadically Late Triassic to Jurassic terrigenous clastic rocks, correspond to the Early Paleozoic and Triassic intracontinental orogeny of the SCB. All the rocks mentioned above were strongly folded, and unconformably overlain by NE-trending small fault depressions filled with Cretaceous-Paleogene alluvial and lacustrine deposits (red beds).

## 2.1 Geology of the granitoids

Four granitic plutons (namely Taohuashan, Dayunshan-Mufushan, Wangxiang and Lianyunshan) in the northeastern Hunan province and adjacent areas have been investigated in this work (Fig. 2). The dominant rock type of these plutons is biotite or two-mica monzogranite, with a minor amount of biotite granodiorite (BGMRHN, 1988; Wang and Deng, 2004; L.X. Wang et al., 2008, 2014; Xu et al., 2009). The main minerals of the monzogranite are quartz, alkali feldspar, plagioclase and biotite, with or without muscovite (Fig. 3a, b, c). Primary muscovite is commonly present in the two-mica monzogranite or leucogranite. Occasionally, minor muscovite (generally <1 %) is also visible in the biotite monzogranite. Accessory minerals in the monzogranite mainly include apatite, zircon and monazite (Fig. 3d). The biotite granodiorite has a mineral assemblage of quartz, plagioclase, alkali feldspar, biotite and minor hornblende, with accessory minerals such as apatite, zircon and titanite as well as epidote and allanite (Fig. 3e, f). Country rocks of these granitoids are predominantly Neoproterozoic slate, as well as locally Early Paleozoic limestone and shale. About 200 m to 2 km wide contact aureoles are usually developed around these plutons, where hornfels and schist are common.

The Taohuashan pluton crops out over an area of about 150 $km^2$, despite its considerable part covered by Quaternary deposits. It is mainly composed of fine- to medium-grained two-mica monzogranite with subordinate porphyritic biotite

monzogranite in the north. Contacts between the two-mica and biotite phases are gradational, and the former usually shows weak gneissic structure.

The Dayunshan-Mufushan batholith is a huge composite pluton, with a total outcrop area of about 2440 $km^2$. It consists of early-stage biotite-rich intrusion and late-stage two-mica intrusion. The former is mainly composed of porphyritic biotite monzogranite, as well as subordinate fine- to medium-grained biotite granodiorite in the northeastern part; while the latter is composed of fine- to medium-grained two-mica monzogranite, with minor phenocrysts sometimes. The early-stage intrusion was dismembered into three larger parts due to the disturbance of the late-stage intrusion. Finally, fine-grained stocks of two-mica or biotite monzogranite intruded the previous facies. As shown later, there is an interval of about 20 Myr between the early and late intrusions. Except for the common andalusite hornfels, garnet- and/or staurolite-bearing schist can also be locally found in the contact zone. In addition, a detachment fault with half-graben basin on the hanging wall developed along the western tongue-shaped margin of the batholith (Dayunshan area), and the late-stage intrusion was involved in mylonitization (Yu et al., 1998).

The Wangxiang batholith is located in the Wangcheng-Xiangyin area, and shows an elliptical shape with an outcrop area of about 1480 $km^2$. The main phase of this batholith is fine- to medium-grained or porphyritic two-mica monzogranite with minor fine- to medium-grained biotite granodiorite as marginal facies in the northern part. Moreover, supplementary pulse of two-mica monzogranite that occurs as stocks or apophysises can be distinguished from the main phase according to field occurrence and petrography.

The Lianyunshan pluton was cut and deformed by a NE-trending fault zone that also constitutes the boundary fault of a narrow and long rift basin to the west. This pluton has an outcrop area about 130 $km^2$, and is lentoid in shape with a bulgy body in the northeast and forked tails in the southwest. It is mainly composed of muscovite-bearing monzogranite with fine- to medium-grained granitic texture or porphyritic texture, usually showing deformation features. Garnet, sillimanite and staurolite are visible in schist of the contact metamorphic zone, indicating a relatively high-temperature metamorphism. Particularly, the thermal metamorphism extends up to 10 km wide to the NE, locally accompanied by weakly migmatization.

## 3. Analytical methods

Fifteen representative samples were collected from the four plutons mentioned above, and zircons from eleven samples therein were determined for SIMS U–Pb dating and LA-MC-ICPMS Hf isotope analyses. In addition, ten samples were selected for whole-rock geochemical analyses.

Zircon grains were separated using standard density and magnetic separation techniques. They were mounted in epoxy mounts together with zircon standards, and then polished to section the crystals in half for analysis. In order to investigate the morphology and internal textures of the zircons, which were documented with transmitted and reflected light micrographs, as well as cathodoluminescence (CL) images (Fig. 4). Measurements of U, Th and Pb isotopes were conducted using a Cameca IMS-1280 at the Institute of Geology and Geophysics, Chinese Academy of Sciences (IGGCAS). The instrument description and analytical procedure can be found in Li et al. (2009b). The beam spot was about 20×30 μm in size, and positive secondary ions were extracted with a 10 KV potential. Standard zircons Plešovice (Sláma et al., 2008) and Qinghu (Li et al., 2013a) were alternately analyzed with unknown zircons from the samples. Measured compositions were corrected for common Pb using the non-radiogenic $^{204}$Pb. Data reduction was carried out using the Isoplot program (Ludwing, 2003). Uncertainties of individual analyses are reported at 1σ in Supplementary Table S1. The concordia diagrams of U–Pb data are shown in Figure 5, where weighted mean $^{206}$Pb/$^{238}$U ages or concordia ages are quoted at either 95% confidence interval or 2σ, as summarized in Table 1.

*In situ* Hf isotope analyses were conducted mostly on the dated zircons with concordant ages by using a Neptune MC-ICPMS, equipped with a Geolas 193 nm laser-ablation system at IGGCAS. The detailed analytical technique and calibration methods are described in Wu et al. (2006). During analyses, zircon standards GJ-1 and Mud Tank were used as reference materials (Woodhead and Hergt, 2005; Morel et al., 2008). The spot size was either 40 or 60 μm depending on grain sizes, with a laser repetition rate of 8 Hz and laser beam energy density of 10 J/cm$^2$. The chondritic Hf-isotope values of Blichert-Toft and Albarède (1997) were used for calculation of εHf(t) values. Depleted-mantle Hf model ages ($T_{DM}$) were calculated using the measured $^{176}$Lu/$^{177}$Hf ratios, in reference to the depleted mantle reservoir with a present-day $^{176}$Hf/$^{177}$Hf = 0.28325 and $^{176}$Lu/$^{177}$Hf = 0.0384 (Griffin et al., 2000). We also present crustal Hf model ages ($T_{DM}^{C}$) for crustal sources that were originally derived from the depleted mantle, assuming that the parental magma was produced from an average continental

crust with $^{176}Lu/^{177}Hf$ = 0.015 (Griffin et al. 2002). The Hf isotope data with uncertainties at 2σ are reported in Supplementary Table S2, and also summarized in Table 1. For comparison, histograms of the εHf(t) values of each samples are shown in Figure 6.

Whole-rock geochemical analyses were carried out at IGGCAS. Major elements were determined by XRF (X-ray fluorescence) using fused glass disks. Trace elements (including rare earth elements, REEs) were determined for the same samples by Agilent 7500a ICP-MS after acid digestion. Analytical uncertainties are generally less than 5% for major elements and 10% for trace elements. The geochemical data are presented in Table 2.

## 4. Results

### 4.1. Zircon U–Pb ages and Hf isotopic data

#### 4.1.1. Taohuashan pluton

Zircons from a biotite monzogranite (JH155) of the Taohuashan pluton are mostly euhedral, colorless and transparent, about 60–200 μm in length. Most grains are characterized by magmatic growth zonation under CL (Fig. 4). Nineteen analyses of zircons were obtained during a single analytical session. Their U and Th contents respectively vary in the ranges of 276–2159 ppm and 235–1194 ppm, with Th/U ratios between 0.28 and 0.95 (Table S1). Excluding one discordant analysis (spot #12), the remaining analyses are concordant in $^{206}Pb/^{238}U$ and $^{207}Pb/^{235}Pb$ within analytical errors and yield a weighted mean $^{206}Pb/^{238}U$ age of 128.0 ± 1.0 Ma (MSWD = 0.79) (Fig. 5a). This age is interpreted as the best estimate of the crystallization age for the Taohuashan biotite monzogranite.

Eighteen spots on the dated zircons were further analyzed for Hf isotopic composition, their $^{176}Hf/^{177}Hf$ ratios range from 0.282409 to 0.282500, corresponding to εHf(t) values of -10.1 to -6.9 and $T_{DM}^{C}$ ages of 1.62–1.82 Ga (Fig. 6a; Table S2).

#### 4.1.2. Dayunshan-Mufushan batholith

Six samples were collected from the Dayunshan-Mufushan batholith for U–Pb dating and Hf isotope analyses, including DM35 and QD69 respectively from the

northern and southern parts of the early-stage biotite monzogranite, DYS14 from the early-stage biotite granodiorite, QD49 and DM80 respectively from the western and eastern parts of the late-stage two-mica monzogranite, as well as QD62 from a later stock of two-mica monzogranite.

Zircons form sample DM35 are commonly euhedral, ranging from 100 to 300 μm in length with aspect ratios of 1.5:1 to 3:1. They show conspicuous oscillatory zoning and rare inherited cores under CL (Fig. 4). Eighteen zircons were analyzed, their U and Th contents respectively range from 517 to 2406 ppm and from 256 to 793 ppm, with Th/U ratios of 0.21–0.65 (Table S1). Two discordant analyses indicate their partially inherited origin, the remaining analyses have similar $^{206}Pb/^{238}U$ ages with a weighted mean age of 151.2 ± 1.1 Ma (MSWD = 0.26) (Fig. 5b).

Zircons from sample QD69 are mostly euhedral, with lengths of 100–250 μm and aspect ratios of 2:1 to 3:1. Most grains are nearly black and display faint zoning in CL images, a few of which contain bright inherited cores (Fig. 4). Nineteen analyses were conducted, which are all concordant. The only spot on an inherited core obtained a $^{206}Pb/^{238}U$ age of 837 ± 12 Ma. Sixteen out of the remaining eighteen analyses yielded a weighted mean $^{206}Pb/^{238}U$ age of 151.4 ± 1.1 Ma (MSWD = 0.43), which agrees with the concordia age of 151.3 ± 1.1 Ma (MSWD of concordance = 0.53) (Fig. 5c). The two rejected analyses with older ages (159.6 and 160.1 Ma) are due to very high U concentrations (up to 5370 and 7007 ppm; Table S1).

Accordingly, ca. 151 Ma is the best estimate of crystallization age for the Dayunshan-Mufushan biotite monzogranite. The zircons with ages around ca. 151 Ma from sample DM35 and sample QD69 have similar Hf isotopic compositions. A total of thirty-three measured $^{176}Hf/^{177}Hf$ ratios vary from 0.282440 to 0.282564, corresponding to εHf(t) values of -8.5 to -4.3 and $T_{DM}^{C}$ ages of 1.47–1.74 Ga (Fig. 6b; Table S2). In addition, the ca. 837 Ma inherited core from sample QD69 shows positive εHf(t) value of 4.3.

Zircons from sample DYS14 are mostly euhedral, about 100-250 μm in length with aspect ratios of 1.5:1 to 3:1. Oscillatory zoning of magmatic origin is common in CL images (Fig. 4). Twenty-one spots on twenty zircons were analyzed, all of which obtained concordant analyses. They have moderate U (261–948 ppm) and Th (74–620 ppm) contents, with Th/U ratios of 0.08–0.98 (Table S1). One analysis of inherited core (spot #15) yielded a $^{206}Pb/^{238}U$ age of 819 ± 12 Ma, nineteen out of the remaining twenty analyses yielded a weighted mean $^{206}Pb/^{238}U$ age of 149.0 ± 1.0 Ma (MSWD =

0.71) (Fig. 5d). This age is interpreted as crystallization age of the Dayunshan-Mufushan biotite granodiorite. In addition, sixteen Hf isotope analyses of the ca. 149 Ma zircons have $^{176}Hf/^{177}Hf$ ratios of 0.282438–0.282524. Their εHf(t) values vary from -8.6 to -5.6, and $T_{DM}^{C}$ ages from 1.55 to 1.75 Ga (Fig. 6c; Table S2). By contrast, the ca. 819 Ma inherited core shows positive εHf(t) value of 3.2.

Zircons from sample QD49 are commonly euhedral, about 80–300 μm in length with aspect ratios varying from 1.5:1 to 4:1. A majority of the grains show magmatic growth zonation under CL, but considerable cores are present with various zoning patters (Fig. 4). Twenty-one analyses show U contents of 88–3685 ppm and Th contents of 81–748 ppm respectively (Table S1). Three spots on the inherited cores obtained concordant analyses respectively with Proterozoic ages of 1246 ± 5 Ma ($^{207}Pb/^{206}Pb$ age, spot #18), 831 ± 12 Ma and 848 ± 12 Ma ($^{206}Pb/^{238}U$ age, spot #10 and #13) (Fig. 5e; Table S1). Apart from two discordant analyses, the remaining fifteen analyses forms a cluster, yielding a concordia age of 131.8 ± 1.5 Ma (MSWD of concordance = 0.21) (Fig. 5e).

Zircons from sample DM80 are predominantly elongated grains (about 80–200 μm in length and 20–50 μm in width) with dark CL images, some of which contains inherited cores (Fig. 4). Besides, there are also several tubby grains with bright zonation but no core-rim textures, which are likely xenolithic zircons. A total of thirty-three analyses were conducted. Nine spots on the xenocrysts or inherited cores obtained informative results, among which several concordant or near-concordant analyses yielded $^{206}Pb/^{238}U$ ages of 850–756 Ma as well as ca. 417 Ma (Fig. 5f). We speculated that these xenocrysts with old ages were captured from the wall-rocks during magma ascent. Twenty-four analyses of the dark crystals and rims show high U contents, mostly higher than 2000 ppm (Table S1). These spots are plotted as a cluster on or near the concordia curve, with apparent $^{206}Pb/^{238}U$ ages varying from 137.0 to 153.4 Ma. Despite a weighted mean age of 143.5 ± 1.8 Ma with a large MSWD value of 3.6 can be concluded, there is a distinct correlation that the apparent ages become older while the U concentrations increasing (Fig. 5f). Such a phenomenon is evident for the present of "high-U matrix effect" (White and Ireland, 2012; Gao et al., 2014). Therefore, the crystallization age of sample DM80 is theoretically younger than ca. 143.5 Ma, and probably approximates to the minimum $^{206}Pb/^{238}U$ age of 137.0 ± 2.1 Ma therein. Considering that sample DM80 was taken from the same intrusion as sample QD49, we suggest that the age of sample QD49 (ca. 132 Ma) is a reliable estimate of crystallization

age for the main body of the Dayunshan-Mufushan two-mica monzogranite.

Zircons from sample QD62 are euhedral to subhedral, about 50–250 μm in length with aspect ratios between 1:1 and 4:1. They are either dark with faint zonation or bright with distinct zonation under CL, and quite a few inherited cores can also be observed (Fig. 4). Twenty-three analyses were performed on twenty-one zircons, with Th/U ratios range from 0.08 to 0.42 (Table S1). Except for two discordant analyses resulted from inherited cores, the other analyses form a slightly scattered population with apparent $^{206}Pb/^{238}U$ ages ranging from 118.8 Ma to 140.4 Ma. Seven analyses therein with a bit older or younger ages were rejected, a weighted mean $^{206}Pb/^{238}U$ age of 127.0 ± 1.4 Ma (MSWD = 1.7) was concluded using the remaining fourteen analyses (Fig. 5i). We consider this age to be the crystallization age for the later stocks within the Dayunshan-Mufushan batholith.

The dated zircons from sample QD49 and sample QD 62 were chosen for *in situ* Hf isotope analyses (Fig. 6d; Table S2). Although crystallization ages of these two samples show a discrepancy about 5 Myr, their Hf isotopic compositions largely overlap with $^{176}Hf/^{177}Hf$ ratios varying from 0.282424 to 0.282589. All the analyses show εHf(t) values of -3.6 to -9.6 and $T_{DM}^{C}$ ages of 1.42–1.79 Ga. However, the three concordant cores with Proterozoic ages from sample QD49 have positive εHf(t) values of 2.0 to 5.7 and $T_{DM}^{C}$ ages of 1.50–1.69 Ga.

4.1.3. Wangxiang batholith

Two samples of two-mica monzogranite DYS01 and DYS03 from the main and supplementary phases of the Wangxiang batholith were dated by SIMS method. Zircons from sample DYS01 are relatively small, mostly less than 150 μm in length. CL images reveal that more than one third of them contain inherited cores (Fig. 4). We analyzed five spots on cores, and three analyses therein are concordant with a weighted $^{206}Pb/^{238}U$ mean age of 837 ± 13 Ma (Fig. 5j). Furthermore, the oldest discordant core with $^{207}Pb/^{206}Pb$ age of ca.1715 Ma indicates the presence of potential Paleoproterozoic material. Other eighteen analyses were conducted on rims or magmatic crystals without core. Apart from two analyses possibly due to high U content or Pb loss, the remaining sixteen analyses yielded a weighted mean $^{206}Pb/^{238}U$ age of 147.3 ± 1.5 Ma (MSWD = 1.7) (Fig. 5j).

Zircons from sample DYS03 are either elongated or stubby grains, the latter

usually contain inherited cores surrounded by dark rims (Fig. 4). A total of twenty-five analyses were performed on twenty-three zircons. Four analyses on zircon cores are discordant possibly due to partial mixing of core-rim domains; the remaining analyses plotted on concordia curve show a relatively wide range of apparent $^{206}Pb/^{238}U$ ages from 135.2 to 155.8 Ma. Excluding six analyses with slightly either older or younger ages therein, the other fifteen analyses yielded a weighted $^{206}Pb/^{238}U$ mean age of 146.0 ± 1.4 Ma (MSWD = 1.3) (Fig. 5k). This age is slightly younger but indistinguishable within error from the age of sample DYS01.

Twenty-one dated zircons from sample DYS01 and seventeen dated zircons from sample DYS03 were measured for Hf isotope determination (Fig. 6e; Table S2). The three inherited cores with ages of ca. 837 Ma from sample DYS01 have variable εHf(t) values (-4.1, 3.9 and 11.7). The remaining thirty-five zircons have similar Hf isotopic compositions with $^{176}Hf/^{177}Hf$ ratios of 0.282327–0.282517, corresponding to εHf(t) values of -12.5 to -5.9 and $T_{DM}^{C}$ ages of 1.57–1.99 Ga.

4.1.4. Lianyunshan pluton

We collected two samples DYS06 (two-mica monzogranite) and DYS07 (biotite monzogranite) from the Lianyunshan pluton for age determinations. Zircons from sample DYS06 are euhedral, commonly 60–150 μm in length. Most grains show magmatic oscillatory zoning in CL images, a few inherited cores are also observed (Fig. 4). Twenty-four analyses were conducted, with Th/U ratios between 0.26 and 3.31 (Table S1). One of the two spots on inherited cores obtained a concordant analysis with $^{206}Pb/^{238}U$ age of 825.8 ± 11.6 Ma. Twenty-one analyses of magmatic crystals yielded a weighted mean $^{206}Pb/^{238}U$ age of 150.4 ± 1.7 Ma (MSWD = 2.3) that represents the crystallization age of sample DYS06 (Fig. 5).

Zircons from sample DYS07 are mostly prismatic, 80–200 μm in length with aspect ratios of 2:1 to 3:1. Although most grains display low luminance under CL, oscillatory zoning is more or less visible (Fig. 4). Furthermore, a few of the zircons also show clear core-rim textures, but most of the cores are homogeneous without zonation. A total of twenty-four spots on twenty-two zircons were analyzed, including five bright cores with low U contents (145–726 ppm) and nineteen dark crystals or rims with high U contents (1529–6341 ppm) (Table S1). Except for one discordant core, all the other analyses with similar apparent $^{206}Pb/^{238}U$ ages are plotted on the concordia curve. Apart

from two relatively discrete analyses, the remaining twenty-one analyses yielded a weighted mean $^{206}Pb/^{238}U$ age of 149.0 ± 1.4 (MSWD = 1.8) (Fig. 5). This age is interpreted as the crystallization age of sample DYS07, which is coincident within error with that of sample DYS06.

Twenty-two dated zircons from sample DYS06 were further analyzed for Hf isotopic compositions (Fig. 6f; Table S2). The ca. 826 Ma inherited core has a negative εHf(t) value of -3.6. The $^{176}Hf/^{177}Hf$ ratios of the other magmatic zircons ranges from 0.282330 to 0.282440, corresponding to εHf(t) values of -12.4 to -8.5 and $T_{DM}^{C}$ ages of 1.74–1.98 Ga. By comparison, twenty-one Hf isotope analyses of the dated zircons from sample DYS07 have higher $^{176}Hf/^{177}Hf$ ratios of 0.282486–0.282579, corresponding to εHf(t) values of -6.9 to -3.7 and $T_{DM}^{C}$ ages of 1.44–1.64 Ga (Fig. 6f; Table S2).

## 4.2. Whole-rock major and trace elements

Except for the major and trace element data of ten granitic samples in this study (Table 2), the data from previous literature for the studied plutons have also been selected for comparison. Together with the data presented by L.X. Wang et al. (2008, 2014), the two-mica and biotite monzogranite from the four plutons show high $SiO_2$ contents mostly varying from 70.2 to 74.0 wt.% (up to 76.6 wt.% for sample DYS07), while about 65.5 wt.% for the biotite granodiorite (Fig. 7a). All the granitic rocks (monzogranites and granodiorites) have moderate total alkali $K_2O+Na_2O$ contents of 5.8–8.6 wt.% with $K_2O/Na_2O$ ratios varying from 0.8 to 1.7, mostly belonging to high-K calc-alkaline series (Fig. 7a). On the A/CNK vs. A/NK diagram, they are weakly to strongly peraluminous, with aluminum saturation index (ASI = A/CNK) mostly between 0.99 and 1.17 (Fig. 7b).

The monzogranites as well as granodiorites have similar chondrite-normalized REE patterns, characterized by enrichment of LREEs relative to HREEs and variable degree of negative Eu anomalies (Fig. 8; Xu et al., 2009; L.X. Wang et al., 2008, 2014). Our samples have total REEs contents of 92–232 ppm, with $(La/Yb)_N$ ratios of 20.6–97.8 and Eu/Eu* ratios of 0.35–0.77 (Table 2). By comparison, the negative Eu anomalies of the 151-149 Ma granitoids (i.e., the early-stage intrusion of the Dayunshan-Mufushan batholith, Lianyunshan pluton) are overall less notable than the other younger granitoids. In the primitive mantle-normalized spidergrams, all the

samples are relatively enriched in large ion lithophile elements (LILEs) such as Rb, Th and K, and show distinct negative Ba, Nb, Sr, P and Ti anomalies with a few exceptions (Fig. 8; Xu et al., 2009; L.X. Wang et al., 2008, 2014). The Nb/Ta ratios of our samples mostly range from 5.9 to 11.7 (average at 9.6, except for the unusual sample DYS07), in accord with crustal-derived granites (Table 2).

## 5. Discussion

### 5.1. Emplacement ages of the granitoids in the northeastern Hunan province

As compiled in Table 1 of Shen et al. (2012), numerous geochronological data for the Late Mesozoic granitoids in the study area has been obtained by different methods. However, we notice that most of the data are whole-rock Rb–Sr isochron and biotite or muscovite K–Ar ages, as well as TIMS zircon U–Pb ages. These ages are highly variable ranging from 170 to 108 Ma, their reliabilities are hard to appraise. The Rb–Sr and K–Ar systems are easy to be reset by diffusion and hydrothermal alteration during post-magmatic process, while traditional TIMS method may give mixing age due to possible involvement of inherited cores in magmatic zircons. In contrast, *in situ* zircon U–Pb dating (LA–ICPMS or SIMS) is capable of providing reliable age for pluton emplacement.

Wang et al. (2008) firstly conducted LA–ICPMS zircon U–Pb dating for the Taohuashan two-mica monzogranite, and the age of 129.4 ± 1.1 Ma was considered as the crystallization age. Shen et al. (2012) also dated the Taohuashan pluton by LA–ICPMS method. They obtained a lower intercept age of 118.0 ± 3.7 Ma calculated mostly using discordant spots, and also a concordia age of 127.4 ± 0.6 Ma from four concordant analyses. However, the former was interpreted as the crystallization age, whereas the latter was considered to be inherited from an earlier intrusion phase. Our SIMS zircon U–Pb dating of the Taohuashan biotite monzogranite yielded a concordia age of 128.0 ± 1.0 Ma, which is in agreement with the age of the Taohuashan two-mica monzogranite reported by Wang et al. (2008). Therefore, we suggest that the emplacement age of Taohuashan pluton occurred during 127–129 Ma, and yet the lower intercept age of Shen et al. (2012) likely holds no significance. Besides, there is a small pluton named Xiaomoshan to the north, which yielded two identical LA–ICPMS zircon U–Pb ages of 117.4 ± 1.0 Ma and 116. 6 ± 0.5 Ma (Wang et al., 2008; Shen et al., 2012).

This pluton is mainly composed of biotite monzogranite, representing the latest magmatic activity in the study area.

Recently, L.X. Wang et al. (2014) obtained several zircon U–Pb ages for the Dayunshan-Mufushan batholith by LA–ICPMS method, including 151.5 ± 1.3 Ma, 148.3 ± 1.4 Ma and 145.8 ± 0.9 Ma for the biotite granodiorite, biotite monzogranite and two-mica monzogranite, respectively. Moreover, a small dioritic stock in the northern part of the batholith yielded an older age of 154.0 ± 1.9 Ma. They suggested that the Dayunshan-Mufushan batholith intruded episodically from 154 to 146 Ma, with a magmatic evolution from mafic to felsic. However, such a prolonged (about 8 Myr) process of fractional crystallization proposed by L.X. Wang et al. (2014) is not supported by our new SIMS zircon U–Pb dating results. The two biotite monzogranite samples (DM35 and QD69) in this study have identical ages of 151.2 ± 1.1 Ma and 151.3 ± 1.1 Ma, while the age of biotite granodiorite sample (DYS14, 149.0 ± 1.0 Ma) is about 2 Myr younger than the former. By contrast, the two samples of two-mica monzogranite (QD49 and QD62) from the main body of the batholith and the later stock present Cretaceous ages of 131.9 ± 1.9 Ma and 127.0 ± 1.4 Ma, respectively. Thus we argued that the Dayunshan-Mufushan batholith is a composite pluton, which was products of multistage magmatic activities during the Late Jurassic (151–149 Ma) and Early Cretaceous (132–127 Ma).

Our SIMS zircon U–Pb dating also shows that the main and supplementary phases of the Wangxiang batholith crystallized in a very short period during 147–146 Ma, while the Lianyunshan pluton was emplaced during 150–149 Ma. So far, no *in situ* zircon U–Pb data was previously available for the Miaoshan, Changlejie, Cenchuan and Jinjing plutons in the study area (Fig. 2). Their rock associations are similar to the early-stage intrusion of the Dayunshan-Mufushan batholith, Wangxiang batholith and Lianyunshan pluton (BGMRHN, 1988; Wang and Deng, 2004; Li et al., 2005). Combining with the unreliable radiometric results in the report of regional geological surveys, we infer that they were likely also emplaced during the Late Jurassic (151–146 Ma). Nevertheless, precise dating of these plutons is expected in the future.

### 5.2. Petrogenetic type

Chappell and White (1974, 2001) initially proposed the classification of I- and S-type granites. The I-type granites are mainly metaluminous (ASI <1.0) and have higher

$Na_2O$ contents (normally >3.2 wt.%), derived largely by partial melting of metaigneous rocks; while the S-type granites are usually strongly peraluminous (ASI >1.1) and have lower $Na_2O$ contents (normally <3.2 wt.% with about 5 wt.% $K_2O$), derived largely by partial melting of metasedimentary rocks. In view of the data from both this study and the literature (L.X. Wang et al., 2008, 2014), the majority of the Late Mesozoic granitoids in the northeastern Hunan province is weakly to strongly peraluminous, and have moderate $Na_2O$ contents of 2.8–3.9 wt.% (average at 3.3 wt.%). In this regard, it seems difficult to attribute these granitoids to typical I-type or S-type granites, implying that source heterogeneity or magma mixing may contribute to their origin (Clemens, 2003). On the ACF diagram, however, all the granitic samples plot within the field of S-type granites, in agreement with their muscovite-bearing or biotite-rich peraluminous compositions (Fig. 9a). Furthermore, there is no obvious decrease of $P_2O_5$ when $SiO_2$ increases (without respect to the granodiorites; Fig. 9b), and increasing of Y and Th against Rb (Fig. 9c, d). These trends are inconsistent with the features of the I-type granites in the Lachlan fold belt (Chappell, 1999), and also the fractionated I-type granites in SE China (Li et al., 2007; Zhang et al., 2015). In addition, most of the granitic samples have relatively low 10000×Ga/Al (<2.6) and Zr+Nb+Y+Ce (<350 ppm), low to moderate FeO*/MgO and $(K_2O+Na_2O)/CaO$, falling into the fields of unfractionated and minor fractionated granites (Fig. 9e, f). The above criterions indicate that these rocks are significantly different from the A-type granites (Whalen et al., 1987). Thus, the Late Mesozoic granitoids in the study area, especially the dominant monzogranites, are more similar to S-type as well as fractionated S-type granites. Such a deduction is further supported by the fact that metasedimentary xenoliths or restites are largely present within these granitic rocks. Moreover, considerable zircons in our dated samples contain old inherited cores, indicative of partial melting of metasedimentary rocks.

Barbarin (1996) once further distinguished two main types of peraluminous granitoids, namely muscovite-bearing granitoids (MPGs, unusually two-mica monzogranite to leucogranite) and biotite-rich, cordierite-bearing granitoids (CPGs, unusually tonalite, granodiorite and monzogranite). It has been suggested that the MPGs are produced through ‘wet’ anatexis of crustal rocks and crystal fractionation of the magmas, while the CPGs are produced through ‘dry’ anatexis of crustal rocks enhanced by underplating or injection of hot mantle-derived magmas. According to the rock types and mineral assemblages, both the MPGs and CPGs occur in the study area.

For example, the late-stage intrusion (two-mica monzogranite) of the Dayunshan-Mufushan batholith, and the Wangxiang batholith are dominantly MPGs, while the early-stage intrusion (biotite monzogranite and biotite granodiorite) of the Dayunshan-Mufushan batholith is similar to CPGs but without cordierite.

### 5.3. Origin of the granitoids

Previous studies on experimental petrology and geochemistry have documented that peraluminous granitoids (including strongly peraluminous or S-type granites) are mainly generated by partial melting of metasedimentary rocks (metapelite, metagreywacke), possibly added with metaigneous rocks (orthogneiss, amphibolite) (e.g., Miller, 1985; Patiňo-Douce and Johnston, 1991; Sylvester, 1998). As demonstrated by Sylvester (1998), strongly peraluminous granites can inherit different $CaO/Na_2O$ ratios by partial melting of different sources, pelite-derived melts tend to have lower $CaO/Na_2O$ ratios (<0.3) than psammite-derived counterparts. The majority of granitic rocks in the study area have high $CaO/Na_2O$ ratios (mostly >0.3), indicating that they mainly derived from partial melting of psammitic rocks (Fig. 10a). On the Rb/Sr vs. Rb/Ba plot, these samples mainly fall into the plagioclase-rich, clay-poor sources field (Fig. 10b). Therefore, we suggest that the source rocks are mostly metagreywacke with minor metaigneous rocks, as shown on the molar $Al_2O_3/(MgO+FeO^*)$ vs. molar $CaO/(MgO+FeO^*)$ diagram (Altherr et al., 2000; Fig. 10c). However, minor mixture of the two end-members consisting of crust-derived melt and basaltic magmas cannot be ruled out, especially for the granodiorites with rather higher $CaO/Na_2O$, lower Rb/Sr and Rb/Ba ratios. Indeed, L.X. Wang et al. (2014) identified a small stock of mantle-derived diorite within the biotite monzogranite of the Dayunshan-Mufuhshan batholith. Underplating of basaltic magma acting as a heat source that triggered partial melting of the middle to lower crust and formation of the felsic magmas is very likely. Nevertheless, a direct input of mantle-derived magma in genesis of these granitoids appears to be insignificant since mafic enclaves are rarely observed in the field. In addition, the $Al_2O_3$, $Fe_2O_3^*$, CaO, MgO and $TiO_2$ contents decrease with increasing $SiO_2$, indicative of fractionation of feldspar, biotite and Fe-Ti oxides. The negative Eu anomaly, depletion in Sr and Ba, and linear trends of Sr vs. Rb and Ba further support the removal of plagioclase and K-feldspar from the original magma (Figs. 8 and 11). Dykes or small stocks of garnet-bearing leucogranite are

particularly abundant in the Taohuashan pluton and Dayunshan-Mufushan batholith. These rocks represent highly-fractionated products, showing geochemical features similar to the Himalaya leucogranite (L.X. Wang et al., 2008, 2014). Thus fractional crystallization probably played an important role during the magmatic evolution, which seems likely more effective for generation of the MPGs.

Zircon as early crystallization mineral from the magma can retain its original isotopic composition, and thus was widely used to trace petrogenetic process (Griffin et al., 2002). Zircons (n = 178) with crystallization ages from the studied granitoids show variable εHf(t) values ranging from -12.5 to -3.6 (Table 1; Fig. 6). The corresponding $T_{DM}^{C}$ ages vary from 1.42 to 1.99 Ga, suggesting that the source rocks were chemically weathered Paleo- to Mesoproterozoic crustal materials of the SCB. As mentioned before, the exposed basement in the study area is predominantly the Lengjiaxi Group, which was traditionally regarded as slightly metamorphosed Mesoproterozoic strata (BGMRHN, 1988; Gu et al., 2002; Xu et al., 2007). Recently, U–Pb dating of detrital zircons as well as tuff beds have demonstrated that the deposition of the Lengjiaxi Group occurred during the early Neoproterozoic (ca. 860-820 Ma; W. Wang et al., 2010, 2012, 2013; Gao et al., 2011; Meng et al., 2013; X.L. Wang et al., 2014; Yan et al., 2015). In our dated samples, there are quite a few Neoproterozoic inherited cores (Table S1), overlapping the major age population of detrital zircons from the Lengjiaxi Group. These relict zircons show εHf(t) values mostly between -4.1 and 4.3 (Table S2), which also fall into the wide range of εHf(t) values of the Neoproterozoic detrital zircons. Moreover, the Lengjiaxi Group also contains older detrital zircons with Paleo- to Mesoproterozoic ages equal to the crustal Hf model ages of these studied granitoids. Accordingly, we infer that the Late Mesozoic peraluminous granitoids in the study area were derived from partial melting of metasedimentary basement analogous to the Neoproterozoic Lengjiaxi Group. The slight variations of Hf isotropic compositions among the different plutons, even different samples from the same pluton (e.g., Lianyunshan), indicate isotope disequilibrium of the magma probably inherited from heterogeneous metasedimentary source or due to wall-rock assimilation.

### 5.4. Geodynamic implications

Subduction of the Paleo-Pacific plate beneath the Eurasia continent is the most

popular model to account for the origin and evolution of the Jurassic-Cretaceous magmatism in SE China so far. For example, Zhou and Li (2000) proposed a comprehensive model of a combination of lithospheric subduction and underplating of mafic magmas, with an increasing subduction angle of the Paleo-Pacific plate to explain the oceanward younging trend of the magmatic activity. Alternatively, Li and Li (2007) presented a flat-slab subduction model to account for the Mesozoic migration of intracontinental orogeny and magmatism in SE China. They interpreted the Jurassic magmatism in the interior as anorogenic products formed in response to the upwelling of asthenosphere mantle after the break-up and foundering of an Early Mesozoic subducted flat-slab, whereas the Cretaceous magmatism with both extensional and arc-related features in the coastal area was regarded as a retreating arc system. Similarly, based on detailed compilations of available geochronological, geochemical and geological data on the Cretaceous plutonism in the coastal Fujian province, a recurrence of slab break-off and rollback of the Paleo-Pacific plate has been suggested (Z. Li et al., 2014). More recently, Jiang et al. (2015) put forward a repeated slab advance-retreat model in view of the identification of several Mesozoic NE-trending A-type granite belts and the Early Jurassic mafic rocks in SE China. In addition, a ridge subduction model has been proposed for genesis of the Cretaceous magmatism (especially "adakitic rocks" and A-type granites) and related polymetallic mineralization in the lower Yangtze River belt (Ling et al., 2009; Sun et al., 2010; H. Li et al., 2012). However, the so-called "adakitic rocks" penetrated perpendicularly into the continental interior more than 1000 km away from the present continental margin, such a spatial distribution would require an unlikely ridge subduction with very shallow angle (X.H. Li et al., 2010, 2013b). Moreover, if there was a slab window formed by ridge subduction, the related magmatism would show a younging trend toward the continental interior, which is contrary to the present observation. Considering the subduction angle variations, Wu et al. (2012) argued that slab tearing instead of ridge subduction might account for the eastward younging trend of the 150-136 Ma magmatism in this area. Nevertheless, it is beyond the scope of this paper to reconstruct the history of the Paleo-Pacific plate, since available data are rare (Engebretson et al., 1985; Maruyama et al., 1997; Sun et al., 2007).

The Jurassic-Cretaceous magmatism in SE China took place in two distinct stages. The Jurassic magmatism includes an subordinate phase of ca. 190 Ma A-type granites, mafic intrusions and bimodal volcanic rocks mainly in the E-W trending Nanling Range

(Chen et al., 2008; He et al., 2010; Jiang et al., 2015), and a major magmatic flare-up at ca. 165–150 Ma throughout the Cathaysia interior dominated by I-type or fractionated I-type granites along with minor A-type granites and syenites (Li et al., 2007; Jiang et al., 2009; Huang et al., 2013, 2015; Zhang et al., 2015; Wang et al., 2016). The Cretaceous intrusive and volcanic rocks are confined mostly to the coastal region, with two major phases at ca. 140–125 Ma and ca. 115–90 Ma. They consist predominantly of calc-alkaline granites and felsic volcanic rocks, and subordinate A-type granites and basaltic rocks (Li, 2000; Wong et al., 2009; Jiang et al., 2011; Guo et al., 2012; Liu et al., 2012, 2014; Z. Li et al., 2014). In view of geochronological statistics, ca. 150–140 Ma is a relatively "magmatic quiescence" in SE China (X.H. Li et al., 2010; Y.J. Wang et al., 2013). As discussed before, the Late Mesozoic magmatic activities in the northeastern Hunan province can be roughly subdivided into three phases, namely 151–146 Ma, 132–127 Ma and ca. 117 Ma. The latter two phases of magmatism are in agreement with the Cretaceous magmatism in SE China. Most of the researchers favor slab rollback of the Paleo-Pacific plate as the geodynamic trigger for the Cretaceous magmatism in SE China (e.g., Zhou and Li, 2000; Li and Li, 2007; Wong et al., 2009; Jiang et al., 2011, 2015; Liu et al., 2012, 2014; Wang et al., 2016). Such a setting is evidently supported by the Cretaceous lithospheric extension in the eastern SCB, as indicated by the development of extensional domes and rift basins (Gilder et al., 1996; Li, 2000; Lin et al., 2000; Shu et al., 2009; Ji et al., 2014; J.H. Li et al., 2014). In the study area, the Dayunshan syntectonic pluton was emplaced under a NW-SE extension according to our unpublished structural and AMS (anisotropy of magnetic susceptibility) data. Moreover, a NW-directed back-thrusting event along the Changle-Nan'ao belt and associated metamorphism occurred between 130 and 110 Ma, as a response to collision of the West Philippines microcontinent with the SCB (Li et al., 2015; Wei et al., 2015). Thus we infer that there might be two episodes of slab rollback during the Cretaceous, respectively corresponding to the two main phases of Cretaceous magmatism (Fig. 12A). Particularly, the early-stage (151–146 Ma) magmatism identified in this study, which overlapped the epilogue of Jurassic magmatic flare-up and the subsequent "magmatic quiescence", is rarely developed in SE China. Nevertheless, a minor amount of 150–140 Ma igneous rocks can also be found in the lower Yangtze River belt and the Changle-Nan'ao belt (e.g., X.H. Li et al., 2010; Cui et al., 2012; Liu et al., 2012; Wu et al., 2012). Such a configuration agrees with the broad outward-younging trend for the Jurassic-Cretaceous magmatism as

suggested by Li et al. (2013a). Thus we support the interpretation that the Jurassic magmatic flare-up in SE China was mainly induced by break-up and foundering of a subducted oceanic flat-slab in an intraplate setting, and the apparent 150–140 Ma magmatic gap probably represented a transition period prior to slab rollback of the Paleo-Pacific plate (Fig. 12A).

The effect of Paleo-Pacific subduction on the Mesozoic geological evolution of SE China is generally acknowledged, and a northwestward polarity is usually assumed (e.g., Zhou et al., 2000; Li and Li, 2007; Jiang et al., 2015). However, when and how far the Paleo-Pacific plate subducted is still highly speculative. It is worth nothing that the tectonic nature and polarity of the Jurassic flat-slab beneath SE China remain an open question. In the present state of knowledge, a continental slab with southeastward polarity cannot be ruled out. Indeed, southward or southeastward continental subduction accounts well for the geodynamic scenarios of the Triassic orogeny along the southern margin of the SCB (from Yunnan province to Hainan Island, possibly farther to the east; see Faure et al., 2014, 2016), and especially in interior of the SCB along the NE-SW trending Jiuling-Xuefengshan belt. (Chu et al., 2012a, 2012b; Chu and Lin, 2014). The pre-existing lithospheric weak zone in the central SCB (e.g., the Jiangshan-Shaoxing fault and the Chenzhou-Linwu fault) was reactivated by the Triassic intracontinental orogeny. At variance to the Paleo-Pacific subduction models, the Jurassic magmatism in SE China might be a protracted consequence of slab foundering after a SE-directed intracontinental subduction (Fig. 12B). However, future work is required to test this new geodynamic interpretation.

## 6. Conclusions

A comprehensive study of zircon U–Pb dating, Hf isotope and geochemical data of the Late Mesozoic granitoids in the northeastern Hunan province allows us to draw the following conclusions:

(1) The Late Mesozoic magmatic activities in this area occurred at 151–146 Ma, 132–127 Ma and ca. 117 Ma;

(2) These high-K calc-alkaline, weakly to strongly peraluminous granitoids are mainly represented by two-mica or biotite monzogranites with minor biotite granodiorites, showing geochemical features similar to S-type as well as fractionated S-type granites;

(3) The source rocks of these granitic rocks were mainly metasedimentary rocks predominantly with psammitic component, without significant involvement of mantle material. Fractional crystallization played an important role in the magma evolution especially for the dominant monzogranites;

(4) The Cretaceous (132–127 Ma and ca. 117 Ma) magmatism might be response to episodic slab rollback of the Paleo-Pacific plate; while the early-stage (151–146 Ma) magmatism probably foreshadowed the transformation from foundering of a subducted flat-slab to slab rollback.

## Acknowledgements

Special thanks are due to Xianhua Li, Qiuli Li and Yueheng Yang in IGGCAS for their help with the SIMS and LA–MC–ICPMC analyses, as well as Fuyuan Wu and Xiaochi Liu in IGGCAS for helpful discussion. This work has been financially supported by the National Natural Science Foundation of China (Grant No. 41225009, 41502202 and 41302161).

## Appendix A. Supplementary data

Supplementary data related to this article can be found online.

## References

Altherr, R., Holl, A., Hegner, E., Langer, C., Kreuzer, H., 2000. High-potassium, calc-alkaline I-type plutonism in the European Variscides: northern Vosges (France) and northern Schwarzwald (Germany). Lithos 50, 51–73.

Barbarin, B., 1996. Genesis of the two main types of peraluminous granitoids. Geology 24, 295–298.

Blichert-Toft, J., Albarède, F., 1997. The Lu-Hf isotope geochemistry of chondrites and the evolution of the mantle-crust system. Earth Planet. Sci. Lett. 148, 243–258.

Bureau of Geology and Mineral Resources of Hunan Province (BGMRHN), 1988. Regional Geology of Hunan Province. Geological Publishing House, Beijing (in Chinese with English abstract).

Chappell, B.W., 1999. Aluminium saturation in I- and S-type granites and the characterization of fractionated haplogranites. Lithos 46, 535–551.

Chappell, B.W., White, A.J.R., 1974. Two contrasting granite types. Pac. Geol. 8, 173–174.

Chappell, B.W., White, A.J.R., 1992. I- and S-type granites in the Lachlan Fold Belt. Trans. R. Soc. Edinburgh: Earth Sci. 83, 1–26.

Chappell, B.W., White, A.J.R., 2001. Two contrasting granite types: 25 years later. Aust. J. Earth Sci. 48, 489–499.

Charvet, J., Shu, L.S., Shi, Y.S., Guo, L.Z., Faure, M., 1996. The building of south China: collision of Yangzi and Cathaysia blocks, problems and tentative answers. J. SE Asian Earth Sci. 13, 223–235.

Charvet, J., Shu, L.S., Faure, M., Choulet, F., Wang, B., Lu, H.F., Le Breton, N., 2010. Structural development of the Lower Paleozoic belt of South China: Genesis of an intracontinental orogen. J. Asian Earth Sci. 39, 309–330.

Chen, C.H., Lee, C.Y., Shinjo, R., 2008. Was there Jurassic paleo-Pacific subduction in South China?: Constraints from $^{40}Ar/^{39}Ar$ dating, elemental and Sr–Nd–Pb isotopic geochemistry of the Mesozoic basalts. Lithos 106, 83–92.

Chu, Y., Faure, M., Lin, W., Wang, Q.C., 2012a. Early Mesozoic tectonics of the South China block: Insights from the Xuefengshan intracontinental orogen. J. Asian Earth Sci. 61,199–220.

Chu, Y., Faure, M., Lin, W., Wang, Q.C., Ji, W.B., 2012b. Tectonics of the Middle Triassic intracontinental Xuefengshan belt, South China: New insights from structural and chronological constraints on the basal décollement zone. Int. J. Earth Sci. 101, 2125–2150.

Chu, Y., Lin, W., 2014. Phanerozoic polyorogenic deformation in southern Jiuling Massif, northern South China block: Constraints from structural analysis and geochronogy. J. Asian Earth Sci. 86, 117–130.

Clemens, J.D., 2003. S-type granitic magmas—petrogenetic issues, models and evidence. Earth-Sci. Rev. 61, 1–18.

Cui, J.J., Zhang, Y.Q., Dong, S.W., Jahn, B.M., Xu, X.B., Ma, L.C., 2013. Zircon U–Pb geochronology of the Mesozoic metamorphic rocks and granitoids in the coastal tectonic zone of SE China: Constraints on the timing of Late Mesozoic orogeny. J. Asian Earth Sci. 62, 237–252.

Engebretson, D.C., Cox, A., Gordon, R.G., 1985. Relative motions between oceanic and continental plates in the Pacific basin. Geological Society of American Special Paper 206, 1–59.

Faure, M., Lin, W., Monié, P., Meffre, S., 2008. Paleozoic collision between the North and South China blocks, Triassic intracontinental tectonics, and the problem of the ultrahigh-pressure metamorphism. Compt. Rendus Geosci. 340, 139–150.

Faure, M., Shu, L.S., Wang, B., Charvet, J., Choulet, F., Monié, P., 2009. Intracontinental subduction: a possible mechanism for the Early Palaeozoic Orogen of SE China. Terra Nova 21, 360–368.

Faure, M., Lepvrier, C., Nguyen, V.V., Vu, V.T., Lin, W., Chen, Z.C, 2014. The South China Block-Indochina collision: Where, when, and how? J. Asian Earth Sci. 79, 260–274.

Faure, M., Lin, W., Chu, Y., Lepvrier, C., 2016. Triassic tectonics of the southern margin of the South China Block. Compt. Rendus Geosci. 348, 5–14.

Gao, L.Z., Chen, J., Ding, X.Z., Liu, Y.R., Zhang, C.H., Zhang, H., Liu, Y.X., Pang, W.H., Zhang, Y.H., 2011. Zircon SHRIMP U–Pb dating of the tuff bed of Lengjiaxi and Banxi Groups, northeastern Hunan: constraints on the Wuling movement. Geol. Bull. China 30, 1001–1008 (in Chinese with English abstract).

Gao, Y.Y, Li, X.H., Griffrin, W.L., O'Reilly, S.Y., Wang, Y.F., 2014. Screening criteria for reliable U–Pb geochronology and oxygen isotope analysis in uranium-rich zircons: A case study from the Suzhou A-type granites, SE China. Lithos 192–195, 180-191.

Gilder, S.A., Gill, J., Coe, R.S., Zhao, X.X., Liu, Z.W., Wang, G.X., Yuan, K.R., Liu, W.L., Kuang, G.D., Wu, H.R., 1996. Isotopic and paleomagnetic constraints on the Mesozoic tectonic evolution of south China. J. Geophys. Res. 101, 16137-16154.

Griffin, W.L., Pearson, N.J., Belousova, E., Jackson, S.E., van Achterbergh, E., O'Reilly, S.Y., Shee, S.R., 2000. The Hf isotope composition of cratonic mantle: LAM-MC-ICPMS analysis of zircon megacrysts in kimberlites. Geochim. Cosmochim. Acta 64, 133–147.

Griffin, W.L., Wang, X., Jackson, S.E., Pearson, N.J., O'Reilly, S.Y., Xu, X.S., Zhou, X.M., 2002. Zircon geochemistry and magma mixing, SE China: In-situ analysis of Hf isotopes, Tonglu and Pingtan igneous complexes. Lithos 61, 237–269.

Gu, X.X., Liu, J.M., Zheng, M.H., Tang, J.X., Qi, L., 2002. Provenance and tectonic setting of the Proterozoic turbidites in Hunan, South China: Geochemical evidence. J. Sediment. Res. 72, 393–407.

Guo, F., Fan, W.M., Li, C.W., Zhao, L., Li, H.X., Yang, J.H, 2012. Multi-stage crust-mantle interaction in SE China: Temporal, thermal and compositional constraints

from the Mesozoic felsic volcanic rocks in eastern Guangdong-Fujian provinces. Lithos 150, 62–84.

He, Z.Y., Xu, X.S., Niu, Y.L., 2010. Petrogenesis and tectonic significance of a Mesozoic granite-syenite-gabbro association from inland South China. Lithos 119, 621–641.

Hsü, K.J., Li, J.L., Chen, H.H., Wang, Q.C., Sun, S., Şengör, A.M.C., 1990. Tectonics of South China: Key to understanding West Pacific geology. Tectonophysics 183, 9–39.

Huang, C.L., Jiang, S.Y., 2014. Highly fractionated S-type granites from the giant Dahutang tungsten deposit in Jiangnan Orogen, Southeast China: geochronology, petrogenesis and their relationship with W-mineralization. Lithos 202-203, 207–226.

Huang, H.Q., Li, X.H., Li, Z.X., Li, W.X., 2013. Intraplate crustal remelting as the genesis of Jurassic high-K granites in the coastal region of the Guangdong Province, SE China. J. Asian Earth Sci. 74, 280–302.

Huang, H.Q., Li, X.H., Li, Z.X., Li, W.X., 2015. Formation of the Jurassic South China Large Granitic Province: Insights from the genesis of the Jiufeng pluton. Chem. Geol. 401, 43–58.

Janoušek, V., Finger, F., Roberts, M., Frýda, J., Pin, C., Dolejš, D., 2004. Deciphering the petrogenesis of deeply buried granites: whole-rock geochemical constraints on the origin of largely undepleted granulites from the Moldanubian Zone of the Bohemian Massif. Trans. R. Soc. Edinburgh: Earth Sci. 95, 141–159.

Ji, W.B., Lin, W., Faure, M., Chu, Y., Wu, L., Wang, F., Wang, J., Wang, Q.C., 2014. Origin and tectonic significance of the Huangling massif within the Yangtze craton, South China. J. Asian Earth Sci. 86, 59–75.

Jiang, Y.H., Jiang, S.Y., Dai, B.Z., Liao, S.Y., Zhao, K.D., Ling, H.F., 2009. Middle to Late Jurassic felsic and mafic magmatism in southern Hunan province, Southeast China: Implications for a continental arc to rifting. Lithos 107, 185–204.

Jiang, Y.H., Zhao, P., Zhou, Q., Liao, S.Y., Jin, G.D., 2011. Petrogenesis and tectonic implications of Early Cretaceous S- and A-type granites in the northwest of the Gan-Hang rift, SE China. Lithos 121, 55–73.

Jiang, Y.H., Wang, G.C., Liu, Z., Ni, C.Y., Qing, L., Zhang, Q., 2015. Repeated slab advance-retreat of the Palaeo-Pacific plate underneath SE China. Int. Geol. Rev. 57, 472–491.

Li, H., Ling, M.X., Li, C.Y., Zhang, H., Ding, X., Yang, X.Y., Fan, W.M., Li, Y.L., Sun, W.D., 2012. A-type granite belts of two chemical subgroups in central eastern China: Indication of ridge subduction. Lithos 150, 26–36.

Li, J.H., Zhang, Y.Q., Dong, S.W., Johnston, S.T., 2014. Cretaceous tectonic evolution of South China: A preliminary synthesis. Earth-Sci. Rev. 134, 98–136.

Li, P.C., Xu, D.R., Chen, G.H., Xia, B., He, Z.L., Fu, G.G., 2005. Constraints of petrography, geochemistry and Sr-Nd isotopes on the Jinjing granitoids from northeastern Hunan province, China: implications for petrogenesis and geodynamic setting. Acta Petrol. Sin. 21, 921–934 (in Chinese with English abstract).

Li, X.H., 2000. Cretaceous magmatism and lithospheric extension in Southeast China. J. Asian Earth Sci. 18, 293–305.

Li, X.H., Li, Z.X., Li, W.X., Liu, Y., Yuan, C., Wei, G.J., Qi, C.S., 2007. U–Pb zircon, geochemical and Sr–Nd–Hf isotopic constraints on age and origin of Jurassic I- and A-type granites from central Guangdong, SE China: A major igneous event in response to foundering of a subducted flat-slab? Lithos 96, 186–204.

Li, X.H., Li, W.X., Li, Z.X., Lo, C.H., Wang, J., Ye, M.F., Yang, Y.H., 2009a. Amalgamation between the Yangtze and Cathaysia Blocks in South China: Constraints from SHRIMP U–Pb zircon ages, geochemistry and Nd–Hf isotopes of the Shuangxiwu volcanic rocks. Precambr. Res. 174, 117–128.

Li, X.H., Liu, Y., Li, Q.L., Guo, C.H., Chamberlain, K.R., 2009b. Precise determination of Phanerozoic zircon Pb/Pb age by multicollector SIMS without external standardization. Geochem. Geophys. Geosyst. 10, Q04010, doi:10.1029/2009GC002400.

Li, X.H., Li, W.X., Wang, X.C., Li, Q.L., Liu, Y., Tang, G.Q., Gao, Y.Y., Wu, F.Y., 2010. SIMS U–Pb zircon geochronology of porphyry Cu–Au–(Mo) deposits in the Yangtze River Metallogenic Belt, eastern China: Magmatic response to early Cretaceous lithospheric extension. Lithos 119, 427–438.

Li, X.H., Tang, G.Q., Gong, B., Yang, Y.H., Hou, K.J., Hu, Z.C., Li, Q.L., Liu, Y., Li, W.X., 2013a. Qinghu zircon: A working reference for microbeam analysis of U–Pb age and Hf–O isotopes. Chin. Sci. Bull. 58, 4647–4654.

Li, X.H., Li, Z.X., Li, W.X., Wang, X.C., Gao, Y.Y., 2013b. Revisiting the “C-type adakites” of the Lower Yangtze River Belt, central eastern China: In-situ zircon Hf–O isotope and geochemical constraints. Chem. Geol. 345, 1–15.

Li, Y., Ma, C,Q., Xing, G.F., Zhou, H.W., 2015. The Early Cretaceous evolution of SE China: Insights from the Changle-Nan'ao Metamorphic Belt. Lithos 230: 94–164.

Li, Z., Qiu, J.S., Yang, X.M., 2014. A review of the geochronology and geochemistry of Late Yanshanian (Cretaceous) plutons along the Fujian coastal area of southeastern China: Implications for magma evolution related to slab break-off and rollback in the Cretaceous. Earth-Sci. Rev. 128, 232–248.

Li, Z.X., Li, X.H., 2007. Formation of the 1300-km-wide intra-continental orogen and postorogenic magmatic province in Mesozoic South China: A flat-slab subduction model. Geology 35, 179–182.

Li, Z.X., Li, X.H., Wartho, J.A., Clark, C., Li, W.X., Zhang, C.L., Bao, C.M., 2010. Magmatic and metamorphic events during the early Paleozoic Wuyi-Yunkai orogeny, southeastern South China: New age constraints and pressure-temperature conditions. Geol. Soc. Am. Bull. 122, 772–793.

Li, Z.X., Li, X.H., Chung, S.L., Lo, C.H., Xu, X.S., Li,W.X., 2012. Magmatic switch-on and switch-off along the South China continental margin since the Permian: Transition from an Andean-type to a Western Pacific-type plate boundary. Tectonophysics 532-535, 271–290.

Lin, W., Faure, M., Monié, P., Schärer, U., Zhang, L.S., Sun, Y., 2000. Tectonics of SE China: New insights from the Lushan massif (Jiangxi Province). Tectonics 19, 852–871.

Lin, W., Wang, Q.C., Chen, K., 2008. Phanerozoic tectonics of south China block: New insights from the polyphase deformation in the Yunkai massif. Tectonics 27, TC6004, doi:10.1029/2007TC002207.

Ling, M.X., Wang, F.Y., Ding, X., Hu, Y.H., Zhou, J.B., Zartman, R.E., Yang, X.Y., Sun, W.D., 2009. Cretaceous ridge subduction along the Lower Yangtze River belt, eastern China. Econ. Geol. 104, 303–321.

Liu, L., Xu, X.S., Zou, H.B., 2012. Episodic eruptions of the Late Mesozoic volcanic sequences in southeastern Zhejiang, SE China: petrogenesis and implications for the geodynamics of paleo-Pacific subduction. Lithos 154, 166–180.

Liu, L., Xu, X.S., Xia, Y., 2014. Cretaceous Pacific plate movement beneath SE China: Evidence from episodic volcanism and related intrusions. Tectonophysics 614: 170–184.

Liu, Q., Yu, J.H., Wang, Q., Su, B., Zhou, M.F., Xu, H., Cui, X., 2012. Ages and geochemistry of granites in the Pingtan-Dongshan Metamorphic Belt, Coastal

South China: New constraints on Late Mesozoic magmatic evolution. Lithos 150, 268–286.

Ludwig, K.R., 2003. User's manual for Isoplot 3.00: A Geochronological Toolkit for Microsoft Excel. Berkeley Geochronology Center Special Publication No. 4.

Maniar, P.D., Piccoli, P.M., 1989. Tectonic discrimination of granitoids. Geol. Soc. Am. Bull. 101, 635–643.

Maruyama, S., Isozaki, Y., Kimura, G., Terabayashi, M., 1997. Paleogeographic maps of the Japanese Islands: Plate tectonic synthesis from 750 Ma to present. Isl. Arc 6, 121–142.

Meng, Q.X., Zhang, J., Geng, J.Z., Zhang, C.L., Huang, W.C., 2013. Zircon U–Pb age and Hf isotope compositions of Lengjiaxi and Banxi Groups in middle Hunan province: implication for Neoproterozoic tectonic evolution in South China. Geol. China 40, 191–216 (in Chinese with English abstract).

Miao, J.W., Cheng, Y.B., Chen, M.H., Pirajno, F., 2013. Major types and time-space distribution of Mesozoic ore deposits in South China and their geodynamic settings. Miner. Deposita 48, 267–294.

Morel, M.L.A., Nebel, O., Nebel-Jacobsen, Y.J., Miller, J.S., Vroon, P.Z., 2008. Hafnium isotope characterization of the GJ-1 zircon reference material by solution and laser-ablation MC-ICPMS. Chem. Geol. 255, 231–235.

Patiňo Douce A.E., Johnston, A.D., 1991. Phase equilibria and melt productivity in the pelitic system: implications for the origin of peraluminous granitoids and aluminous granulites. Contrib. Miner. Petrol. 107, 202–218.

Peccerillo, A., Taylor, S.R., 1976. Geochemistry of Eocene calc-alkaline volcanic rocks from the Kastamonu area, northern Turkey. Contrib. Miner. Petrol. 58, 63–81.

Shen, C.B., Mei, L.F., Min, K., Jonckheere, R., Ratschbacher, L., Yang, Z., Peng, L., Liu, Z,Q., 2012. Multi-chronometric dating of the Huarong granitoids from the middle Yangtze Craton: Implications for the tectonic evolution of eastern China. J. Asian Earth Sci. 52, 73–87.

Shu, L.S., Zhou, X.M., Deng, P., Wang, B., Jiang, S.Y., Yu, J.H., Zhao, X.X., 2009. Mesozoic tectonic evolution of the Southeast China Block: New insights from basin analysis, J. Asian Earth Sci. 34, 376–391.

Shu, L.S., Jahn, B.M., Charvet, J., Santosh, M., Wang, B., Xu, X.S., Jiang, S.Y., 2014. Intraplate tectono-magmatism in the Cathaysia Block (South China): Evidence from stratigraphic, structural, geochemical and geochronological investigations.

Am. J. Sci. 314, 154–186.

Shu, L.S., Wang, B., Cawood, P.A., Santosh, M., Xu, Z.Q., 2015. Early Paleozoic and Early Mesozoic intraplate tectonic and magmatic events in the Cathaysia Block, South China. Tectonics 34, 1600–1621.

Sláma, J., Košler, J., Condon, D.J., Crowley, J.L., Gerdes, A., Hanchar, J.M., Horstwood, M.S.A., Morris, G.A., Nasdala, L., Norberg, N., Schaltegger, U., Schoene, B., Tubrett, M.N., Whitehouse, M.J., 2008. Plešovice zircon—A new natural reference material for U–Pb and Hf isotopic microanalysis. Chem. Geol. 249, 1–35.

Sun, S.S., McDonough, W.F., 1989. Chemical and isotopic systematic of oceanic basalts: implications for mantle composition and processes. In: Saunders, A.D., Norry, M.J. (Eds.), Magmatism in the Ocean Basins. Geological Society of London Special Publications 42, 313–345.

Sun, W.D., Ding, X., Hu, Y.H., Li, X.H., 2007. The golden transformation of the Cretaceous plate subduction in the west Pacific. Earth Planet. Sci. Lett. 262, 533–542.

Sun, W.D., Ling, M.X., Yang, X.Y., Fan, W.M., Ding, X., Liang, H.Y., 2010. Ridge subduction and porphyry copper-gold mineralization: An overview. Sci. China Earth Sci. 53, 475–484.

Sylvester, P.J., 1998. Post-collisional stongly peraluminous granites. Lithos 45, 29–44.

Wang, F.Y., Ling, M.X., Ding, X., Hu, Y.H., Zhou, J.B., Yang, X.Y., Liang, H.Y., Fan, W.M., Sun, W.D., 2011. Mesozoic large magmatic events and mineralization in SE China: oblique subduction of the Pacific plate. Int. Geol. Rev. 53, 704–726.

Wang, G.C., Jiang, Y.H., Liu, Z., Ni, C.Y., Qing, L., Zhang, Q., Zhou, S.Q., 2016. Multiple origins for the Middle Jurassic to Early Cretaceous high-K calc-alkaline I-type granites in northwestern Fujian province, SE China and tectonic implications. Lithos 246-247, 197–211.

Wang, J., Li, Z.X., 2003. History of Neoproterozoic rift basins in South China: implications for Rodinia break-up. Precambr. Res. 122: 141–158.

Wang, L.X., Ma, C.Q., Zhang, J.Y., Chen, L., Zhang, C., 2008. Petrological and geochemical characteristics and petrogenesis of the Early Cretaceous Taohuashan-Xiaomoshan granites in northeastern Hunan province. Geol. J. China Univ. 14, 334–349 (in Chinese with English abstract).

Wang, L.X., Ma, C.Q., Zhang, C., Zhang, J.Y., Marks, M.A.W., 2014. Genesis of

leucogranite by prolonged fractional crystallization: A case study of the Mufushan complex, South China. Lithos 206–207, 147–163.

Wang, W., Wang, F., Chen, F.K., Zhu, X.Y., Xiao, P., Siebel, W., 2010. Detrital zircon ages and Hf–Nd isotopic composition of Neoproterozoic sedimentary rocks in the Yangtze block: constraints on the deposition age and provenance. J. Geol. 118, 79–94.

Wang, W., Chen, F.K., Hu, R., Chu, Y., Yang, Y.Z., 2012. Provenance and tectonic setting of Neoproterozoic sedimentary sequences in the South China Block: evidence from detrital zircon ages and Hf–Nd isotopes. Int. J. Earth Sci. 101, 1723–1744.

Wang, W., Zhou, M.F., Yan, D.P., Li, L., Malpas, J., 2013. Detrital zircon record of Neoproterozoic active-margin sedimentation in the eastern Jiangnan Orogen, South China. Precambr. Res. 235, 1–19.

Wang, X.L., Zhou, J.C., Wan, Y.S., Kitajima, K., Wang, D., Bonamici, C., Qiu, J.S., Sun, T., 2013. Magmatic evolution and crustal recycling for Neoproterozoic strongly peraluminous granitoids from southern China: Hf and O isotopes in zircon. Earth Planet. Sci. Lett. 366, 71–82.

Wang, X.L., Zhou, J.C., Griffin, W.L., Zhao, G.C., Yu, J.H., Qiu, J.S., Zhang, Y.J., Xing, G.F., 2014. Geochemical zonation across a Neoproterozoic orogenic belt: Isotopic evidence from granitoids and metasedimentary rocks of the Jiangnan orogen, China. Precambr. Res. 242, 154–171.

Wang, Y., Deng, J.F., 2004. Petrochemical features and tectonic setting of Late Yanshanian strongly peraluminous granites in the northeastern part of Hunan province. Geotecton. Metallog. 28, 60–68 (in Chinese with English abstract).

Wang, Y.J., Fan, W.M., Zhang, G.W., Zhang, Y.H., 2013. Phanerozoic tectonics of the South China Block: Key observations and controversies. Gondwana Res. 23, 1273–1305.

Wei, W., Faure, M., Chen, Y., Ji, W.B., Lin, W., Wang, Q.C., Yan, Q.R., Hou, Q.L., 2015. Back-thrusting response of continental collision: Early Cretaceous NW-directed thrusting in the Changle-Nan'ao belt (Southeast China). J. Asian Earth Sci. 100, 98–114.

Whalen, J.B., Currie, K.L., Chappell, B.W., 1987. A-type granites: geochemical characteristics, discrimination and petrogenesis. Contrib. Miner. Petrol. 95, 407–419.

White, L.T., Ireland, T.R., 2012. High-uranium matrix effect in zircon and its implications for SHRIMP U–Pb age determinations. Chem. Geol. 306–307, 78–91.

Wong, J., Sun, M., Xing, G.F., Li, X.H., Zhao, G.C., Wong, K., Yuan, C., Xia, X.P., Li, L.M., Wu, F.Y., 2009. Geochemical and zircon U–Pb and Hf isotopic study of the Baijuhuajian metaluminous A-type granite: Extension at 125–100 Ma and its tectonic significance for South China. Lithos 112, 289–305.

Woodhead, J.D., Hergt, J.M., 2005. A preliminary appraisal of seven natural zircon reference materials for *in situ* Hf isotope determination. Geostand. Geoanal. Res. 29, 183–195.

Wu, F.Y., Yang, Y.H., Xie, L.W., Yang, J.H., Xu, P., 2006. Hf isotopic compositions of the standard zircons and baddeleyites used in U–Pb geochronology. Chem. Geol. 234, 105–126.

Wu, F.Y., Ji, W.Q., Sun, D.H., Yang, Y.H., Li, X.H., 2012. Zircon U–Pb geochronology and Hf isotopic compositions of the Mesozoic granites in southern Anhui Province, China. Lithos 150, 6–25.

Xu, D.R., Gu, X.X., Li, P.C., Chen, G.H., Xia, B., Bachlinski, R., He, Z.L., Fu, G.G., 2007. Mesoproterozoic-Neoproterozoic transition: Geochemistry, provenance and tectonic setting of clastic sedimentary rocks on the SE margin of the Yangtze Block, South China. J. Asian Earth Sci. 29, 637–650.

Xu, D.R., Wang, L., Li, P.C., Chen, G.H., He, Z.L., Fu, G.G., Wu, J., 2009. Petrogenesis of the Lianyunshan granites in northeastern Hunan province, South China, and its geodynamic implications. Acta Petrol. Sin. 25, 1056–1078 (in Chinese with English abstract).

Xu, J.W., 1993. The Tancheng-Lujiang wrench fault system. John Wiley & Sons, Chichester.

Yan, C.L., Shu, L.S., Santosh, M., Yao, J.L., Li, J.Y., Li, C., 2015. The Precambrian tectonic evolution of the western Jiangnan Orogen and western Cathaysia Block: Evidence from detrital zircon age spectra and geochemistry of clastic rocks. Precambr. Res. 268, 33–60.

Yu, A.N., Ye, B.L., Peng, E.S., 1998. Relationship between the Dayunshan metamorphic core complex and mineralization, Taolin, Hunan province. Geotecton. Metallog. 22, 82–88 (in Chinese with English Abstract).

Zhang, Y., Yang, J.H., Sun, J.F., Zhang, J.H., Chen, J.Y., Li, X.H., 2015. Petrogenesis of Jurassic fractionated I-type granites in Southeast China: Constraints from whole-

rock geochemical and zircon U–Pb and Hf–O isotopes. J. Asian Earth Sci. 111, 268–283.

Zhao, G.C., 2015. The Jiangnan Orogen in South China: Developing from divergent double subduction. Gondwana Res. 27, 1173–1180.

Zhao, J.H., Zhou, M.F., Yan, D.P., Zheng, J.P., Li, J.W., 2011. Reappraisal of the ages of Neoproterozoic strata in South China: No connection with the Grenvillian orogeny. Geology 39, 299–302.

Zhao, J.H., Zhou, M.F., Zheng, J.P., 2013. Constraints from zircon U–Pb ages, O and Hf isotopic compositions on the origin of Neoproterozoic peraluminous granitoids from the Jiangnan Fold Belt, South China. Contrib. Miner. Petrol. 166, 1505–1519

Zhou, X.M., Li, W.X., 2000. Origin of Late Mesozoic igneous rocks in Southeastern China: implications for lithosphere subduction and underplating of mafic magmas. Tectonophysics 326, 269–287.

Zhou, X.M., Sun, T., Shen, W.Z., Shu, L.S., Niu, Y.L., 2006. Petrogenesis of Mesozoic granitoids and volcanic rocks in South China: A response to tectonic evolution. Episodes 29, 26–33.

**Figure captions**

Fig. 1. Schematic map showing distribution of the Jurassic-Cretaceous magmatic rocks in SE China (modified after Zhou et al., 2006) and location of the study area. The dashed line indicates the Jiangshan-Shaoxing fault at the northeastern segment (representing the reworked Neoproterozoic suture zone) and the Chenzhou-Linwu fault at the southwestern segment (probably as a scar of the Triassic intracontinental orogeny). Inset shows the tectonic sketch of the SCB, with the Jiuling-Xuefengshan belt in the central part.

Fig. 2. Geological map of the northeastern Hunan province and adjacent areas showing the main Late Jurassic to Early Cretaceous granitic plutons including those studied in this paper.

Fig. 3. Microphotographs of the representative granitic samples. (a) Plagioclase with compositional zoning in biotite monzogranite (sample JH155). (b) Euhedral to subhedral muscovite, along with biotite and K-feldspar in two-mica monzogranite (sample DYS01). (c) Secondary muscovite replacing biotite and plagioclase in biotite

monzogranite, note also myrmekite developed in feldspar (sample QD69). (d) Monazite enclosed within biotite in biotite monzogranite (sample QD69). (e) Biotite mostly altered to chlorite in granodiorite (sample DYS14). (f) Magmatic epidote including allanite in granodiorite (sample DYS14). Mineral abbreviations: Bt, biotite; Mus, muscovite; Kfs, K-feldspar; Pl, plagioclase; Qtz, quartz; Mnz, monazite; Ep, epidote; Aln, allanite; Myr, myrmekite.

Fig. 4. Cathodoluminescence images of representative zircons from the granitic samples. White ellipses indicate the analytical spots with measured ages.

Fig. 5. Concordia diagrams of the analyzed zircons, sample locations are shown in Figure 2.

Fig. 6. Histograms of the zircon εHf(t) values, n is the number of analyzed grains.

Fig. 7. (a) $K_2O$ vs. $SiO_2$ diagram (after Peccerillo and Taylor, 1976); (b) A/NK vs. A/CNK diagram: A/NK = molar $Al_2O_3/(Na_2O+K_2O)$, A/CNK (alumina saturation index, ASI) = molar $Al_2O_3/(CaO+Na_2O+K_2O)$ (after Maniar and Piccoli, 1989).

Fig. 8. Chondrite-normalized REE patterns (left column), and primitive mantle-normalized trace element spidergrams (right column). The normalization values are from McDonough and Sun (1989).

Fig. 9. (a) ACF diagram: A = $Al_2O_3$-$Na_2O$-$K_2O$, C = CaO, F = MgO+FeO* (after Chappell and White, 1992); (b) variation of $SiO_2$ vs. $P_2O_5$, (c) and (d) plots of Y and Th against Rb (for the I- and S-type granites trends, cf. Chappell, 1999); (e) and (t) classification diagrams of 10000×Ga/Al vs. FeO*/MgO and Zr+Nb+Ce+Y vs. $(K_2O+Na_2O)/CaO$, respectively (after Whalen et al., 1987). Symbols are the same as those in Figure 7.

Fig. 10. (a) $Al_2O_3/TiO_2$ vs. $CaO/Na_2O$ and (b) Rb/Sr vs. Rb/Ba (after Sylvester, 1998); (c) molar CaO/(MgO+FeO*) vs. molar $Al_2O_3$/(MgO+FeO*) (after Altherr et al., 2000). Symbols are the same as those in Figure 7.

Fig. 11. Sr vs. Ba (a) and Rb (b) plots. Labeled vectors correspond to up to 50% fractionation crystallization of the main rock-forming minerals (after Janoušek et al.,

2004). Symbols are the same as those in Figure 7.

Fig. 12. Tectonic model for the Mesozoic tectono-magmatic evolution in SE China. (A) Northwestward subduction of the Paleo-Pacific plate (modified after Li and Li, 2007; Li et al., 2007); (B) Jurassic slab foundering after a SE-directed intracontinental subduction (modified after Faure et al., 2016).

**Table captions**

Table 1 Summary of zircon U–Pb ages and Hf isotopic data for the granitic samples

Table 2 Major (wt.%) and trace element (ppm) compositions of the granitic samples

**Supplementary data**

Table S1 SIMS zircon U–Pb data of the granitic samples

Table S2 Zircon Hf isotopic data of the granitic samples

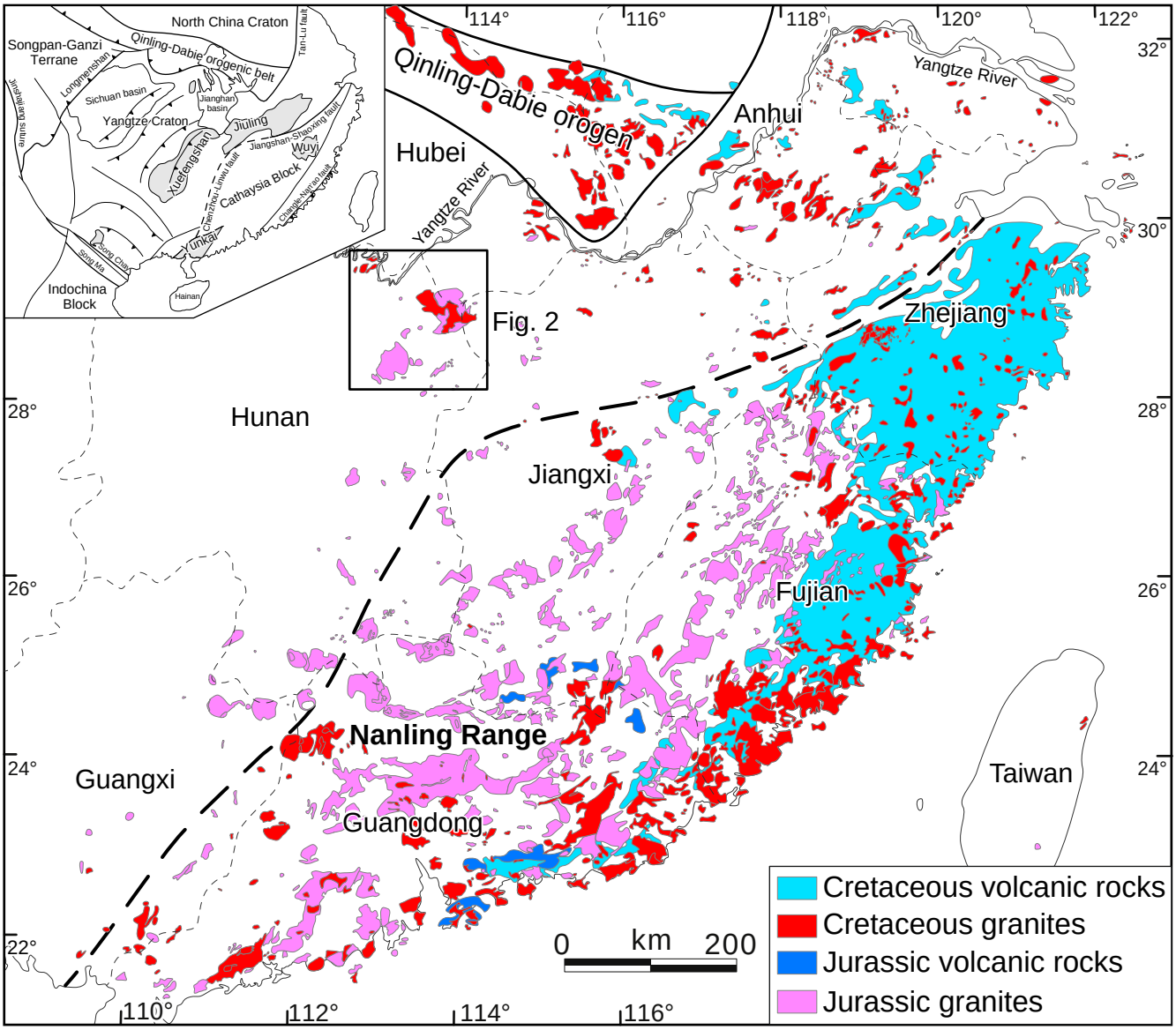
North China Craton
Songpan-Ganzi Terrane
Qinling-Dabie orogenic belt
Tan-Lu fault
Longmenshan
Sichuan basin
Jianghan basin
Yangtze Craton
Jiuling
Jiangshan-Shaoxing fault
Wuyi
Xuefengshan
Cathaysia Block
Chenzhou-Linwu fault
Changle-Nanao fault
Ailaoshan suture
Red River fault
Song Chay
Song Ma
Yunkai
Indochina Block
Hainan
Qinling-Dabie orogen
Hubei
Yangtze River
Anhui
Fig. 2
Zhejiang
Hunan
Jiangxi
Fujian
Nanling Range
Guangxi
Guangdong
Taiwan
114°
116°
118°
120°
122°
32°
30°
28°
26°
24°
22°
110°
112°
0 km 200
Cretaceous volcanic rocks
Cretaceous granites
Jurassic volcanic rocks
Jurassic granites

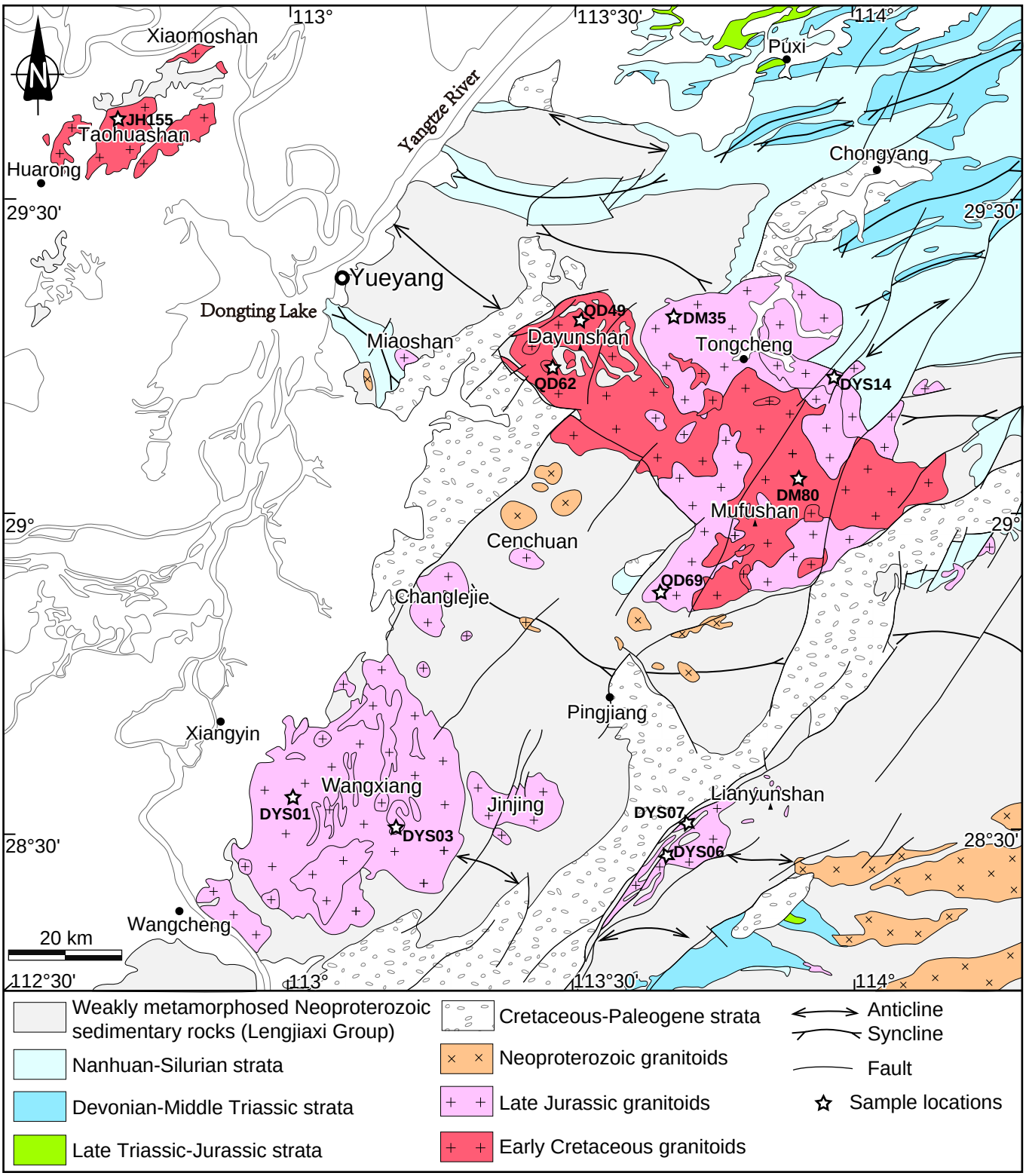
Xiaomoshan
JH155
Taohuashan
Huarong
113°
113°30'
114°
Puxi
Yangtze River
Chongyang
29°30'
Yueyang
Dongting Lake
Miaoshan
QD49
Dayunshan
DM35
Tongcheng
QD62
DYS14
DM80
Mufushan
29°
Cenchuan
QD69
Changlejie
Pingjiang
Xiangyin
Wangxiang
DYS01
DYS03
Jinjing
DYS07
Lianyunshan
DYS06
28°30'
Wangcheng
20 km
112°30'
Weakly metamorphosed Neoproterozoic sedimentary rocks (Lengjiaxi Group)
Nanhuan-Silurian strata
Devonian-Middle Triassic strata
Late Triassic-Jurassic strata
Cretaceous-Paleogene strata
Neoproterozoic granitoids
Late Jurassic granitoids
Early Cretaceous granitoids
Anticline
Syncline
Fault
Sample locations

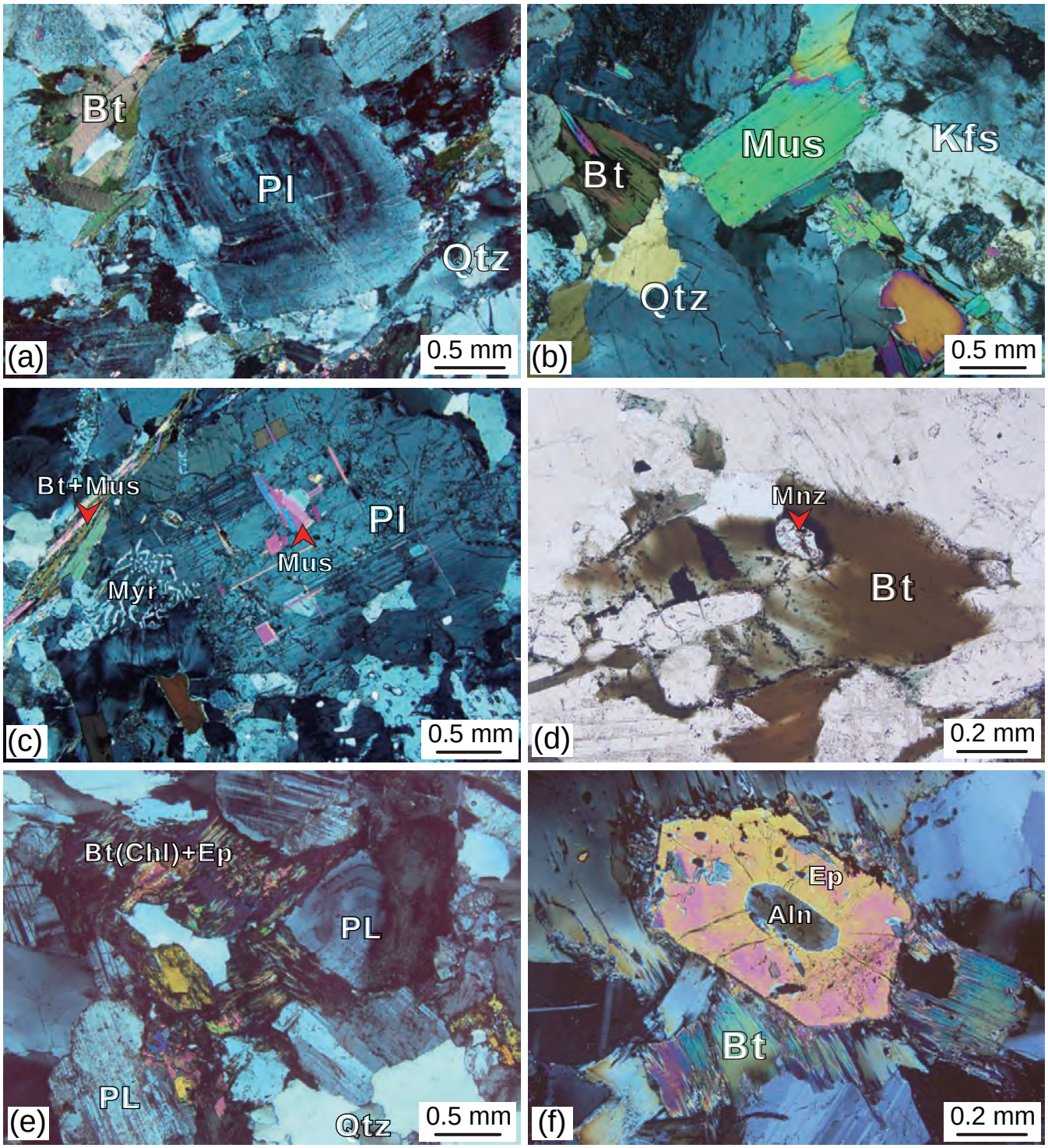
Bt
Pl
Qtz
(a)
0.5 mm
Mus
Kfs
Bt
Qtz
(b)
0.5 mm
Bt+Mus
Pl
Mus
Myr
(c)
0.5 mm
Mnz
Bt
(d)
0.2 mm
Bt(Chl)+Ep
PL
PL
Qtz
(e)
0.5 mm
Ep
Aln
Bt
(f)
0.2 mm

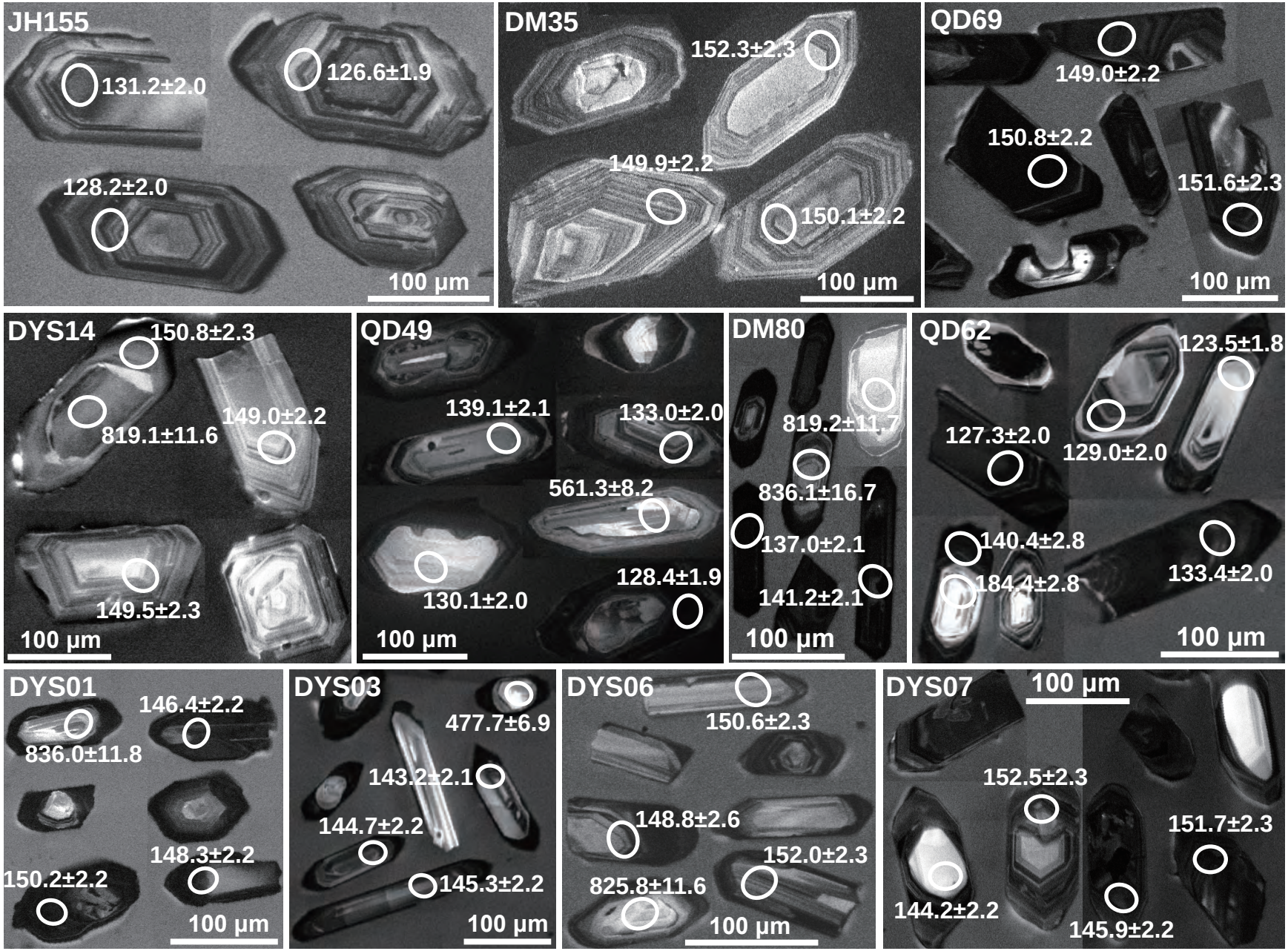
JH155
131.2±2.0
126.6±1.9
128.2±2.0
100 μm
DM35
152.3±2.3
149.9±2.2
150.1±2.2
100 μm
QD69
149.0±2.2
150.8±2.2
151.6±2.3
100 μm
DYS14
150.8±2.3
819.1±11.6
149.0±2.2
149.5±2.3
100 μm
QD49
139.1±2.1
133.0±2.0
561.3±8.2
130.1±2.0
128.4±1.9
100 μm
DM80
819.2±11.7
836.1±16.7
137.0±2.1
141.2±2.1
100 μm
QD62
123.5±1.8
127.3±2.0
129.0±2.0
140.4±2.8
184.4±2.8
133.4±2.0
100 μm
DYS01
146.4±2.2
836.0±11.8
148.3±2.2
150.2±2.2
100 μm
DYS03
477.7±6.9
143.2±2.1
144.7±2.2
145.3±2.2
100 μm
DYS06
150.6±2.3
148.8±2.6
152.0±2.3
825.8±11.6
100 μm
DYS07
100 μm
152.5±2.3
151.7±2.3
144.2±2.2
145.9±2.2

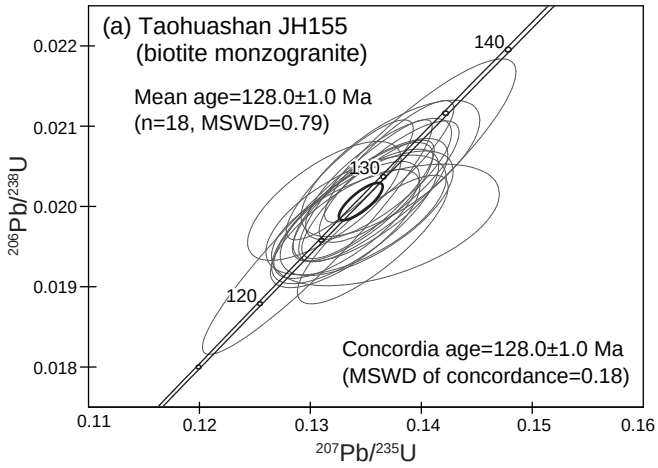
(a) Taohuashan JH155
(biotite monzogranite)
Mean age=128.0±1.0 Ma
(n=18, MSWD=0.79)
Concordia age=128.0±1.0 Ma
(MSWD of concordance=0.18)
140
130
120
$^{206}Pb/^{238}U$
$^{207}Pb/^{235}U$

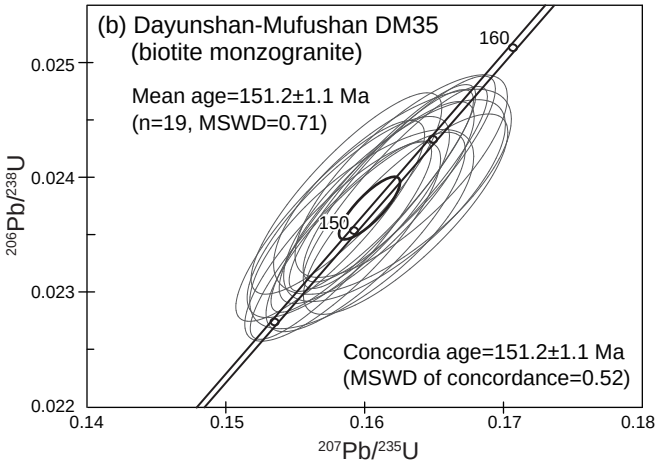
(b) Dayunshan-Mufushan DM35
(biotite monzogranite)
Mean age=151.2±1.1 Ma
(n=19, MSWD=0.71)
Concordia age=151.2±1.1 Ma
(MSWD of concordance=0.52)
160
150
$^{206}Pb/^{238}U$
$^{207}Pb/^{235}U$

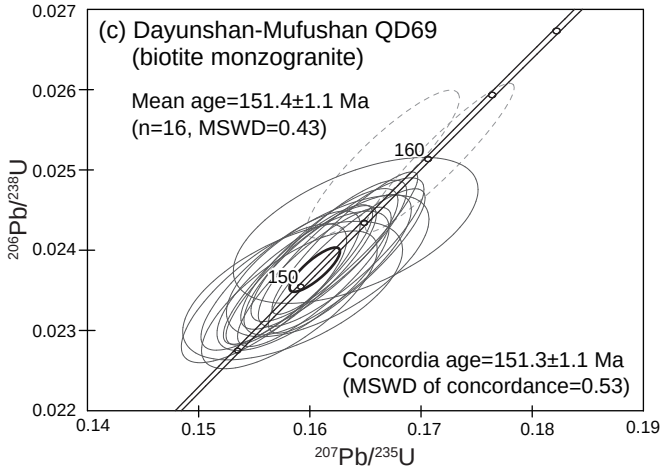
(c) Dayunshan-Mufushan QD69
(biotite monzogranite)
Mean age=151.4±1.1 Ma
(n=16, MSWD=0.43)
Concordia age=151.3±1.1 Ma
(MSWD of concordance=0.53)
160
150
$^{206}Pb/^{238}U$
$^{207}Pb/^{235}U$

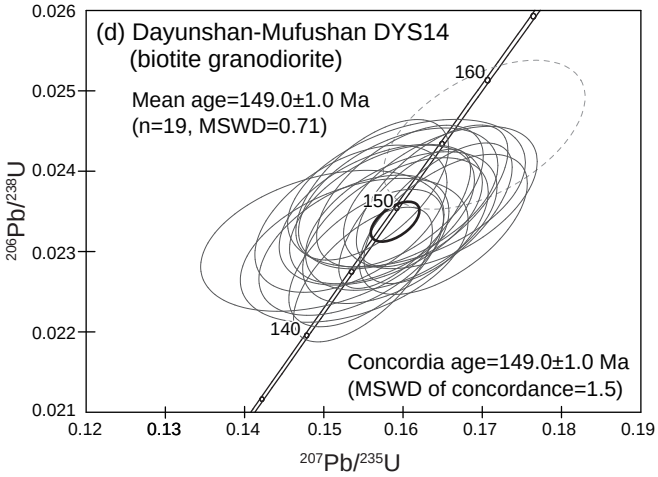
(d) Dayunshan-Mufushan DYS14
(biotite granodiorite)
Mean age=149.0±1.0 Ma
(n=19, MSWD=0.71)
Concordia age=149.0±1.0 Ma
(MSWD of concordance=1.5)
160
150
140
$^{206}Pb/^{238}U$
$^{207}Pb/^{235}U$

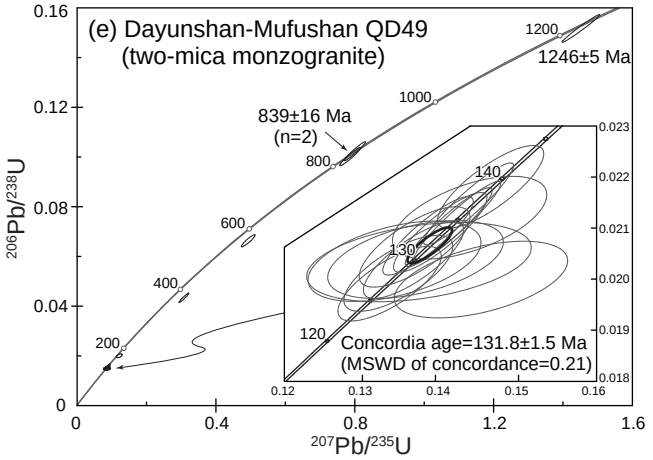
(e) Dayunshan-Mufushan QD49
(two-mica monzogranite)
1246±5 Ma
839±16 Ma
(n=2)
Concordia age=131.8±1.5 Ma
(MSWD of concordance=0.21)
1200
1000
800
600
400
200
140
130
120
$^{206}Pb/^{238}U$
$^{207}Pb/^{235}U$

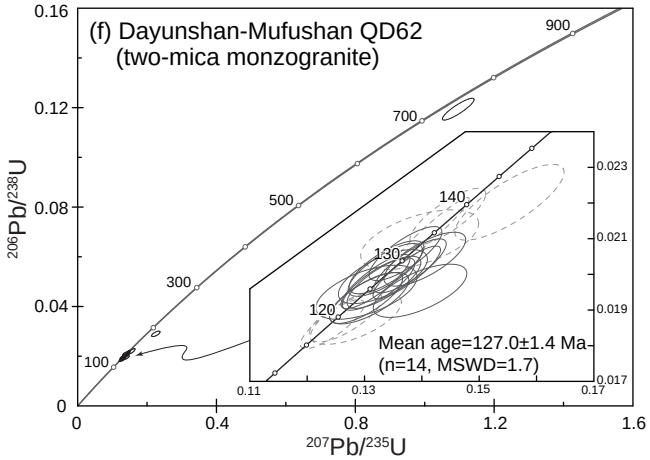
(f) Dayunshan-Mufushan QD62
(two-mica monzogranite)
Mean age=127.0±1.4 Ma
(n=14, MSWD=1.7)
900
700
500
300
100
140
130
120
$^{206}Pb/^{238}U$
$^{207}Pb/^{235}U$

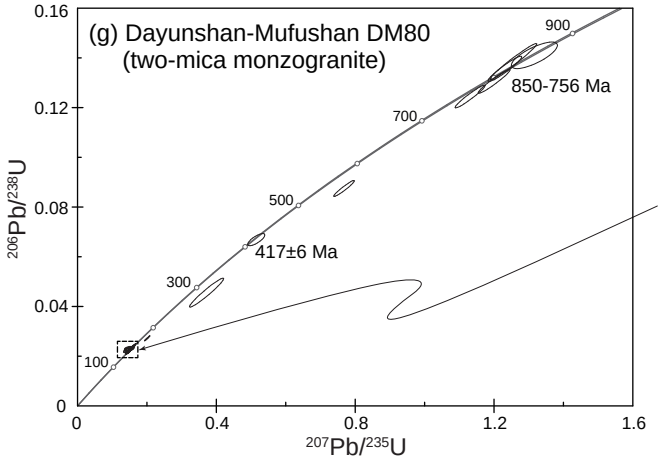
(g) Dayunshan-Mufushan DM80
(two-mica monzogranite)
850-756 Ma
417±6 Ma
900
700
500
300
100
$^{206}Pb/^{238}U$
$^{207}Pb/^{235}U$

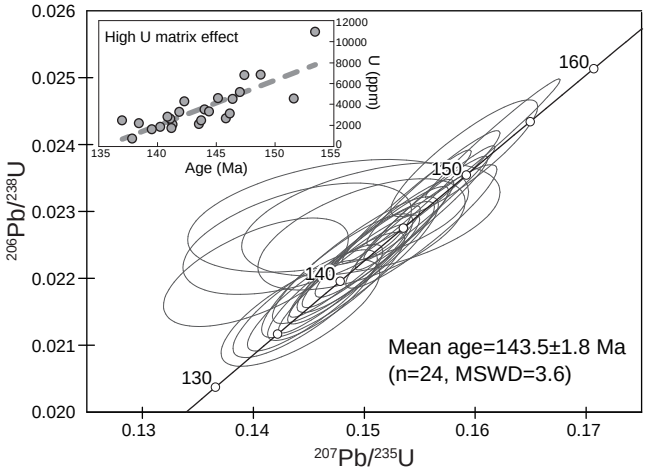
High U matrix effect
U (ppm)
Age (Ma)
160
150
140
130
Mean age=143.5±1.8 Ma
(n=24, MSWD=3.6)
$^{206}Pb/^{238}U$
$^{207}Pb/^{235}U$

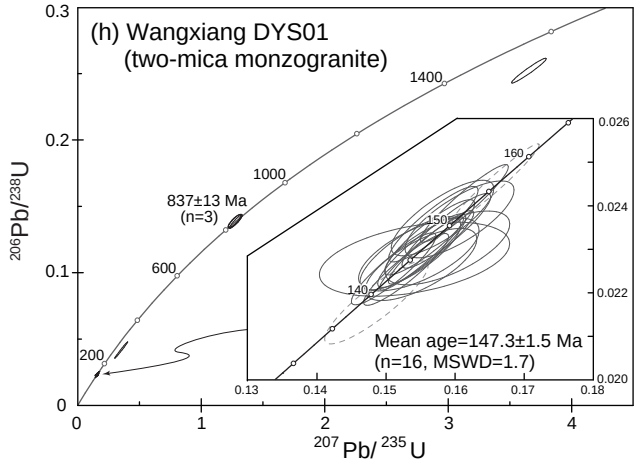
(h) Wangxiang DYS01
(two-mica monzogranite)
837±13 Ma
(n=3)
1400
1000
600
200
Mean age=147.3±1.5 Ma
(n=16, MSWD=1.7)
$^{206}Pb/^{238}U$
$^{207}Pb/^{235}U$

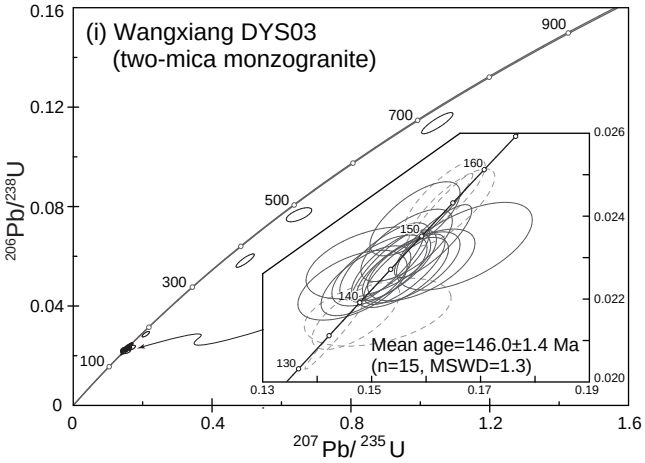
(i) Wangxiang DYS03
(two-mica monzogranite)
900
700
500
300
100
Mean age=146.0±1.4 Ma
(n=15, MSWD=1.3)
$^{206}Pb/^{238}U$
$^{207}Pb/^{235}U$

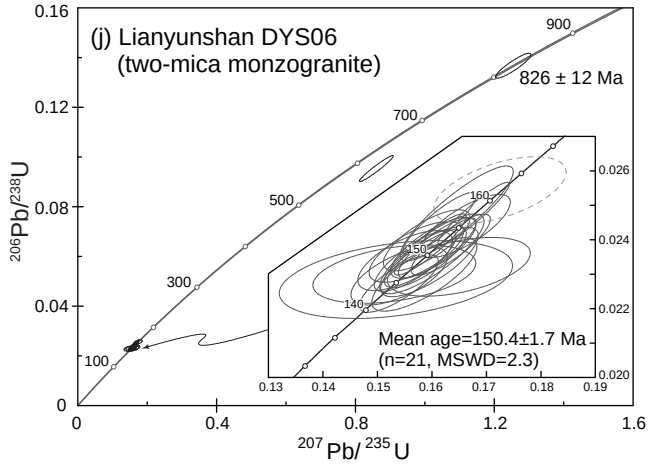
(j) Lianyunshan DYS06
(two-mica monzogranite)
826 ± 12 Ma
900
700
500
300
100
Mean age=150.4±1.7 Ma
(n=21, MSWD=2.3)
$^{206}Pb/^{238}U$
$^{207}Pb/^{235}U$

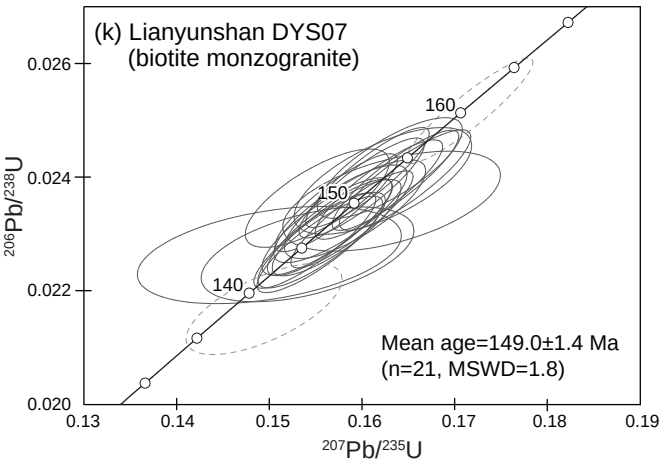
(k) Lianyunshan DYS07
(biotite monzogranite)
160
150
140
Mean age=149.0±1.4 Ma
(n=21, MSWD=1.8)
$^{206}Pb/^{238}U$
$^{207}Pb/^{235}U$

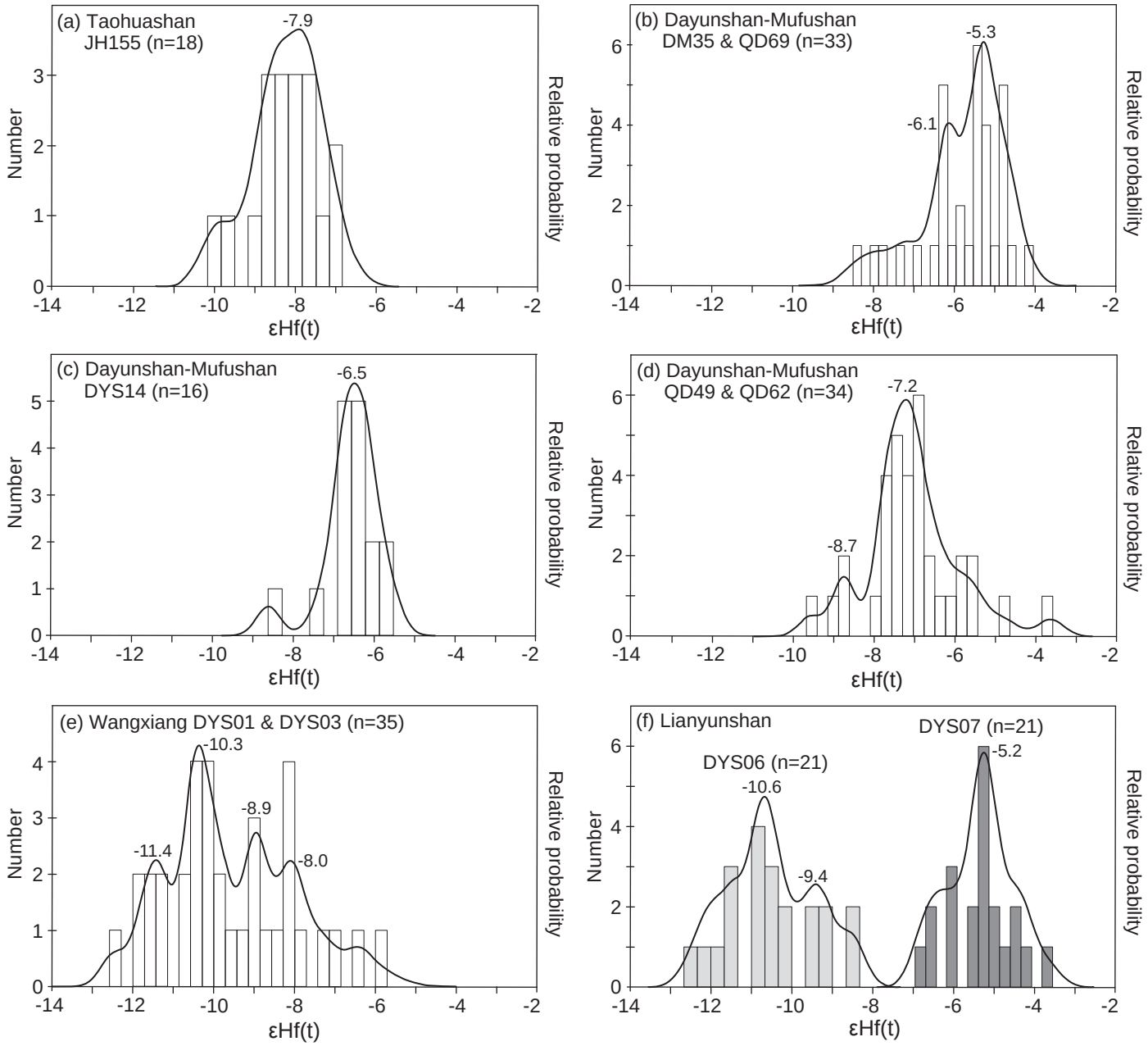
(a) Taohuashan
JH155 (n=18)
-7.9
(b) Dayunshan-Mufushan
DM35 & QD69 (n=33)
-5.3
-6.1
(c) Dayunshan-Mufushan
DYS14 (n=16)
-6.5
(d) Dayunshan-Mufushan
QD49 & QD62 (n=34)
-7.2
-8.7
(e) Wangxiang DYS01 & DYS03 (n=35)
-10.3
-8.9
-11.4
-8.0
(f) Lianyunshan
DYS07 (n=21)
-5.2
DYS06 (n=21)
-10.6
-9.4
Number
Relative probability
εHf(t)

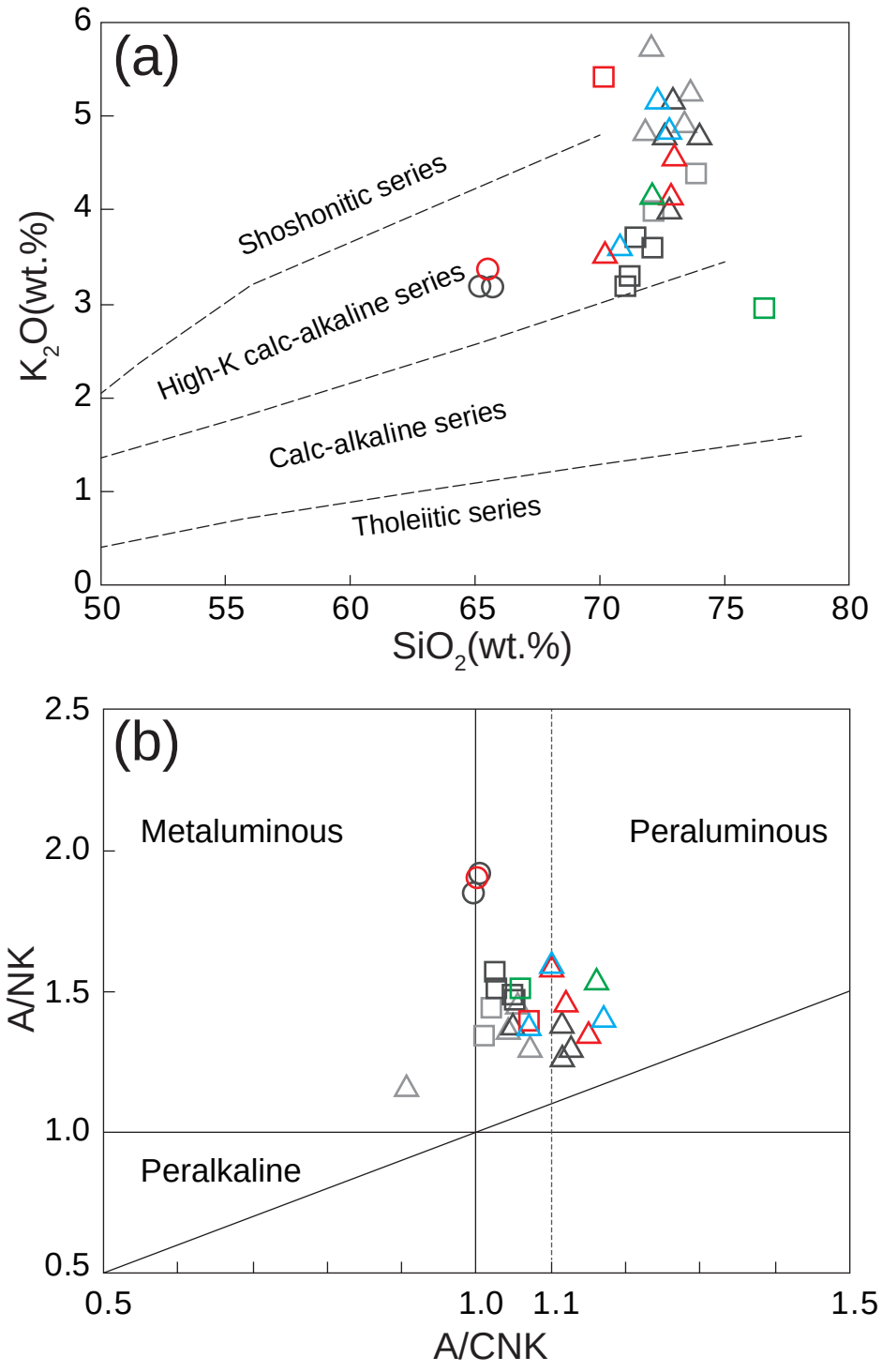


TM BM BG

Taohuashan (Wang et al., 2008)

Dayunshan-Mufushan
(red: this study; grey: L.X. Wang et al., 2014)

Wangxiang

Lianyunshan

TM: two-mica monzogranite

BM: biotite monzogranite

BG: biotite granodiorite

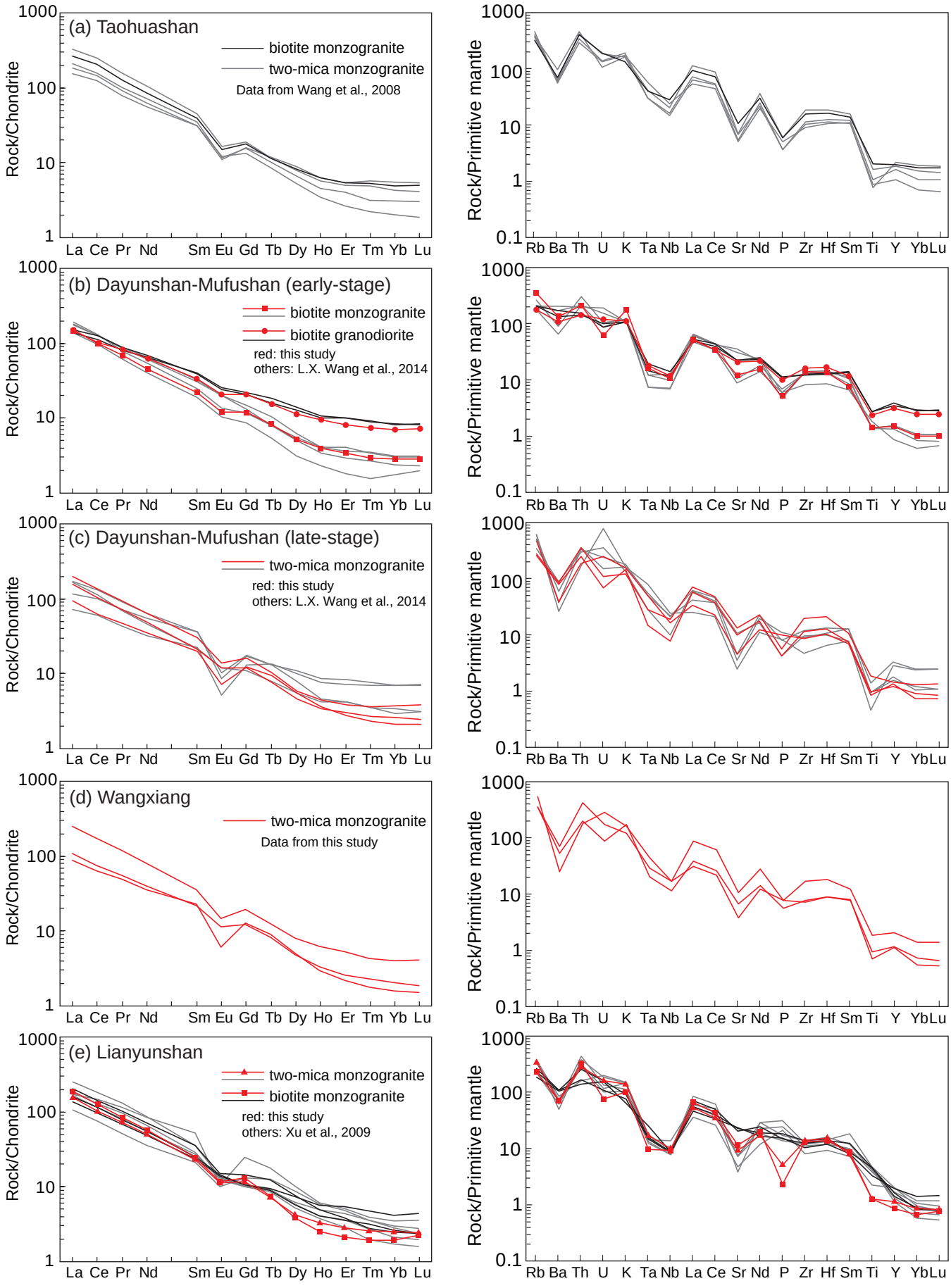
(a) Taohuashan
biotite monzogranite
two-mica monzogranite
Data from Wang et al., 2008
(b) Dayunshan-Mufushan (early-stage)
biotite monzogranite
biotite granodiorite
red: this study
others: L.X. Wang et al., 2014
(c) Dayunshan-Mufushan (late-stage)
two-mica monzogranite
red: this study
others: L.X. Wang et al., 2014
(d) Wangxiang
two-mica monzogranite
Data from this study
(e) Lianyunshan
two-mica monzogranite
biotite monzogranite
red: this study
others: Xu et al., 2009
Rock/Chondrite
Rock/Primitive mantle
1000
100
10
1
0.1
La Ce Pr Nd Sm Eu Gd Tb Dy Ho Er Tm Yb Lu
Rb Ba Th U K Ta Nb La Ce Sr Nd P Zr Hf Sm Ti Y YbLu

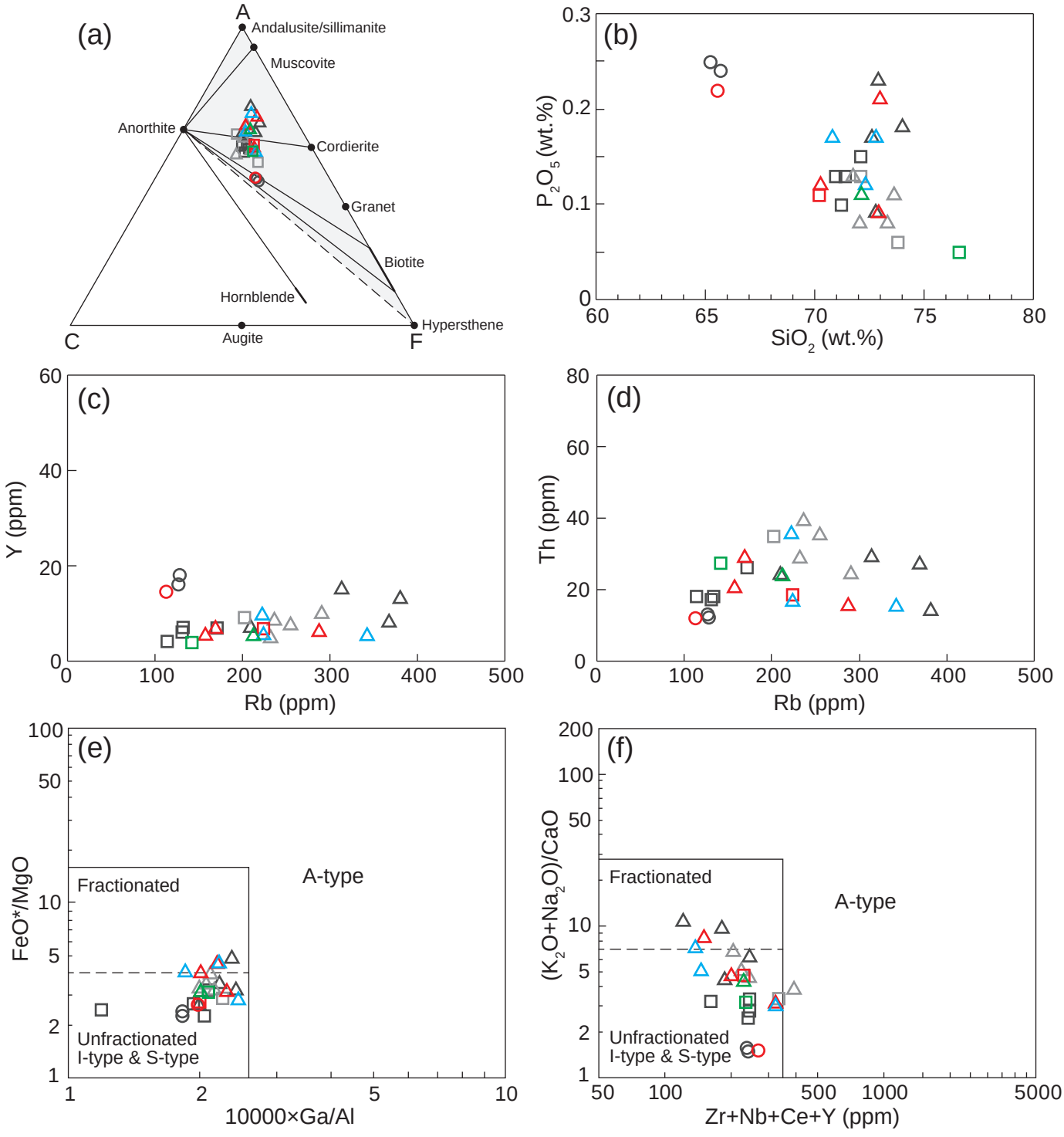
(a)
A
Andalusite/sillimanite
Muscovite
Anorthite
Cordierite
Granet
Biotite
Hornblende
Hypersthene
C
Augite
F
(b)
$P_2O_5$ (wt.%)
$SiO_2$ (wt.%)
(c)
Y (ppm)
Rb (ppm)
(d)
Th (ppm)
Rb (ppm)
(e)
FeO*/MgO
Fractionated
A-type
Unfractionated
I-type & S-type
10000×Ga/Al
(f)
$(K_2O+Na_2O)/CaO$
Fractionated
A-type
Unfractionated
I-type & S-type
Zr+Nb+Ce+Y (ppm)

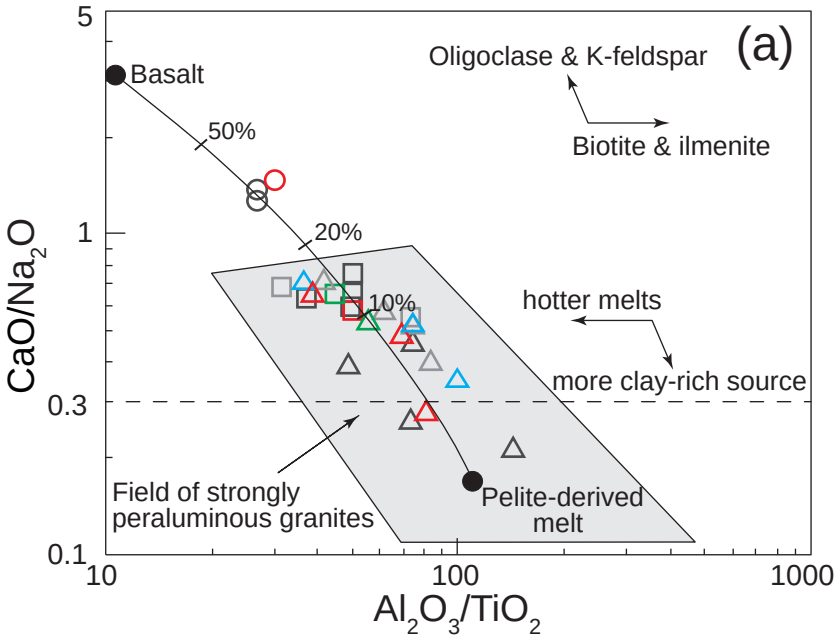
(a)
Basalt
Oligoclase & K-feldspar
Biotite & ilmenite
50%
20%
10%
hotter melts
more clay-rich source
Field of strongly peraluminous granites
Pelite-derived melt
CaO/Na2O
Al2O3/TiO2
5
1
0.3
0.1
10
100
1000

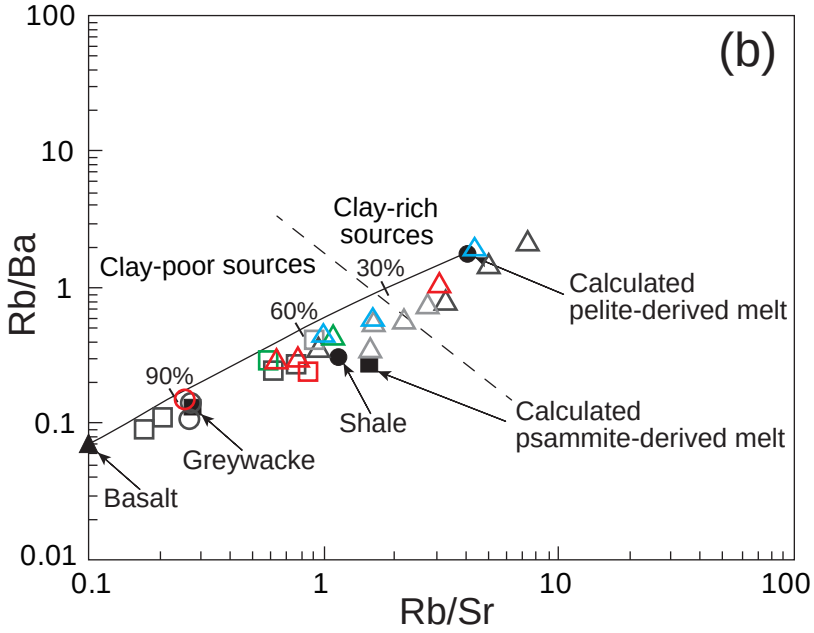
(b)
Clay-rich sources
Clay-poor sources
30%
60%
90%
Calculated pelite-derived melt
Calculated psammite-derived melt
Shale
Greywacke
Basalt
Rb/Ba
Rb/Sr
100
10
1
0.1
0.01
0.1
1
10
100

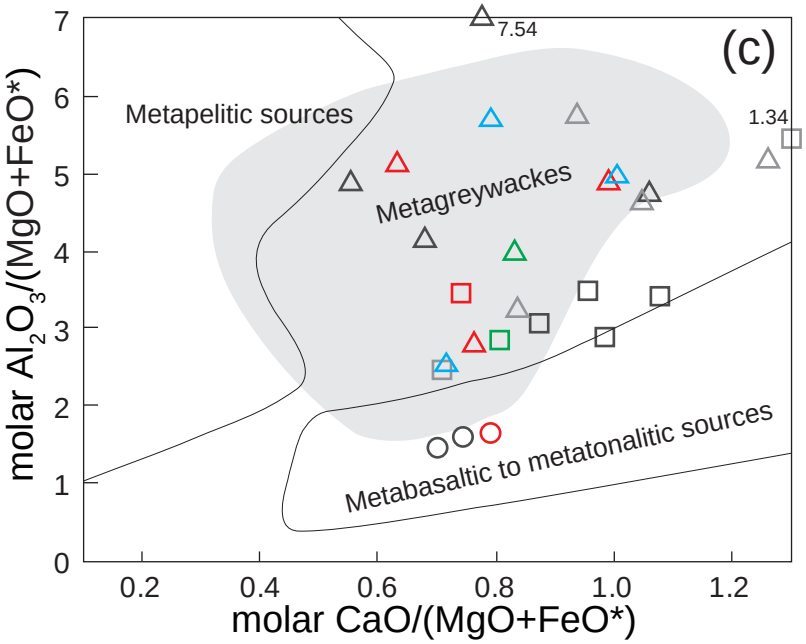
(c)
7.54
1.34
Metapelitic sources
Metagreywackes
Metabasaltic to metatonalitic sources
molar Al2O3/(MgO+FeO*)
molar CaO/(MgO+FeO*)
7
6
5
4
3
2
1
0
0.2
0.4
0.6
0.8
1.0
1.2

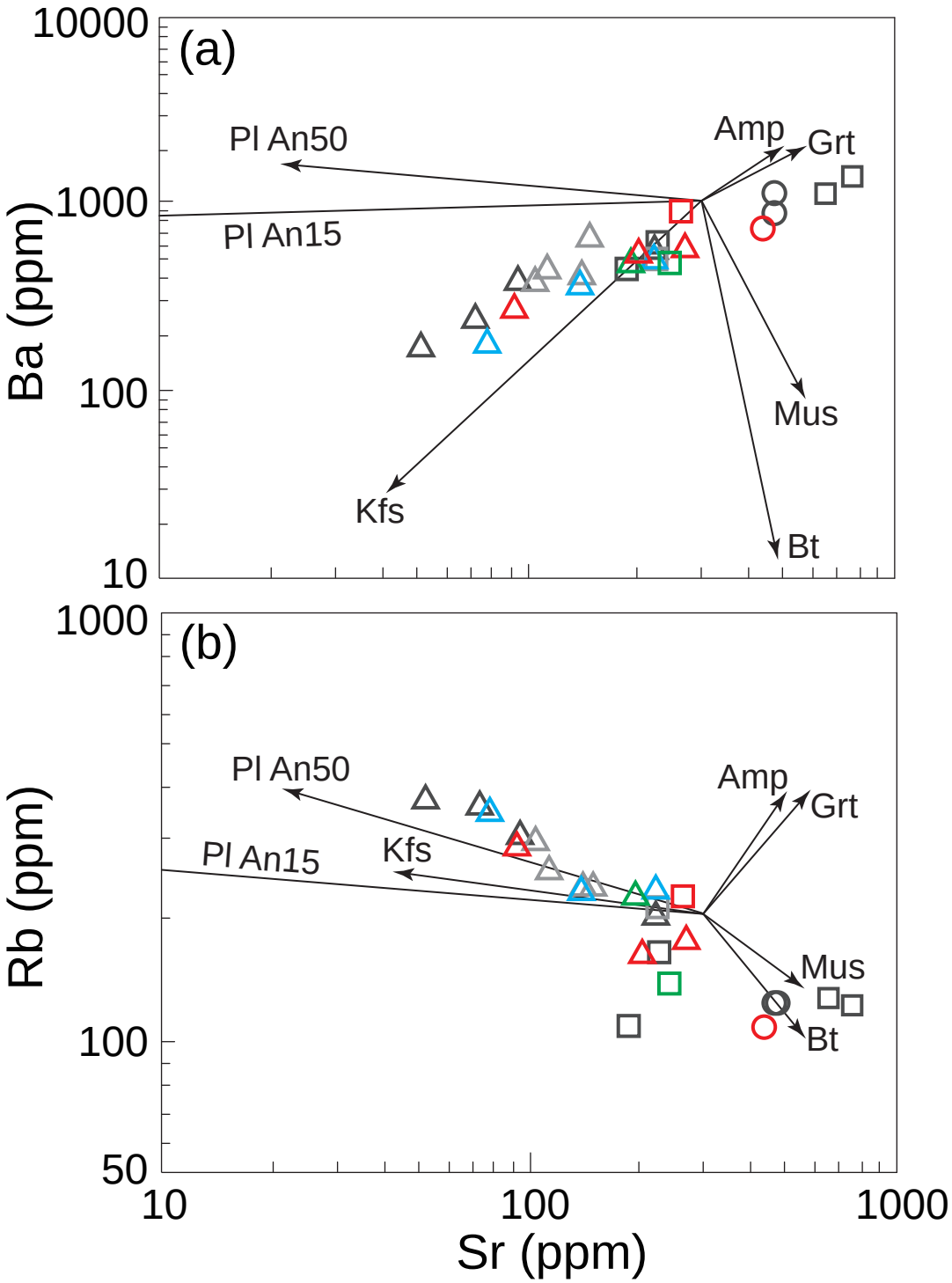
(a)
10000
1000
100
10
Ba (ppm)
Pl An50
Pl An15
Amp
Grt
Mus
Kfs
Bt
(b)
1000
100
50
Rb (ppm)
Pl An50
Pl An15
Kfs
Amp
Grt
Mus
Bt
10
100
1000
Sr (ppm)

A) Northwestward subduction of the Paleo-Pacific plate

(a) Jurassic: foundering of a subducted oceanic flat-slab

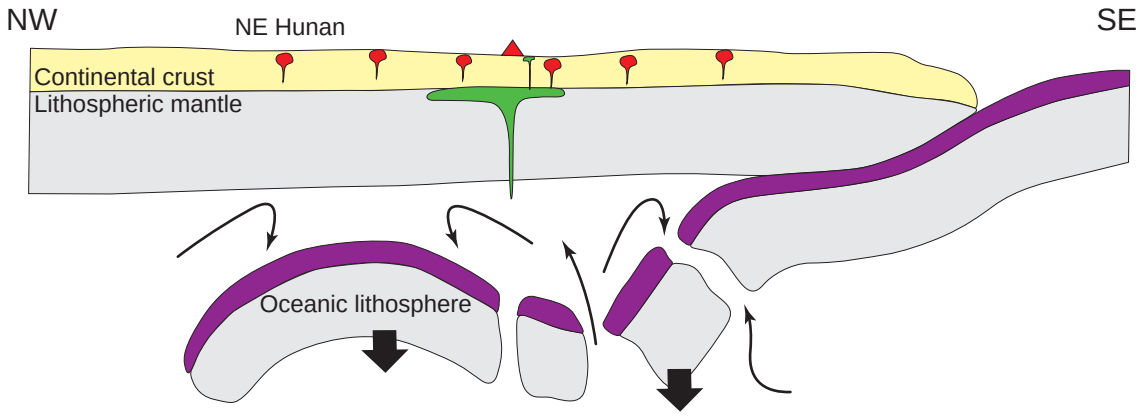


(b) 140-90 Ma: episodic slab rollback with collision during the interval

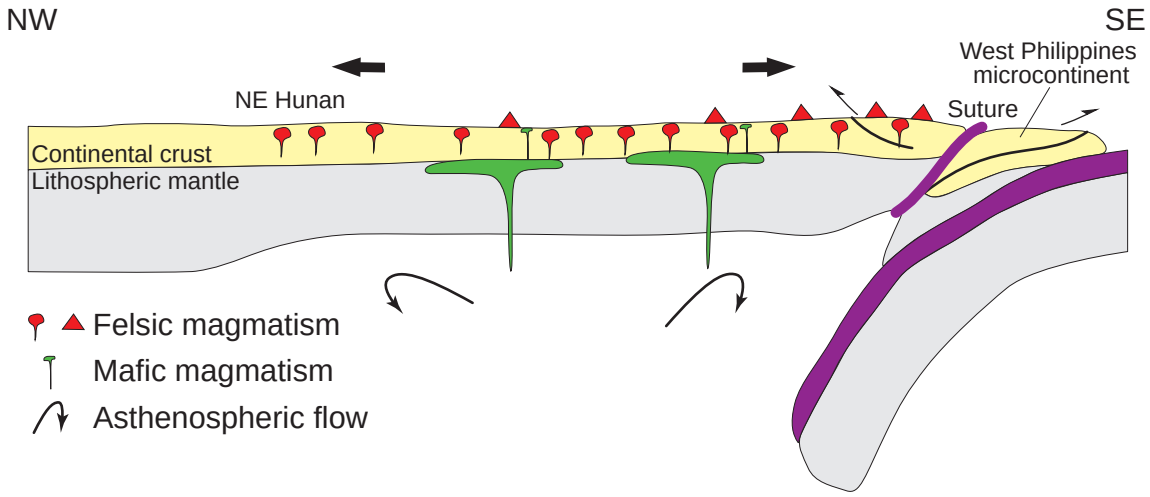


B) Jurassic slab foundering after a SE-directed intracontinental subduction

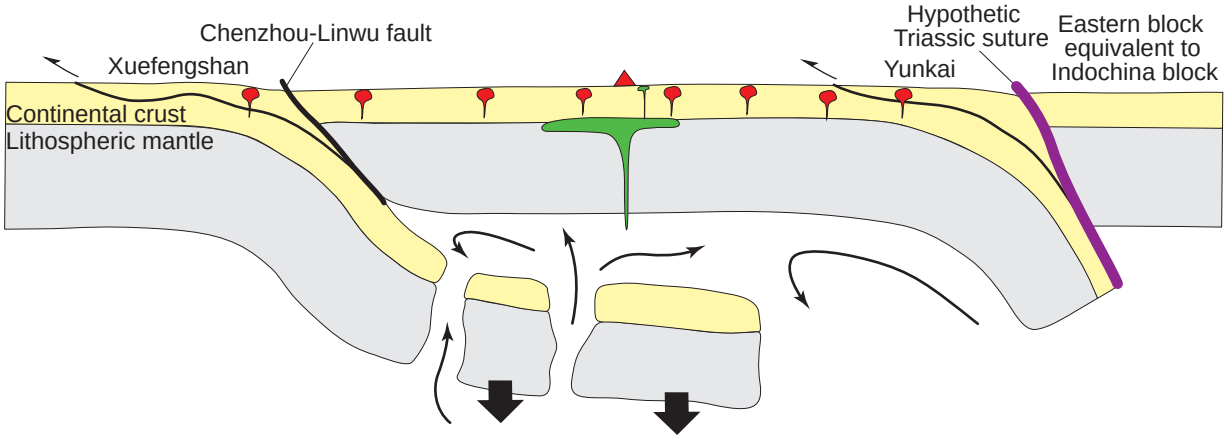

**Table 1**

Summary of zircon U-Pb ages and Hf isotopic data for the granitic samples

| Sample | Site | Lithology | GPS location | Zircon U-Pb age | εHf(t) | $T_{DM}^{C}$ |
|---|---|---|---|---|---|---|
| JH155 | Taohuashan | biotite monzogranite | N29°37'59", E112°40'40" | 128.0 ± 1.0 Ma | -10.1 to -6.9 | 1.62–1.82 Ga |
| DM35 | Dayunshan-Mufushan | biotite monzogranite | N29°19'35", E113°40'12" | 151.2 ± 1.1 Ma | -8.5 to -4.7 | 1.50–1.74 Ga |
| QD69 | Dayunshan-Mufushan | biotite monzogranite | N28°51'56", E113°37'21" | 151.3 ± 1.1 Ma | -7.3 to -4.3 | 1.47–1.66 Ga |
| DYS14 | Dayunshan-Mufushan | biotite granodiorite | N29°13'19", E113°56'48" | 149.0 ± 1.0 Ma | -8.6 to -5.6 | 1.55–1.75 Ga |
| QD49 | Dayunshan-Mufushan | two-mica monzogranite | N29°17'58", E113°30'52" | 131.8 ± 1.5 Ma | -7.9 to -3.6 | 1.42–1.69 Ga |
| DM80 | Dayunshan-Mufushan | two-mica monzogranite | N29°03'02", E113°53'44" | | | |
| QD62 | Dayunshan-Mufushan | two-mica monzogranite | N29°13'52", E113°27'56" | 127.0 ± 1.4 Ma | -9.6 to -6.2 | 1.58–1.79 Ga |
| DYS01 | Wangxiang | two-mica monzogranite | N28°28'49", E112°57'56" | 147.3 ± 1.5 Ma | -12.5 to -6.4 | 1.61–1.99 Ga |
| DYS03 | Wangxiang | two-mica monzogranite | N28°30'08", E113°10'28" | 146.0 ± 1.4 Ma | -11.6 to -5.9 | 1.57–1.93 Ga |
| DYS06 | Lianyunshan | two-mica monzogranite | N28°28'16", E113°40'12" | 150.4 ± 1.7 Ma | -12.4 to -8.5 | 1.74–1.98 Ga |
| DYS07 | Lianyunshan | biotite monzogranite | N28°30'34", E113°42'11" | 149.0 ± 1.4 Ma | -6.9 to -3.7 | 1.44–1.64 Ga |

**Table 2**

Major (wt.%) and trace element (ppm) compositions of the granitic samples

| Site | Dayunshan-Mufushan | | | | | Wangxiang | | | Lianyunshan | |
|---|---|---|---|---|---|---|---|---|---|---|
| Sample | QD70 | DYS14 | QD49 | DYS10 | DYS15 | DYS01 | DYS02 | DYS03 | DYS06 | DYS07 |
| Lithology | BM | BG | TM | TM | TM | TM | TM | TM | TM | BM |
| Major elements (wt.%) | | | | | | | | | | |
| $SiO_2$ | 70.2 | 65.5 | 72.9 | 73.0 | 70.3 | 72.3 | 70.8 | 72.8 | 72.1 | 76.6 |
| $TiO_2$ | 0.31 | 0.52 | 0.21 | 0.18 | 0.40 | 0.20 | 0.41 | 0.15 | 0.27 | 0.27 |
| $Al_2O_3$ | 15.5 | 15.7 | 14.5 | 14.5 | 15.3 | 14.8 | 14.8 | 14.8 | 15.0 | 12.0 |
| $Fe_2O_3$* | 2.13 | 4.39 | 1.60 | 1.58 | 2.72 | 1.61 | 2.75 | 1.44 | 1.88 | 2.09 |
| FeO* | 1.92 | 3.95 | 1.44 | 1.42 | 2.45 | 1.45 | 2.48 | 1.30 | 1.69 | 1.88 |
| MnO | 0.03 | 0.07 | 0.02 | 0.03 | 0.03 | 0.02 | 0.04 | 0.03 | 0.03 | 0.02 |
| MgO | 0.70 | 1.51 | 0.36 | 0.32 | 0.79 | 0.36 | 0.89 | 0.29 | 0.54 | 0.61 |
| CaO | 1.83 | 4.10 | 1.61 | 0.98 | 2.30 | 1.64 | 2.27 | 1.12 | 1.72 | 1.87 |
| $Na_2O$ | 3.20 | 2.79 | 3.37 | 3.57 | 3.57 | 3.15 | 3.25 | 3.21 | 3.23 | 2.86 |
| $K_2O$ | 5.43 | 3.38 | 4.15 | 4.58 | 3.54 | 5.19 | 3.63 | 4.87 | 4.17 | 2.96 |
| $P_2O_5$ | 0.11 | 0.22 | 0.09 | 0.21 | 0.12 | 0.12 | 0.17 | 0.17 | 0.11 | 0.05 |
| LOI | 0.44 | 1.52 | 0.44 | 0.70 | 0.50 | 0.46 | 0.54 | 0.96 | 0.66 | 0.54 |
| Total | 99.9 | 99.7 | 99.3 | 99.7 | 99.6 | 99.9 | 99.6 | 99.8 | 99.8 | 99.9 |
| $K_2O+Na_2O$ | 8.6 | 6.2 | 7.5 | 8.2 | 7.1 | 8.3 | 6.9 | 8.1 | 7.4 | 5.8 |
| $K_2O/Na_2O$ | 1.7 | 1.2 | 1.2 | 1.3 | 1.0 | 1.6 | 1.1 | 1.5 | 1.3 | 1.0 |
| ASI | 1.07 | 1.00 | 1.12 | 1.15 | 1.10 | 1.07 | 1.10 | 1.17 | 1.16 | 1.06 |
| Trace elements (ppm) | | | | | | | | | | |
| Sc | 4.21 | 8.75 | 3.86 | 2.38 | 4.46 | 2.83 | 4.94 | 2.34 | 3.65 | 3.70 |
| V | 32.2 | 82.7 | 13.9 | 17.5 | 31.3 | 11.9 | 42.0 | 7.6 | 21.8 | 28.3 |
| Cr | 201 | 241 | 218 | 221 | 229 | 262 | 234 | 232 | 172 | 358 |
| Co | 5.76 | 11.0 | 4.26 | 3.61 | 6.43 | 4.60 | 7.70 | 3.42 | 4.56 | 6.30 |
| Ni | 10.3 | 12.6 | 12.7 | 15.5 | 13.7 | 40.6 | 17.1 | 9.39 | 11.3 | 22.9 |
| Ga | 21.3 | 21.2 | 20.0 | 21.7 | 24.2 | 18.8 | 24.8 | 22.3 | 20.6 | 17.2 |
| Rb | 224 | 112 | 157 | 287 | 169 | 224 | 222 | 343 | 213 | 141 |
| Sr | 261 | 437 | 202 | 92.9 | 270 | 139 | 222 | 78.2 | 193 | 242 |
| Y | 6.77 | 14.5 | 5.49 | 6.03 | 6.60 | 5.32 | 9.45 | 5.09 | 5.09 | 3.94 |
| Zr | 155 | 183 | 126 | 93.7 | 215 | 87.2 | 191 | 81.2 | 155 | 146 |
| Nb | 7.44 | 8.56 | 5.49 | 11.6 | 13.15 | 8.04 | 12.1 | 12.1 | 7.10 | 6.59 |
| Cs | 10.9 | 3.90 | 6.61 | 44.9 | 8.83 | 9.13 | 13.8 | 36.4 | 15.0 | 5.61 |
| Ba | 929 | 740 | 527 | 267 | 584 | 376 | 495 | 177 | 479 | 484 |
| La | 36.0 | 34.7 | 37.8 | 22.8 | 48.1 | 26.1 | 60.2 | 20.9 | 36.6 | 44.7 |
| Ce | 60.7 | 62.0 | 64.0 | 38.9 | 83.6 | 46.1 | 107.1 | 39.1 | 61.4 | 76.8 |
| Pr | 6.59 | 7.96 | 6.87 | 4.63 | 9.13 | 5.38 | 11.4 | 4.67 | 6.85 | 8.05 |
| Nd | 21.4 | 29.3 | 23.0 | 16.5 | 30.1 | 18.8 | 38.5 | 16.8 | 23.2 | 27.0 |
| Sm | 3.45 | 5.21 | 3.30 | 3.09 | 4.66 | 3.39 | 5.51 | 3.50 | 3.44 | 3.80 |

| | | | | | | | | | | |
|---|---|---|---|---|---|---|---|---|---|---|
| Eu | 0.71 | 1.23 | 0.70 | 0.43 | 0.82 | 0.68 | 0.87 | 0.36 | 0.65 | 0.68 |
| Gd | 2.53 | 4.28 | 2.44 | 2.55 | 3.41 | 2.53 | 4.07 | 2.68 | 2.36 | 2.70 |
| Tb | 0.31 | 0.59 | 0.28 | 0.35 | 0.38 | 0.31 | 0.48 | 0.35 | 0.27 | 0.28 |
| Dy | 1.33 | 2.90 | 1.16 | 1.43 | 1.49 | 1.24 | 2.09 | 1.30 | 1.07 | 0.97 |
| Ho | 0.23 | 0.55 | 0.19 | 0.21 | 0.25 | 0.19 | 0.36 | 0.17 | 0.19 | 0.14 |
| Er | 0.57 | 1.35 | 0.50 | 0.46 | 0.65 | 0.44 | 0.88 | 0.37 | 0.46 | 0.35 |
| Tm | 0.08 | 0.19 | 0.07 | 0.06 | 0.09 | 0.06 | 0.11 | 0.05 | 0.07 | 0.05 |
| Yb | 0.49 | 1.21 | 0.44 | 0.36 | 0.64 | 0.35 | 0.70 | 0.27 | 0.42 | 0.33 |
| Lu | 0.07 | 0.19 | 0.06 | 0.05 | 0.10 | 0.05 | 0.11 | 0.04 | 0.06 | 0.06 |
| Hf | 4.21 | 5.24 | 3.84 | 3.14 | 6.40 | 2.72 | 5.59 | 2.71 | 4.68 | 4.23 |
| Ta | 0.67 | 0.74 | 0.59 | 1.98 | 1.12 | 0.84 | 1.19 | 1.79 | 0.69 | 0.39 |
| Th | 18.4 | 12.1 | 20.6 | 15.5 | 29.0 | 16.7 | 35.7 | 15.2 | 23.9 | 27.4 |
| U | 1.30 | 2.55 | 1.41 | 5.07 | 2.20 | 1.86 | 3.60 | 6.02 | 3.39 | 1.59 |
| ΣREEs | 134 | 152 | 141 | 91.8 | 183 | 106 | 232 | 90.6 | 137 | 166 |
| $(La/Yb)_N$ | 53.4 | 62.1 | 55.4 | 62.3 | 97.8 | 44.9 | 20.6 | 54.0 | 61.7 | 52.6 |
| Eu/Eu* | 0.68 | 0.54 | 0.35 | 0.66 | 0.62 | 0.45 | 0.77 | 0.60 | 0.72 | 0.70 |
| Nb/Ta | 11.1 | 11.5 | 9.3 | 5.9 | 11.7 | 9.6 | 10.2 | 6.8 | 10.3 | 16.9 |
| Zr/Hf | 36.9 | 34.9 | 32.9 | 29.9 | 33.6 | 32.1 | 34.1 | 30.0 | 33.2 | 34.5 |

**Supplementary Table S1**

SIMS zircon U-Pb data of the granitic samples

| Sample#spot | U ppm | Th ppm | Th/U | $f_{206}$% | $\frac{^{207}Pb}{^{235}U}$ | ±σ (%) | $\frac{^{206}Pb}{^{238}U}$ | ±σ (%) | $t_{207/206}$ (Ma) | ±σ (Ma) | $t_{207/235}$ (Ma) | ±σ (Ma) | $t_{206/238}$ (Ma) | ±σ (Ma) |
|---|---|---|---|---|---|---|---|---|---|---|---|---|---|---|
| **JH155** | | | | | | | | | | | | | | |
| JH155#1 | 829 | 621 | 0.75 | 0.08 | 0.13126 | 2.16 | 0.0201 | 1.51 | 71.2 | 36.2 | 125.2 | 2.5 | 128.1 | 1.9 |
| JH155#2 | 2159 | 1194 | 0.55 | 0.08 | 0.13520 | 1.81 | 0.0201 | 1.50 | 138.8 | 23.4 | 128.8 | 2.2 | 128.2 | 1.9 |
| JH155#3 | 651 | 583 | 0.90 | 0.07 | 0.13328 | 2.01 | 0.0198 | 1.50 | 135.3 | 31.3 | 127.0 | 2.4 | 126.6 | 1.9 |
| JH155#4 | 652 | 452 | 0.69 | 0.03 | 0.13542 | 2.10 | 0.0201 | 1.56 | 143.4 | 33.0 | 129.0 | 2.6 | 128.2 | 2.0 |
| JH155#5 | 1510 | 1053 | 0.70 | 0.00 | 0.13712 | 1.74 | 0.0206 | 1.51 | 117.3 | 20.2 | 130.5 | 2.1 | 131.2 | 2.0 |
| JH155#6 | 1345 | 372 | 0.28 | 0.01 | 0.13563 | 2.05 | 0.0196 | 1.67 | 205.1 | 27.2 | 129.1 | 2.5 | 125.1 | 2.1 |
| JH155#7 | 748 | 502 | 0.67 | 0.06 | 0.13508 | 2.36 | 0.0199 | 1.59 | 157.0 | 40.2 | 128.7 | 2.9 | 127.1 | 2.0 |
| JH155#8 | 1176 | 662 | 0.56 | 0.00 | 0.13710 | 1.88 | 0.0203 | 1.52 | 145.8 | 25.7 | 130.5 | 2.3 | 129.6 | 2.0 |
| JH155#9 | 803 | 463 | 0.58 | 0.06 | 0.13471 | 1.92 | 0.0201 | 1.50 | 133.8 | 27.9 | 128.3 | 2.3 | 128.0 | 1.9 |
| JH155#10 | 494 | 374 | 0.76 | 0.00 | 0.13404 | 2.30 | 0.0199 | 1.72 | 143.5 | 35.2 | 127.7 | 2.8 | 126.9 | 2.2 |
| JH155#11 | 276 | 261 | 0.95 | 0.00 | 0.13677 | 3.07 | 0.0198 | 1.57 | 203.1 | 60.2 | 130.2 | 3.8 | 126.2 | 2.0 |
| JH155#12 | 623 | 235 | 0.38 | 0.11 | 0.42838 | 1.90 | 0.0513 | 1.67 | 622.6 | 19.6 | 362.0 | 5.8 | 322.7 | 5.2 |
| JH155#13 | 1160 | 703 | 0.61 | 0.09 | 0.13615 | 1.98 | 0.0203 | 1.52 | 125.8 | 29.6 | 129.6 | 2.4 | 129.8 | 1.9 |
| JH155#14 | 1401 | 472 | 0.34 | 0.02 | 0.13355 | 1.75 | 0.0203 | 1.50 | 81.5 | 21.3 | 127.3 | 2.1 | 129.8 | 1.9 |
| JH155#15 | 668 | 593 | 0.89 | 0.04 | 0.13315 | 2.07 | 0.0197 | 1.52 | 145.8 | 32.5 | 126.9 | 2.5 | 125.9 | 1.9 |
| JH155#16 | 1224 | 1166 | 0.95 | 0.09 | 0.13875 | 2.88 | 0.0206 | 2.51 | 143.5 | 32.9 | 131.9 | 3.6 | 131.3 | 3.3 |
| JH155#17 | 751 | 477 | 0.63 | 0.06 | 0.13413 | 2.48 | 0.0199 | 1.53 | 142.9 | 45.1 | 127.8 | 3.0 | 127.0 | 1.9 |
| JH155#18 | 934 | 547 | 0.59 | 0.05 | 0.13063 | 3.24 | 0.0196 | 3.04 | 113.4 | 26.0 | 124.7 | 3.8 | 125.2 | 3.8 |
| JH155#19 | 722 | 546 | 0.76 | 0.00 | 0.13722 | 2.40 | 0.0205 | 1.70 | 128.9 | 39.5 | 130.6 | 2.9 | 130.7 | 2.2 |
| **DM35** | | | | | | | | | | | | | | |
| DM35#1 | 874 | 289 | 0.33 | 0.07 | 0.16198 | 2.16 | 0.0239 | 1.53 | 157.5 | 35.4 | 152.4 | 3.1 | 152.1 | 2.3 |
| DM35#2 | 917 | 392 | 0.43 | 0.10 | 0.15749 | 1.77 | 0.0236 | 1.51 | 116.6 | 21.4 | 148.5 | 2.4 | 150.5 | 2.2 |
| DM35#3 | 1121 | 585 | 0.52 | 0.04 | 0.15880 | 1.88 | 0.0237 | 1.51 | 132.7 | 26.0 | 149.7 | 2.6 | 150.7 | 2.3 |
| DM35#4 | 1288 | 751 | 0.58 | 0.06 | 0.15827 | 1.69 | 0.0235 | 1.50 | 144.9 | 17.9 | 149.2 | 2.3 | 149.5 | 2.2 |
| DM35#5 | 1195 | 583 | 0.49 | 0.03 | 0.16061 | 1.88 | 0.0238 | 1.70 | 143.3 | 18.6 | 151.2 | 2.6 | 151.7 | 2.5 |

| | | | | | | | | | | | | | | |
|---|---|---|---|---|---|---|---|---|---|---|---|---|---|---|
| DM35#6 | 1448 | 793 | 0.55 | 0.07 | 0.16219 | 1.67 | 0.0239 | 1.50 | 156.9 | 17.1 | 152.6 | 2.4 | 152.3 | 2.3 |
| DM35#7 | 942 | 419 | 0.45 | 0.02 | 0.15977 | 2.07 | 0.0236 | 1.50 | 157.4 | 32.8 | 150.5 | 2.9 | 150.1 | 2.2 |
| DM35#8 | 709 | 256 | 0.36 | 0.00 | 0.16005 | 1.83 | 0.0235 | 1.51 | 164.0 | 24.3 | 150.7 | 2.6 | 149.9 | 2.2 |
| DM35#9 | 517 | 334 | 0.65 | 0.03 | 0.16261 | 1.92 | 0.0240 | 1.50 | 153.3 | 28.0 | 153.0 | 2.7 | 153.0 | 2.3 |
| DM35#10 | 1292 | 725 | 0.56 | 0.04 | 0.16118 | 1.68 | 0.0239 | 1.50 | 144.8 | 17.8 | 151.7 | 2.4 | 152.2 | 2.3 |
| DM35#11 | 836 | 334 | 0.40 | 0.07 | 0.16293 | 1.85 | 0.0237 | 1.50 | 190.4 | 24.8 | 153.3 | 2.6 | 150.9 | 2.2 |
| DM35#12 | 2406 | 497 | 0.21 | 0.08 | 0.43199 | 7.53 | 0.0427 | 6.80 | 1022.7 | 64.2 | 364.6 | 23.3 | 269.7 | 18.0 |
| DM35#13 | 917 | 510 | 0.56 | 0.03 | 0.16085 | 1.79 | 0.0238 | 1.51 | 150.3 | 22.2 | 151.4 | 2.5 | 151.5 | 2.3 |
| DM35#14 | 882 | 394 | 0.45 | 0.17 | 0.15866 | 1.77 | 0.0239 | 1.50 | 110.4 | 22.1 | 149.5 | 2.5 | 152.0 | 2.3 |
| DM35#15 | 893 | 420 | 0.47 | 0.06 | 0.16213 | 2.02 | 0.0238 | 1.51 | 167.2 | 30.9 | 152.6 | 2.9 | 151.6 | 2.3 |
| DM35#16 | 1227 | 694 | 0.57 | 0.07 | 0.15839 | 1.82 | 0.0234 | 1.51 | 148.0 | 23.7 | 149.3 | 2.5 | 149.4 | 2.2 |
| DM35#17 | 887 | 287 | 0.32 | 0.22 | 1.07765 | 1.61 | 0.1156 | 1.50 | 856.9 | 11.7 | 742.5 | 8.5 | 705.1 | 10.0 |
| DM35#18 | 1075 | 584 | 0.54 | 0.15 | 0.16247 | 1.74 | 0.0240 | 1.53 | 153.8 | 19.6 | 152.9 | 2.5 | 152.8 | 2.3 |
| **QD69** | | | | | | | | | | | | | | |
| QD69#1 | 1839 | 345 | 0.19 | 0.05 | 0.15737 | 1.86 | 0.0236 | 1.50 | 115.3 | 25.8 | 148.4 | 2.6 | 150.5 | 2.2 |
| QD69#2 | 3341 | 422 | 0.13 | 0.00 | 0.16283 | 1.87 | 0.0240 | 1.58 | 160.5 | 23.3 | 153.2 | 2.7 | 152.7 | 2.4 |
| QD69#3 | 2516 | 271 | 0.11 | 0.00 | 0.16042 | 1.76 | 0.0237 | 1.50 | 155.8 | 21.5 | 151.1 | 2.5 | 150.8 | 2.2 |
| QD69#4 | 755 | 27 | 0.04 | 0.00 | 0.16162 | 2.31 | 0.0238 | 1.52 | 159.8 | 40.2 | 152.1 | 3.3 | 151.6 | 2.3 |
| QD69#5 | 7007 | 979 | 0.14 | 0.00 | 0.17165 | 1.60 | 0.0251 | 1.50 | 172.0 | 12.7 | 160.8 | 2.4 | 160.1 | 2.4 |
| QD69#6 | 4952 | 771 | 0.16 | 0.34 | 0.16161 | 1.91 | 0.0238 | 1.50 | 158.3 | 27.3 | 152.1 | 2.7 | 151.7 | 2.3 |
| QD69#7 | 4816 | 700 | 0.15 | 0.01 | 0.16316 | 1.64 | 0.0241 | 1.51 | 154.2 | 15.4 | 153.5 | 2.3 | 153.4 | 2.3 |
| QD69#8 | 3176 | 612 | 0.19 | 0.06 | 0.16086 | 1.80 | 0.0239 | 1.50 | 140.2 | 23.2 | 151.5 | 2.5 | 152.2 | 2.3 |
| QD69#9 | 2483 | 405 | 0.16 | 0.01 | 0.16172 | 1.77 | 0.0240 | 1.50 | 142.8 | 21.9 | 152.2 | 2.5 | 152.8 | 2.3 |
| QD69#10 | 126 | 85 | 0.68 | 0.08 | 1.26671 | 2.11 | 0.1387 | 1.50 | 814.3 | 30.7 | 830.9 | 12.1 | 837.1 | 11.8 |
| QD69#11 | 521 | 397 | 0.76 | 0.15 | 0.15846 | 2.56 | 0.0235 | 1.50 | 144.0 | 47.8 | 149.4 | 3.6 | 149.7 | 2.2 |
| QD69#12 | 1466 | 106 | 0.07 | 0.00 | 0.15587 | 1.95 | 0.0235 | 1.51 | 108.6 | 29.0 | 147.1 | 2.7 | 149.5 | 2.2 |
| QD69#13 | 3703 | 727 | 0.20 | 0.07 | 0.15923 | 1.74 | 0.0237 | 1.50 | 136.3 | 20.4 | 150.0 | 2.4 | 150.9 | 2.2 |
| QD69#14 | 5370 | 652 | 0.12 | 0.23 | 0.16664 | 1.69 | 0.0251 | 1.50 | 110.0 | 18.5 | 156.5 | 2.5 | 159.6 | 2.4 |
| QD69#15 | 2129 | 217 | 0.10 | 0.12 | 0.15816 | 2.05 | 0.0234 | 1.50 | 151.2 | 32.3 | 149.1 | 2.8 | 149.0 | 2.2 |
| QD69#16 | 2873 | 246 | 0.09 | 0.01 | 0.16333 | 1.77 | 0.0239 | 1.54 | 178.3 | 20.0 | 153.6 | 2.5 | 152.0 | 2.3 |

| | | | | | | | | | | | | | | |
|---|---|---|---|---|---|---|---|---|---|---|---|---|---|---|
| QD69#17 | 2996 | 340 | 0.11 | 0.04 | 0.15894 | 1.73 | 0.0237 | 1.50 | 131.1 | 20.1 | 149.8 | 2.4 | 151.0 | 2.2 |
| QD69#18 | 427 | 250 | 0.59 | 0.14 | 0.16414 | 2.74 | 0.0242 | 1.53 | 152.8 | 52.5 | 154.3 | 3.9 | 154.4 | 2.3 |
| QD69#19 | 1295 | 1783 | 1.38 | 0.06 | 0.15940 | 1.99 | 0.0236 | 1.50 | 145.7 | 30.2 | 150.2 | 2.8 | 150.5 | 2.2 |
| **DYS14** | | | | | | | | | | | | | | |
| DYS14#1 | 303 | 185 | 0.61 | 0.31 | 0.17024 | 3.05 | 0.0245 | 1.55 | 217.8 | 59.8 | 159.6 | 4.5 | 155.7 | 2.4 |
| DYS14#2 | 381 | 298 | 0.78 | 0.15 | 0.16478 | 3.04 | 0.0237 | 1.53 | 217.4 | 59.7 | 154.9 | 4.4 | 150.8 | 2.3 |
| DYS14#3 | 439 | 226 | 0.52 | 0.26 | 0.15967 | 2.70 | 0.0237 | 1.52 | 142.2 | 51.5 | 150.4 | 3.8 | 150.9 | 2.3 |
| DYS14#4 | 330 | 258 | 0.78 | 0.29 | 0.15909 | 3.02 | 0.0233 | 1.59 | 176.6 | 58.7 | 149.9 | 4.2 | 148.2 | 2.3 |
| DYS14#5 | 457 | 216 | 0.47 | 0.02 | 0.16518 | 2.63 | 0.0233 | 1.53 | 255.7 | 48.4 | 155.2 | 3.8 | 148.7 | 2.2 |
| DYS14#6 | 378 | 372 | 0.98 | 0.40 | 0.16049 | 3.83 | 0.0237 | 1.58 | 150.7 | 79.8 | 151.1 | 5.4 | 151.2 | 2.4 |
| DYS14#7 | 517 | 168 | 0.32 | 0.15 | 0.15539 | 2.58 | 0.0229 | 1.52 | 156.1 | 47.9 | 146.7 | 3.5 | 146.1 | 2.2 |
| DYS14#8 | 532 | 301 | 0.57 | 0.11 | 0.15615 | 2.53 | 0.0238 | 1.50 | 81.9 | 47.6 | 147.3 | 3.5 | 151.4 | 2.2 |
| DYS14#9 | 627 | 281 | 0.45 | 0.13 | 0.16374 | 2.39 | 0.0237 | 1.52 | 200.7 | 42.4 | 154.0 | 3.4 | 151.0 | 2.3 |
| DYS14#10 | 942 | 529 | 0.56 | 0.06 | 0.16027 | 2.13 | 0.0234 | 1.51 | 179.0 | 34.5 | 150.9 | 3.0 | 149.2 | 2.2 |
| DYS14#11 | 414 | 277 | 0.67 | 0.38 | 0.15388 | 3.83 | 0.0230 | 1.59 | 123.3 | 80.1 | 145.3 | 5.2 | 146.7 | 2.3 |
| DYS14#12 | 326 | 162 | 0.50 | 0.12 | 0.15723 | 3.34 | 0.0235 | 1.52 | 129.2 | 68.6 | 148.3 | 4.6 | 149.5 | 2.3 |
| DYS14#13 | 294 | 258 | 0.88 | 0.11 | 0.15983 | 3.10 | 0.0234 | 1.51 | 175.5 | 62.0 | 150.6 | 4.3 | 149.0 | 2.2 |
| DYS14#14r | 694 | 117 | 0.17 | 0.14 | 0.15945 | 3.23 | 0.0237 | 1.51 | 141.8 | 65.8 | 150.2 | 4.5 | 150.8 | 2.3 |
| DYS14#14c | 948 | 74 | 0.08 | 0.01 | 1.24630 | 1.61 | 0.1355 | 1.51 | 829.0 | 11.6 | 821.7 | 9.1 | 819.1 | 11.6 |
| DYS14#15 | 699 | 620 | 0.89 | 0.34 | 0.15739 | 3.04 | 0.0235 | 1.50 | 131.3 | 61.0 | 148.4 | 4.2 | 149.5 | 2.2 |
| DYS14#16 | 261 | 166 | 0.64 | 0.72 | 0.14985 | 4.20 | 0.0231 | 1.55 | 48.2 | 90.8 | 141.8 | 5.6 | 147.4 | 2.3 |
| DYS14#17 | 676 | 370 | 0.55 | 0.17 | 0.16449 | 2.33 | 0.0235 | 1.52 | 232.5 | 40.3 | 154.6 | 3.4 | 149.6 | 2.3 |
| DYS14#18 | 629 | 381 | 0.61 | 0.47 | 0.15384 | 3.19 | 0.0231 | 1.54 | 116.1 | 64.7 | 145.3 | 4.3 | 147.1 | 2.2 |
| DYS14#19 | 726 | 561 | 0.77 | 0.00 | 0.15499 | 2.32 | 0.0227 | 1.51 | 171.0 | 40.6 | 146.3 | 3.2 | 144.8 | 2.2 |
| DYS14#20 | 674 | 504 | 0.75 | 0.23 | 0.15346 | 3.24 | 0.0234 | 1.60 | 76.8 | 65.6 | 145.0 | 4.4 | 149.2 | 2.4 |
| **QD49** | | | | | | | | | | | | | | |
| QD49#1 | 5166 | 109 | 0.02 | 0.03 | 0.14105 | 1.62 | 0.0210 | 1.50 | 132.1 | 14.1 | 134.0 | 2.0 | 134.1 | 2.0 |
| QD49#2 | 2432 | 358 | 0.15 | 0.04 | 0.13996 | 1.75 | 0.0209 | 1.53 | 125.5 | 20.2 | 133.0 | 2.2 | 133.4 | 2.0 |
| QD49#3 | 3685 | 438 | 0.12 | 0.04 | 0.14215 | 1.60 | 0.0211 | 1.50 | 137.3 | 12.6 | 135.0 | 2.0 | 134.8 | 2.0 |
| QD49#4 | 88 | 81 | 0.92 | 0.72 | 0.13724 | 4.29 | 0.0203 | 1.56 | 145.7 | 91.2 | 130.6 | 5.3 | 129.8 | 2.0 |

| | | | | | | | | | | | | | | |
|---|---|---|---|---|---|---|---|---|---|---|---|---|---|---|
| QD49#5 | 831 | 697 | 0.84 | 0.07 | 0.14644 | 1.90 | 0.0218 | 1.52 | 133.5 | 26.5 | 138.8 | 2.5 | 139.1 | 2.1 |
| QD49#6 | 162 | 154 | 0.95 | 0.15 | 0.13679 | 3.37 | 0.0204 | 1.53 | 132.3 | 69.0 | 130.2 | 4.1 | 130.1 | 2.0 |
| QD49#7 | 157 | 164 | 1.04 | 0.13 | 0.14519 | 3.13 | 0.0200 | 1.54 | 315.0 | 60.9 | 137.7 | 4.0 | 127.6 | 1.9 |
| QD49#8 | 2981 | 675 | 0.23 | 0.02 | 0.14360 | 1.64 | 0.0215 | 1.53 | 123.8 | 14.0 | 136.2 | 2.1 | 137.0 | 2.1 |
| QD49#9 | 938 | 325 | 0.35 | 0.00 | 0.13668 | 2.13 | 0.0206 | 1.56 | 101.9 | 33.8 | 130.1 | 2.6 | 131.6 | 2.0 |
| QD49#10 | 525 | 334 | 0.64 | 0.01 | 1.27868 | 1.56 | 0.1377 | 1.50 | 849.3 | 9.1 | 836.3 | 8.9 | 831.4 | 11.7 |
| QD49#11 | 161 | 92 | 0.57 | 0.16 | 0.19698 | 2.96 | 0.0273 | 1.64 | 299.6 | 55.4 | 182.6 | 5.0 | 173.6 | 2.8 |
| QD49#12 | 367 | 278 | 0.76 | 0.16 | 0.14373 | 2.82 | 0.0212 | 1.56 | 155.7 | 53.9 | 136.4 | 3.6 | 135.3 | 2.1 |
| QD49#13 | 618 | 416 | 0.67 | 0.01 | 1.29991 | 1.56 | 0.1406 | 1.51 | 839.8 | 8.3 | 845.7 | 9.0 | 847.9 | 12.0 |
| QD49#14 | 706 | 748 | 1.06 | 0.13 | 0.13346 | 2.03 | 0.0199 | 1.50 | 129.6 | 31.9 | 127.2 | 2.4 | 127.1 | 1.9 |
| QD49#15 | 427 | 188 | 0.44 | 0.02 | 0.80096 | 1.63 | 0.0910 | 1.51 | 736.9 | 13.0 | 597.4 | 7.4 | 561.3 | 8.1 |
| QD49#16 | 252 | 222 | 0.88 | 0.36 | 0.13409 | 3.38 | 0.0203 | 1.58 | 89.0 | 69.4 | 127.8 | 4.1 | 129.9 | 2.0 |
| QD49#17 | 1186 | 442 | 0.37 | 0.03 | 0.49973 | 1.86 | 0.0594 | 1.80 | 639.8 | 10.3 | 411.5 | 6.3 | 372.0 | 6.5 |
| QD49#18 | 413 | 119 | 0.29 | 0.08 | 0.13458 | 2.12 | 0.0201 | 1.51 | 125.3 | 34.6 | 128.2 | 2.6 | 128.4 | 1.9 |
| QD49#19 | 1272 | 375 | 0.29 | 0.04 | 0.13839 | 1.71 | 0.0208 | 1.51 | 106.6 | 19.2 | 131.6 | 2.1 | 133.0 | 2.0 |
| QD49#20 | 632 | 148 | 0.23 | 0.08 | 0.13654 | 1.93 | 0.0204 | 1.51 | 129.0 | 27.9 | 130.0 | 2.4 | 130.0 | 1.9 |
| QD49#21 | 975 | 525 | 0.54 | 0.01 | 2.35906 | 1.53 | 0.2087 | 1.50 | 1245.5 | 5.4 | 1230.3 | 10.9 | 1221.6 | 16.7 |
| **QD62** | | | | | | | | | | | | | | |
| DQ62#1 | 3724 | 483 | 0.13 | 0.06 | 0.13365 | 1.99 | 0.0201 | 1.50 | 107.4 | 30.4 | 127.4 | 2.4 | 128.4 | 1.9 |
| DQ62#2 | 1266 | 474 | 0.37 | 0.02 | 1.09491 | 1.71 | 0.1195 | 1.51 | 820.2 | 16.6 | 750.9 | 9.1 | 727.8 | 10.4 |
| DQ62#3 | 537 | 50 | 0.09 | 0.18 | 0.13033 | 2.77 | 0.0195 | 1.58 | 122.4 | 52.7 | 124.4 | 3.2 | 124.5 | 2.0 |
| DQ62#4 | 9826 | 1410 | 0.14 | 0.04 | 0.14160 | 1.93 | 0.0212 | 1.85 | 121.6 | 12.6 | 134.5 | 2.4 | 135.2 | 2.5 |
| DQ62#5r | 1170 | 245 | 0.21 | 0.04 | 0.13080 | 2.16 | 0.0193 | 1.53 | 151.2 | 35.3 | 124.8 | 2.5 | 123.4 | 1.9 |
| DQ62#5c | 3033 | 397 | 0.13 | 0.32 | 0.15528 | 2.50 | 0.0220 | 1.98 | 247.2 | 34.6 | 146.6 | 3.4 | 140.4 | 2.8 |
| DQ62#6 | 1719 | 321 | 0.19 | 0.32 | 0.22448 | 2.22 | 0.0290 | 1.53 | 456.4 | 35.1 | 205.6 | 4.1 | 184.4 | 2.8 |
| DQ62#7 | 2839 | 425 | 0.15 | 0.33 | 0.13321 | 2.37 | 0.0199 | 1.55 | 121.3 | 41.8 | 127.0 | 2.8 | 127.3 | 2.0 |
| DQ62#8 | 1708 | 363 | 0.21 | 0.07 | 0.13338 | 1.97 | 0.0198 | 1.51 | 143.4 | 29.5 | 127.1 | 2.4 | 126.3 | 1.9 |
| DQ62#9 | 2516 | 533 | 0.21 | 0.16 | 0.12682 | 2.01 | 0.0188 | 1.52 | 143.4 | 30.6 | 121.2 | 2.3 | 120.1 | 1.8 |
| DQ62#10 | 1260 | 526 | 0.42 | 0.00 | 0.14053 | 2.07 | 0.0204 | 1.51 | 190.0 | 32.8 | 133.5 | 2.6 | 130.4 | 1.9 |
| DQ62#11 | 602 | 96 | 0.16 | 0.08 | 0.13963 | 3.02 | 0.0210 | 1.63 | 113.2 | 58.8 | 132.7 | 3.8 | 133.8 | 2.2 |

| | | | | | | | | | | | | | | |
|---|---|---|---|---|---|---|---|---|---|---|---|---|---|---|
| DQ62#12 | 2099 | 541 | 0.26 | 0.01 | 0.14456 | 1.87 | 0.0216 | 1.50 | 123.4 | 26.2 | 137.1 | 2.4 | 137.9 | 2.0 |
| DQ62#13 | 2693 | 376 | 0.14 | 0.08 | 0.12438 | 1.83 | 0.0186 | 1.51 | 123.3 | 24.3 | 119.0 | 2.1 | 118.8 | 1.8 |
| DQ62#14 | 1634 | 186 | 0.11 | 0.12 | 0.13385 | 1.99 | 0.0202 | 1.50 | 102.3 | 30.7 | 127.5 | 2.4 | 128.9 | 1.9 |
| DQ62#15 | 2636 | 509 | 0.19 | 0.06 | 0.13191 | 1.87 | 0.0198 | 1.57 | 114.8 | 23.7 | 125.8 | 2.2 | 126.4 | 2.0 |
| DQ62#16 | 1802 | 321 | 0.18 | 0.02 | 0.13246 | 1.94 | 0.0197 | 1.52 | 132.6 | 28.2 | 126.3 | 2.3 | 126.0 | 1.9 |
| DQ62#17 | 1967 | 244 | 0.12 | 0.06 | 0.13716 | 1.90 | 0.0206 | 1.50 | 115.1 | 27.1 | 130.5 | 2.3 | 131.4 | 2.0 |
| DQ62#18-1 | 1619 | 291 | 0.18 | 0.04 | 0.13025 | 2.00 | 0.0193 | 1.51 | 140.3 | 30.6 | 124.3 | 2.3 | 123.5 | 1.8 |
| DQ62#18-2 | 1702 | 130 | 0.08 | 0.01 | 0.12839 | 2.55 | 0.0188 | 1.59 | 176.6 | 45.8 | 122.7 | 3.0 | 119.9 | 1.9 |
| DQ62#19 | 2239 | 227 | 0.10 | 0.01 | 0.13796 | 1.87 | 0.0202 | 1.53 | 168.8 | 25.1 | 131.2 | 2.3 | 129.2 | 2.0 |
| DQ62#20 | 3402 | 420 | 0.12 | 0.02 | 0.13739 | 1.75 | 0.0201 | 1.50 | 180.0 | 20.5 | 130.7 | 2.1 | 128.0 | 1.9 |
| DQ62#21 | 851 | 106 | 0.12 | 0.06 | 0.13970 | 2.39 | 0.0195 | 1.56 | 278.8 | 41.0 | 132.8 | 3.0 | 124.8 | 1.9 |
| **DM80** | | | | | | | | | | | | | | |
| DM80#1 | 4582 | 500 | 0.11 | 0.02 | 0.15123 | 1.85 | 0.0225 | 1.74 | 167.3 | 16.0 | 146.5 | 2.4 | 145.2 | 2.4 |
| DM80#2 | 5175 | 1926 | 0.37 | 0.01 | 0.15517 | 1.57 | 0.0230 | 1.51 | 116.7 | 8.9 | 145.3 | 2.1 | 147.0 | 2.2 |
| DM80#3 | 2666 | 3332 | 1.25 | 0.12 | 0.15158 | 1.62 | 0.0225 | 1.50 | 86.1 | 64.5 | 142.4 | 4.2 | 145.8 | 2.2 |
| DM80#4 | 2093 | 623 | 0.30 | 0.04 | 0.14557 | 1.71 | 0.0217 | 1.50 | 131.6 | 23.6 | 140.8 | 2.9 | 141.3 | 2.7 |
| DM80#5 | 2611 | 941 | 0.36 | 2.31 | 0.14396 | 2.92 | 0.0226 | 1.51 | 140.4 | 14.9 | 141.1 | 2.2 | 141.1 | 2.1 |
| DM80#6 | 3496 | 563 | 0.16 | 0.14 | 0.15515 | 1.79 | 0.0228 | 1.66 | 0.0 | 68.1 | 136.6 | 3.7 | 144.0 | 2.1 |
| DM80#7 | 2806 | 366 | 0.13 | 0.00 | 0.15902 | 1.70 | 0.0238 | 1.50 | -0.1 | 45.4 | 133.3 | 3.0 | 140.8 | 2.1 |
| DM80#8 | 1861 | 331 | 0.18 | 0.58 | 0.14024 | 2.43 | 0.0221 | 1.50 | 140.0 | 12.9 | 140.2 | 2.1 | 140.3 | 2.1 |
| DM80#9 | 726 | 264 | 0.36 | 0.08 | 0.14425 | 2.03 | 0.0215 | 1.52 | 125.4 | 24.1 | 137.2 | 2.4 | 137.9 | 2.1 |
| DM80#10 | 2183 | 654 | 0.30 | 0.03 | 0.14872 | 2.19 | 0.0222 | 1.94 | 130.3 | 19.3 | 138.0 | 2.2 | 138.4 | 2.1 |
| DM80#11 | 4500 | 2228 | 0.50 | 0.02 | 0.14916 | 1.62 | 0.0222 | 1.53 | 147.1 | 10.2 | 146.5 | 2.1 | 146.4 | 2.2 |
| DM80#12 | 607 | 97 | 0.16 | 0.05 | 1.25570 | 2.19 | 0.1385 | 2.13 | 798.9 | 10.0 | 826.0 | 12.4 | 836.1 | 16.7 |
| DM80#13 | 6792 | 217 | 0.03 | 0.02 | 0.15381 | 1.55 | 0.0231 | 1.50 | 142.2 | 8.5 | 147.1 | 2.1 | 147.4 | 2.2 |
| DM80#14 | 2125 | 692 | 0.33 | 0.09 | 0.14805 | 1.75 | 0.0221 | 1.51 | 133.8 | 14.5 | 143.0 | 2.5 | 143.6 | 2.5 |
| DM80#15 | 4550 | 1187 | 0.26 | 0.02 | 0.15624 | 1.57 | 0.0233 | 1.50 | 122.3 | 18.8 | 149.8 | 2.4 | 151.6 | 2.2 |
| DM80#16 | 3131 | 761 | 0.24 | 1.79 | 0.14674 | 3.53 | 0.0229 | 1.50 | 18.9 | 74.9 | 139.0 | 4.6 | 146.2 | 2.2 |
| DM80#17 | 2475 | 875 | 0.35 | 0.61 | 0.15060 | 3.16 | 0.0229 | 1.51 | 133.6 | 31.3 | 136.8 | 2.6 | 137.0 | 2.1 |
| DM80#18 | 1743 | 710 | 0.41 | 0.03 | 0.14746 | 1.71 | 0.0219 | 1.51 | 123.4 | 20.4 | 140.2 | 2.3 | 141.2 | 2.1 |

| | | | | | | | | | | | | | | |
|---|---|---|---|---|---|---|---|---|---|---|---|---|---|---|
| DM80#19 | 3337 | 1885 | 0.56 | 0.07 | 0.14905 | 1.63 | 0.0221 | 1.50 | 96.4 | 48.0 | 141.7 | 3.4 | 144.4 | 2.1 |
| DM80#20 | 4268 | 1384 | 0.32 | 0.85 | 0.14976 | 2.55 | 0.0227 | 1.50 | 137.8 | 17.0 | 142.0 | 2.2 | 142.3 | 2.1 |
| DM80#21 | 3295 | 499 | 0.15 | 0.04 | 0.14811 | 1.61 | 0.0220 | 1.51 | 129.6 | 12.4 | 141.2 | 2.1 | 141.9 | 2.1 |
| DM80#22 | 810 | 113 | 0.14 | 0.02 | 0.16159 | 1.54 | 0.0241 | 1.51 | 804.4 | 9.1 | 768.1 | 8.5 | 755.7 | 10.8 |
| DM80#23 | 405 | 70 | 0.17 | 0.03 | 0.19986 | 1.54 | 0.0270 | 1.51 | 802.7 | 10.7 | 814.8 | 9.1 | 819.2 | 11.7 |
| DM80#24 | 68 | 43 | 0.63 | 0.07 | 0.15588 | 1.55 | 0.0231 | 1.51 | 860.0 | 27.9 | 852.8 | 11.9 | 850.1 | 12.3 |
| DM80#25 | 690 | 535 | 0.78 | 0.04 | 1.20012 | 1.56 | 0.1305 | 1.50 | 828.5 | 9.0 | 800.6 | 8.7 | 790.7 | 11.2 |
| DM80#26 | 260 | 255 | 0.98 | 0.06 | 1.13078 | 1.57 | 0.1244 | 1.51 | 447.6 | 27.8 | 421.3 | 6.8 | 416.5 | 6.1 |
| DM80#27 | 1452 | 262 | 0.18 | 0.04 | 0.76740 | 1.57 | 0.0874 | 1.50 | 575.7 | 30.4 | 320.4 | 15.0 | 286.3 | 14.7 |
| DM80#28 | 1633 | 595 | 0.36 | 0.06 | 1.23105 | 1.61 | 0.1355 | 1.53 | 142.3 | 18.8 | 139.7 | 2.2 | 139.5 | 2.1 |
| DM80#29 | 2488 | 784 | 0.32 | 0.02 | 0.15014 | 1.68 | 0.0223 | 1.52 | 136.6 | 14.3 | 143.3 | 2.2 | 143.7 | 2.1 |
| DM80#30 | 10911 | 941 | 0.09 | 0.02 | 0.14468 | 1.84 | 0.0216 | 1.52 | 131.1 | 6.3 | 152.1 | 2.2 | 153.4 | 2.3 |
| DM80#31 | 1329 | 584 | 0.44 | 0.05 | 0.51429 | 1.96 | 0.0668 | 1.50 | 731.9 | 9.6 | 578.3 | 6.9 | 539.9 | 7.8 |
| DM80#32 | 7413 | 115 | 0.02 | 0.01 | 1.31618 | 2.06 | 0.1410 | 1.55 | 355.1 | 7.4 | 185.0 | 2.6 | 172.0 | 2.6 |
| DM80#33 | 6842 | 244 | 0.04 | 0.03 | 0.37095 | 5.43 | 0.0454 | 5.24 | 125.3 | 10.8 | 147.4 | 2.2 | 148.8 | 2.2 |
| **DYS01** | | | | | | | | | | | | | | |
| DYS01#1 | 2497 | 18 | 0.01 | 0.03 | 0.15107 | 1.66 | 0.0225 | 1.50 | 128.1 | 16.3 | 142.9 | 2.2 | 143.7 | 2.1 |
| DYS01#2 | 6697 | 339 | 0.05 | 0.01 | 0.16590 | 1.55 | 0.0245 | 1.50 | 150.0 | 8.6 | 155.9 | 2.2 | 156.2 | 2.3 |
| DYS01#3 | 533 | 39 | 0.07 | 0.09 | 0.15502 | 2.13 | 0.0226 | 1.50 | 178.3 | 34.9 | 146.3 | 2.9 | 144.4 | 2.1 |
| DYS01#4 | 3374 | 41 | 0.01 | 0.04 | 0.15511 | 1.60 | 0.0229 | 1.51 | 153.3 | 12.6 | 146.4 | 2.2 | 146.0 | 2.2 |
| DYS01#5 | 656 | 206 | 0.31 | 0.00 | 0.15348 | 1.94 | 0.0229 | 1.50 | 128.0 | 28.6 | 145.0 | 2.6 | 146.0 | 2.2 |
| DYS01#6 | 12087 | 689 | 0.06 | 3.39 | 0.15409 | 3.65 | 0.0228 | 1.53 | 151.5 | 75.9 | 145.5 | 5.0 | 145.1 | 2.2 |
| DYS01#7 | 7008 | 369 | 0.05 | 0.02 | 0.16130 | 1.62 | 0.0241 | 1.52 | 129.9 | 12.8 | 151.8 | 2.3 | 153.3 | 2.3 |
| DYS01#8 | 373 | 202 | 0.54 | 0.02 | 3.65417 | 1.57 | 0.2523 | 1.52 | 1715.1 | 7.4 | 1561.4 | 12.6 | 1450.3 | 19.7 |
| DYS01#9 | 3687 | 269 | 0.07 | 0.10 | 0.15628 | 1.70 | 0.0233 | 1.52 | 133.2 | 17.8 | 147.4 | 2.3 | 148.3 | 2.2 |
| DYS01#10 | 6866 | 1318 | 0.19 | 0.59 | 0.15681 | 1.69 | 0.0236 | 1.51 | 110.8 | 17.8 | 147.9 | 2.3 | 150.2 | 2.2 |
| DYS01#11 | 1757 | 1615 | 0.92 | 0.01 | 0.15514 | 1.68 | 0.0230 | 1.51 | 147.2 | 17.2 | 146.4 | 2.3 | 146.4 | 2.2 |
| DYS01#12 | 1396 | 285 | 0.20 | 0.05 | 0.16061 | 2.01 | 0.0237 | 1.53 | 156.0 | 30.1 | 151.2 | 2.8 | 150.9 | 2.3 |
| DYS01#13 | 351 | 419 | 1.20 | 0.01 | 1.28026 | 1.61 | 0.1385 | 1.50 | 839.4 | 12.2 | 837.0 | 9.2 | 836.0 | 11.8 |
| DYS01#14 | 227 | 79 | 0.35 | 0.03 | 1.26987 | 1.69 | 0.1388 | 1.50 | 817.6 | 16.0 | 832.3 | 9.6 | 837.9 | 11.8 |

| | | | | | | | | | | | | | | |
|---|---|---|---|---|---|---|---|---|---|---|---|---|---|---|
| DYS01#15 | 1878 | 245 | 0.13 | 0.32 | 0.35173 | 6.10 | 0.0416 | 6.06 | 649.5 | 16.1 | 306.0 | 16.3 | 262.9 | 15.6 |
| DYS01#16 | 3882 | 55 | 0.01 | 0.01 | 0.15649 | 1.61 | 0.0230 | 1.50 | 159.8 | 13.7 | 147.6 | 2.2 | 146.9 | 2.2 |
| DYS01#17 | 122 | 104 | 0.85 | 0.05 | 1.27447 | 1.80 | 0.1389 | 1.50 | 823.5 | 20.6 | 834.4 | 10.3 | 838.5 | 11.8 |
| DYS01#18 | 2085 | 464 | 0.22 | 1.29 | 0.15886 | 2.32 | 0.0230 | 1.51 | 196.2 | 40.4 | 149.7 | 3.2 | 146.8 | 2.2 |
| DYS01#19 | 2960 | 22 | 0.01 | 0.01 | 0.15287 | 1.64 | 0.0225 | 1.50 | 157.3 | 15.5 | 144.4 | 2.2 | 143.7 | 2.1 |
| DYS01#20 | 1975 | 238 | 0.12 | 0.01 | 0.15870 | 1.65 | 0.0234 | 1.50 | 154.3 | 16.0 | 149.6 | 2.3 | 149.3 | 2.2 |
| DYS01#21 | 1516 | 734 | 0.48 | 0.04 | 0.14858 | 2.05 | 0.0218 | 1.81 | 170.9 | 22.6 | 140.7 | 2.7 | 138.9 | 2.5 |
| DYS01#22 | 319 | 245 | 0.77 | 0.00 | 0.15471 | 2.30 | 0.0229 | 1.51 | 149.6 | 40.4 | 146.1 | 3.1 | 145.8 | 2.2 |
| DYS01#23 | 658 | 690 | 1.05 | 0.07 | 0.15814 | 1.92 | 0.0237 | 1.50 | 116.5 | 27.9 | 149.1 | 2.7 | 151.1 | 2.2 |
| **DYS03** | | | | | | | | | | | | | | |
| DYS03#1 | 710 | 356 | 0.50 | 0.03 | 1.05139 | 1.76 | 0.1138 | 1.53 | 837.9 | 17.8 | 729.6 | 9.2 | 694.8 | 10.1 |
| DYS03#2 | 519 | 120 | 0.23 | 0.10 | 0.65209 | 2.30 | 0.0769 | 1.50 | 656.5 | 37.0 | 509.8 | 9.3 | 477.7 | 6.9 |
| DYS03#3 | 1980 | 86 | 0.04 | 0.57 | 0.14649 | 2.80 | 0.0224 | 1.52 | 75.7 | 55.1 | 138.8 | 3.6 | 142.5 | 2.1 |
| DYS03#4 | 2124 | 867 | 0.41 | 0.55 | 0.14896 | 2.27 | 0.0225 | 1.51 | 104.3 | 39.5 | 141.0 | 3.0 | 143.2 | 2.1 |
| DYS03#5 | 857 | 748 | 0.87 | 0.05 | 0.15144 | 2.36 | 0.0227 | 1.52 | 117.8 | 42.2 | 143.2 | 3.2 | 144.7 | 2.2 |
| DYS03#6 | 3677 | 1087 | 0.30 | 0.11 | 0.15293 | 1.76 | 0.0228 | 1.51 | 131.3 | 21.2 | 144.5 | 2.4 | 145.3 | 2.2 |
| DYS03#7 | 1651 | 336 | 0.20 | 0.15 | 0.15799 | 2.14 | 0.0239 | 1.50 | 93.3 | 35.8 | 148.9 | 3.0 | 152.5 | 2.3 |
| DYS03#8c | 756 | 135 | 0.18 | 0.09 | 0.49649 | 2.17 | 0.0584 | 1.89 | 661.1 | 22.5 | 409.3 | 7.3 | 366.1 | 6.7 |
| DYS03#8r | 12950 | 115 | 0.01 | 0.00 | 0.16242 | 1.57 | 0.0241 | 1.51 | 139.5 | 10.0 | 152.8 | 2.2 | 153.7 | 2.3 |
| DYS03#9 | 4548 | 728 | 0.16 | 1.75 | 0.16132 | 1.80 | 0.0234 | 1.51 | 194.7 | 22.6 | 151.9 | 2.5 | 149.1 | 2.2 |
| DYS03#10 | 1959 | 1694 | 0.86 | 0.04 | 0.15565 | 2.23 | 0.0227 | 1.50 | 186.8 | 38.0 | 146.9 | 3.1 | 144.4 | 2.1 |
| DYS03#11c | 1754 | 121 | 0.07 | 0.22 | 0.20955 | 2.05 | 0.0288 | 1.57 | 321.2 | 29.7 | 193.2 | 3.6 | 182.9 | 2.8 |
| DYS03#11r | 38596 | 271 | 0.01 | 0.01 | 0.14310 | 1.54 | 0.0212 | 1.51 | 146.3 | 6.5 | 135.8 | 2.0 | 135.2 | 2.0 |
| DYS03#12 | 884 | 466 | 0.53 | 0.09 | 0.15729 | 2.33 | 0.0228 | 1.51 | 198.9 | 40.7 | 148.3 | 3.2 | 145.2 | 2.2 |
| DYS03#13 | 1579 | 108 | 0.07 | 0.01 | 0.15413 | 2.07 | 0.0228 | 1.51 | 146.7 | 33.0 | 145.5 | 2.8 | 145.5 | 2.2 |
| DYS03#14 | 592 | 786 | 1.33 | 0.34 | 0.15113 | 3.64 | 0.0217 | 1.53 | 217.1 | 74.8 | 142.9 | 4.9 | 138.5 | 2.1 |
| DYS03#15 | 361 | 188 | 0.52 | 0.61 | 0.16708 | 3.05 | 0.0233 | 1.83 | 287.6 | 54.9 | 156.9 | 4.4 | 148.4 | 2.7 |
| DYS03#16 | 608 | 16 | 0.03 | 0.10 | 0.15914 | 2.54 | 0.0228 | 1.52 | 220.0 | 46.3 | 150.0 | 3.5 | 145.6 | 2.2 |
| DYS03#17 | 1540 | 722 | 0.47 | 0.04 | 0.15604 | 1.95 | 0.0227 | 1.50 | 185.0 | 28.8 | 147.2 | 2.7 | 144.9 | 2.2 |
| DYS03#18 | 2625 | 1269 | 0.48 | 0.17 | 0.16346 | 1.85 | 0.0245 | 1.50 | 122.5 | 25.4 | 153.7 | 2.6 | 155.8 | 2.3 |

| | | | | | | | | | | | | | | |
|---|---|---|---|---|---|---|---|---|---|---|---|---|---|---|
| DYS03#19 | 3181 | 949 | 0.30 | 0.50 | 0.15240 | 2.21 | 0.0229 | 1.64 | 110.8 | 34.7 | 144.0 | 3.0 | 146.1 | 2.4 |
| DYS03#20 | 6468 | 1230 | 0.19 | 0.59 | 0.15644 | 2.20 | 0.0233 | 1.51 | 133.2 | 37.2 | 147.6 | 3.0 | 148.5 | 2.2 |
| DYS03#21 | 2076 | 402 | 0.19 | 0.06 | 0.16477 | 1.95 | 0.0242 | 1.55 | 166.3 | 27.5 | 154.9 | 2.8 | 154.1 | 2.4 |
| DYS03#22 | 867 | 171 | 0.20 | 0.00 | 0.14711 | 2.24 | 0.0216 | 1.50 | 164.6 | 38.3 | 139.4 | 2.9 | 137.9 | 2.0 |
| DYS03#23 | 584 | 329 | 0.56 | 0.07 | 0.14941 | 3.14 | 0.0229 | 1.52 | 67.0 | 64.0 | 141.4 | 4.1 | 145.9 | 2.2 |
| **DYS06** | | | | | | | | | | | | | | |
| DYS06#1 | 1784 | 775 | 0.43 | 0.00 | 0.15970 | 1.68 | 0.0239 | 1.52 | 125.9 | 16.9 | 150.4 | 2.4 | 152.0 | 2.3 |
| DYS06#2 | 611 | 450 | 0.74 | 0.04 | 0.15862 | 2.49 | 0.0230 | 1.89 | 197.1 | 37.1 | 149.5 | 3.5 | 146.5 | 2.7 |
| DYS06#3 | 2394 | 7919 | 3.31 | 1.57 | 0.15341 | 5.70 | 0.0228 | 2.02 | 134.0 | 120.8 | 144.9 | 7.7 | 145.6 | 2.9 |
| DYS06#4 | 1028 | 1036 | 1.01 | 0.03 | 0.16456 | 2.58 | 0.0248 | 2.27 | 109.3 | 28.4 | 154.7 | 3.7 | 157.7 | 3.5 |
| DYS06#5 | 1371 | 910 | 0.66 | 0.26 | 0.15392 | 1.92 | 0.0227 | 1.50 | 153.8 | 28.0 | 145.4 | 2.6 | 144.9 | 2.1 |
| DYS06#6 | 478 | 877 | 1.83 | 0.78 | 0.16495 | 3.25 | 0.0232 | 1.50 | 265.4 | 64.8 | 155.0 | 4.7 | 147.9 | 2.2 |
| DYS06#7 | 660 | 1346 | 2.04 | 0.02 | 0.15882 | 1.93 | 0.0235 | 1.53 | 150.5 | 27.4 | 149.7 | 2.7 | 149.6 | 2.3 |
| DYS06#8 | 721 | 350 | 0.49 | 0.04 | 0.15692 | 1.96 | 0.0234 | 1.55 | 131.8 | 27.7 | 148.0 | 2.7 | 149.0 | 2.3 |
| DYS06#9 | 1420 | 376 | 0.26 | 0.05 | 0.16141 | 1.70 | 0.0245 | 1.50 | 91.7 | 18.7 | 151.9 | 2.4 | 155.8 | 2.3 |
| DYS06#10 | 551 | 808 | 1.47 | 0.10 | 0.16026 | 2.00 | 0.0238 | 1.52 | 143.8 | 30.2 | 150.9 | 2.8 | 151.4 | 2.3 |
| DYS06#11 | 487 | 575 | 1.18 | 0.08 | 0.15906 | 2.04 | 0.0240 | 1.51 | 104.9 | 32.2 | 149.9 | 2.9 | 152.7 | 2.3 |
| DYS06#12 | 499 | 788 | 1.58 | 0.14 | 0.15510 | 2.29 | 0.0234 | 1.51 | 103.9 | 40.1 | 146.4 | 3.1 | 149.0 | 2.2 |
| DYS06#13 | 1107 | 982 | 0.89 | 0.05 | 0.16099 | 1.81 | 0.0238 | 1.51 | 154.5 | 23.2 | 151.6 | 2.6 | 151.4 | 2.3 |
| DYS06#14 | 908 | 653 | 0.72 | 0.03 | 0.15714 | 2.25 | 0.0236 | 1.52 | 109.6 | 38.7 | 148.2 | 3.1 | 150.6 | 2.3 |
| DYS06#15 | 571 | 931 | 1.63 | 0.07 | 0.15955 | 2.30 | 0.0233 | 1.76 | 174.6 | 34.1 | 150.3 | 3.2 | 148.8 | 2.6 |
| DYS06#16 | 628 | 1052 | 1.67 | 1.19 | 0.15311 | 3.99 | 0.0230 | 1.50 | 113.4 | 85.0 | 144.7 | 5.4 | 146.6 | 2.2 |
| DYS06#17 | 975 | 279 | 0.29 | 0.21 | 0.85995 | 2.32 | 0.0953 | 2.24 | 789.1 | 12.8 | 630.1 | 11.0 | 586.7 | 12.6 |
| DYS06#18 | 4980 | 1882 | 0.38 | 0.82 | 0.15399 | 2.35 | 0.0229 | 1.50 | 132.5 | 41.9 | 145.4 | 3.2 | 146.2 | 2.2 |
| DYS06#19 | 920 | 775 | 0.84 | 0.00 | 0.16346 | 1.82 | 0.0239 | 1.52 | 181.2 | 23.2 | 153.7 | 2.6 | 152.0 | 2.3 |
| DYS06#20 | 230 | 124 | 0.54 | 0.01 | 1.25457 | 1.67 | 0.1367 | 1.50 | 824.7 | 15.1 | 825.5 | 9.5 | 825.8 | 11.6 |
| DYS06#21 | 4792 | 1949 | 0.41 | 0.01 | 0.16767 | 1.59 | 0.0248 | 1.50 | 154.1 | 12.6 | 157.4 | 2.3 | 157.6 | 2.3 |
| DYS06#22 | 1404 | 1519 | 1.08 | 0.94 | 0.17251 | 2.86 | 0.0254 | 1.57 | 157.1 | 55.1 | 161.6 | 4.3 | 161.9 | 2.5 |
| DYS06#23 | 880 | 992 | 1.13 | 0.04 | 0.16616 | 2.03 | 0.0244 | 1.53 | 166.8 | 30.7 | 156.1 | 2.9 | 155.4 | 2.4 |
| DYS06#24 | 3364 | 1432 | 0.43 | 0.07 | 0.16000 | 2.45 | 0.0236 | 2.00 | 157.4 | 32.6 | 150.7 | 3.4 | 150.3 | 3.0 |

| **DYS07** | | | | | | | | | | | | | | |
|---|---|---|---|---|---|---|---|---|---|---|---|---|---|---|
| DYS07#1 | 1529 | 33 | 0.02 | 0.01 | 0.15926 | 1.96 | 0.0234 | 1.52 | 161.6 | 28.6 | 150.1 | 2.7 | 149.3 | 2.2 |
| DYS07#2 | 3377 | 537 | 0.16 | 0.04 | 0.15724 | 1.72 | 0.0235 | 1.50 | 120.4 | 19.5 | 148.3 | 2.4 | 150.0 | 2.2 |
| DYS07#3 | 5009 | 929 | 0.19 | 0.33 | 0.16301 | 1.96 | 0.0242 | 1.50 | 144.9 | 29.4 | 153.3 | 2.8 | 153.9 | 2.3 |
| DYS07#4c | 282 | 197 | 0.70 | 0.15 | 0.15002 | 3.88 | 0.0226 | 1.55 | 103.7 | 82.1 | 141.9 | 5.2 | 144.2 | 2.2 |
| DYS07#5c | 381 | 65 | 0.17 | 0.11 | 0.16321 | 2.94 | 0.0236 | 1.53 | 204.7 | 57.3 | 153.5 | 4.2 | 150.2 | 2.3 |
| DYS07#6 | 2291 | 466 | 0.20 | 0.06 | 0.15768 | 1.86 | 0.0234 | 1.51 | 146.6 | 25.5 | 148.7 | 2.6 | 148.8 | 2.2 |
| DYS07#7 | 3255 | 142 | 0.04 | 0.01 | 0.15493 | 1.73 | 0.0229 | 1.50 | 153.2 | 20.3 | 146.3 | 2.4 | 145.8 | 2.2 |
| DYS07#8 | 2586 | 173 | 0.07 | 0.04 | 0.15546 | 1.78 | 0.0228 | 1.52 | 168.2 | 21.5 | 146.7 | 2.4 | 145.4 | 2.2 |
| DYS07#9 | 2868 | 135 | 0.05 | 0.01 | 0.15566 | 1.80 | 0.0229 | 1.50 | 163.4 | 23.1 | 146.9 | 2.5 | 145.9 | 2.2 |
| DYS07#10 | 3319 | 774 | 0.23 | 0.04 | 0.15999 | 1.73 | 0.0238 | 1.51 | 135.2 | 19.7 | 150.7 | 2.4 | 151.7 | 2.3 |
| DYS07#11 | 4070 | 263 | 0.06 | 0.06 | 0.16061 | 1.69 | 0.0240 | 1.50 | 126.2 | 18.4 | 151.2 | 2.4 | 152.8 | 2.3 |
| DYS07#12 | 3025 | 239 | 0.08 | 0.01 | 0.16184 | 1.74 | 0.0238 | 1.51 | 165.0 | 20.1 | 152.3 | 2.5 | 151.5 | 2.3 |
| DYS07#13 | 2690 | 296 | 0.11 | 0.04 | 0.16467 | 1.76 | 0.0239 | 1.51 | 189.0 | 20.9 | 154.8 | 2.5 | 152.6 | 2.3 |
| DYS07#14 | 2715 | 427 | 0.16 | 0.39 | 0.14944 | 2.30 | 0.0217 | 1.51 | 195.1 | 39.9 | 141.4 | 3.0 | 138.2 | 2.1 |
| DYS07#15c | 339 | 129 | 0.38 | 0.00 | 0.15414 | 3.04 | 0.0226 | 1.51 | 166.2 | 60.6 | 145.6 | 4.1 | 144.3 | 2.2 |
| DYS07#16r | 3354 | 364 | 0.11 | 0.03 | 0.16363 | 1.71 | 0.0239 | 1.51 | 174.7 | 18.6 | 153.9 | 2.4 | 152.5 | 2.3 |
| DYS07#16c | 726 | 287 | 0.40 | 0.03 | 0.16227 | 2.41 | 0.0239 | 1.61 | 156.2 | 41.6 | 152.7 | 3.4 | 152.5 | 2.4 |
| DYS07#17 | 2776 | 88 | 0.03 | 0.02 | 0.15623 | 1.83 | 0.0231 | 1.51 | 147.4 | 24.0 | 147.4 | 2.5 | 147.4 | 2.2 |
| DYS07#18 | 2683 | 105 | 0.04 | 0.02 | 0.15656 | 1.76 | 0.0231 | 1.50 | 154.1 | 21.5 | 147.7 | 2.4 | 147.3 | 2.2 |
| DYS07#19r | 6341 | 793 | 0.13 | 0.03 | 0.17159 | 1.63 | 0.0252 | 1.51 | 169.4 | 14.8 | 160.8 | 2.4 | 160.2 | 2.4 |
| DYS07#19c | 145 | 95 | 0.66 | 0.20 | 0.95262 | 2.27 | 0.1060 | 1.51 | 779.2 | 35.2 | 679.5 | 11.3 | 649.8 | 9.4 |
| DYS07#20 | 5820 | 518 | 0.09 | 0.01 | 0.15894 | 1.69 | 0.0233 | 1.50 | 175.0 | 18.2 | 149.8 | 2.4 | 148.2 | 2.2 |
| DYS07#21 | 5384 | 916 | 0.17 | 1.24 | 0.15518 | 2.05 | 0.0236 | 1.50 | 81.2 | 32.7 | 146.5 | 2.8 | 150.5 | 2.2 |
| DYS07#22 | 2926 | 94 | 0.03 | 0.13 | 0.15728 | 1.81 | 0.0231 | 1.50 | 165.1 | 23.4 | 148.3 | 2.5 | 147.3 | 2.2 |

**Supplementary Table S2**

Zircon Hf isotopic data of the granitic samples

| Sample#spot | $^{176}Yb/^{177}Hf$ | $^{176}Lu/^{177}Hf$ | $^{176}Hf/^{177}Hf$ | 2σ | $^{176}Hf/^{177}Hf_i$ | Age (Ma) | $\varepsilon_{Hf}(t)$ | 2σ | $T_{DM}$ (Ma) | $T_{DM}^{C}$ (Ma) | $f_{Lu/Hf}$ |
|---|---|---|---|---|---|---|---|---|---|---|---|
| **JH155** | | | | | | | | | | | |
| JH155#01 | 0.0224 | 0.0008 | 0.282409 | 0.000021 | 0.282407 | 128 | -10.1 | 0.7 | 1187 | 1823 | -0.97 |
| JH155#02 | 0.0233 | 0.0009 | 0.282481 | 0.000019 | 0.282478 | 128 | -7.6 | 0.7 | 1089 | 1663 | -0.97 |
| JH155#03 | 0.0130 | 0.0005 | 0.282450 | 0.000021 | 0.282449 | 128 | -8.6 | 0.7 | 1119 | 1728 | -0.99 |
| JH155#04 | 0.0137 | 0.0005 | 0.282480 | 0.000020 | 0.282479 | 128 | -7.6 | 0.7 | 1078 | 1662 | -0.98 |
| JH155#05 | 0.0246 | 0.0009 | 0.282420 | 0.000020 | 0.282418 | 128 | -9.7 | 0.7 | 1173 | 1798 | -0.97 |
| JH155#06 | 0.0227 | 0.0009 | 0.282465 | 0.000020 | 0.282463 | 128 | -8.1 | 0.7 | 1110 | 1698 | -0.97 |
| JH155#07 | 0.0148 | 0.0005 | 0.282482 | 0.000021 | 0.282481 | 128 | -7.5 | 0.7 | 1076 | 1658 | -0.98 |
| JH155#08 | 0.0211 | 0.0008 | 0.282475 | 0.000021 | 0.282473 | 128 | -7.8 | 0.7 | 1094 | 1676 | -0.98 |
| JH155#09 | 0.0182 | 0.0007 | 0.282437 | 0.000019 | 0.282436 | 128 | -9.1 | 0.7 | 1144 | 1758 | -0.98 |
| JH155#10 | 0.0238 | 0.0009 | 0.282473 | 0.000018 | 0.282471 | 128 | -7.8 | 0.6 | 1099 | 1680 | -0.97 |
| JH155#11 | 0.0129 | 0.0005 | 0.282500 | 0.000024 | 0.282499 | 128 | -6.9 | 0.9 | 1051 | 1619 | -0.98 |
| JH155#12 | 0.0165 | 0.0006 | 0.282445 | 0.000019 | 0.282444 | 128 | -8.8 | 0.7 | 1130 | 1740 | -0.98 |
| JH155#13 | 0.0169 | 0.0007 | 0.282454 | 0.000018 | 0.282453 | 128 | -8.5 | 0.6 | 1119 | 1721 | -0.98 |
| JH155#14 | 0.0170 | 0.0006 | 0.282461 | 0.000019 | 0.282460 | 128 | -8.2 | 0.7 | 1107 | 1704 | -0.98 |
| JH155#15 | 0.0231 | 0.0008 | 0.282472 | 0.000018 | 0.282470 | 128 | -7.9 | 0.6 | 1100 | 1683 | -0.97 |
| JH155#16 | 0.0203 | 0.0008 | 0.282456 | 0.000019 | 0.282454 | 128 | -8.4 | 0.7 | 1119 | 1717 | -0.98 |
| JH155#17 | 0.0148 | 0.0006 | 0.282492 | 0.000019 | 0.282490 | 128 | -7.2 | 0.7 | 1064 | 1637 | -0.98 |
| JH155#18 | 0.0166 | 0.0006 | 0.282447 | 0.000022 | 0.282446 | 128 | -8.7 | 0.8 | 1128 | 1737 | -0.98 |
| **DM35** | | | | | | | | | | | |
| DM35#01 | 0.0393 | 0.0012 | 0.282463 | 0.000021 | 0.282460 | 151 | -7.7 | 0.8 | 1122 | 1692 | -0.97 |
| DM35#02 | 0.0279 | 0.0009 | 0.282541 | 0.000020 | 0.282539 | 151 | -4.9 | 0.7 | 1003 | 1515 | -0.97 |
| DM35#03 | 0.0293 | 0.0009 | 0.282529 | 0.000019 | 0.282527 | 151 | -5.4 | 0.7 | 1021 | 1542 | -0.97 |
| DM35#04 | 0.0270 | 0.0008 | 0.282517 | 0.000018 | 0.282515 | 151 | -5.8 | 0.7 | 1036 | 1569 | -0.97 |
| DM35#05 | 0.0316 | 0.0010 | 0.282548 | 0.000021 | 0.282545 | 151 | -4.7 | 0.7 | 997 | 1501 | -0.97 |
| DM35#06 | 0.0266 | 0.0008 | 0.282483 | 0.000018 | 0.282481 | 151 | -7.0 | 0.6 | 1083 | 1645 | -0.98 |
| DM35#07 | 0.0226 | 0.0007 | 0.282440 | 0.000019 | 0.282438 | 151 | -8.5 | 0.7 | 1139 | 1739 | -0.98 |

| | | | | | | | | | | | |
|---|---|---|---|---|---|---|---|---|---|---|---|
| DM35#08 | 0.0220 | 0.0007 | 0.282533 | 0.000018 | 0.282531 | 151 | -5.2 | 0.6 | 1011 | 1533 | -0.98 |
| DM35#09 | 0.0304 | 0.0009 | 0.282547 | 0.000019 | 0.282544 | 151 | -4.7 | 0.7 | 997 | 1503 | -0.97 |
| DM35#10 | 0.0249 | 0.0008 | 0.282543 | 0.000022 | 0.282540 | 151 | -4.9 | 0.8 | 1000 | 1511 | -0.98 |
| DM35#11 | 0.0268 | 0.0009 | 0.282549 | 0.000018 | 0.282547 | 151 | -4.6 | 0.6 | 992 | 1497 | -0.97 |
| DM35#12 | 0.0231 | 0.0008 | 0.282456 | 0.000020 | 0.282454 | 151 | -7.9 | 0.7 | 1120 | 1705 | -0.98 |
| DM35#13 | 0.0261 | 0.0009 | 0.282544 | 0.000019 | 0.282542 | 151 | -4.8 | 0.7 | 999 | 1508 | -0.97 |
| DM35#14 | 0.0303 | 0.0010 | 0.282504 | 0.000021 | 0.282501 | 151 | -6.3 | 0.7 | 1059 | 1599 | -0.97 |
| DM35#15 | 0.0278 | 0.0009 | 0.282528 | 0.000020 | 0.282525 | 151 | -5.4 | 0.7 | 1023 | 1546 | -0.97 |
| **QD69** | | | | | | | | | | | |
| QD69#01 | 0.0355 | 0.0013 | 0.282506 | 0.000015 | 0.282503 | 151 | -6.2 | 0.5 | 1063 | 1595 | -0.96 |
| QD69#02 | 0.0319 | 0.0011 | 0.282533 | 0.000015 | 0.282530 | 151 | -5.2 | 0.5 | 1020 | 1534 | -0.97 |
| QD69#03 | 0.0288 | 0.0011 | 0.282514 | 0.000015 | 0.282511 | 151 | -5.9 | 0.5 | 1048 | 1578 | -0.97 |
| QD69#04 | 0.0308 | 0.0011 | 0.282533 | 0.000012 | 0.282530 | 151 | -5.3 | 0.4 | 1021 | 1536 | -0.97 |
| QD69#05 | 0.0295 | 0.0010 | 0.282503 | 0.000015 | 0.282500 | 151 | -6.3 | 0.5 | 1060 | 1601 | -0.97 |
| QD69#06 | 0.0402 | 0.0014 | 0.282548 | 0.000014 | 0.282544 | 151 | -4.8 | 0.5 | 1007 | 1504 | -0.96 |
| QD69#07 | 0.0490 | 0.0018 | 0.282530 | 0.000016 | 0.282525 | 151 | -5.4 | 0.6 | 1043 | 1545 | -0.95 |
| QD69#08 | 0.0229 | 0.0008 | 0.282534 | 0.000012 | 0.282532 | 151 | -5.2 | 0.4 | 1011 | 1530 | -0.98 |
| QD69#09 | 0.0355 | 0.0013 | 0.282477 | 0.000015 | 0.282473 | 151 | -7.3 | 0.5 | 1106 | 1662 | -0.96 |
| QD69#10 | 0.0415 | 0.0015 | 0.282394 | 0.000014 | 0.282370 | 837 | 4.3 | 0.5 | 1230 | 1465 | -0.95 |
| QD69#11 | 0.0520 | 0.0016 | 0.282532 | 0.000016 | 0.282527 | 151 | -5.3 | 0.5 | 1037 | 1541 | -0.95 |
| QD69#12 | 0.0366 | 0.0013 | 0.282511 | 0.000014 | 0.282507 | 151 | -6.1 | 0.5 | 1056 | 1585 | -0.96 |
| QD69#13 | 0.0595 | 0.0020 | 0.282564 | 0.000019 | 0.282558 | 151 | -4.3 | 0.7 | 1001 | 1472 | -0.94 |
| QD69#14 | 0.0418 | 0.0014 | 0.282521 | 0.000014 | 0.282517 | 151 | -5.7 | 0.5 | 1046 | 1564 | -0.96 |
| QD69#15 | 0.0251 | 0.0008 | 0.282506 | 0.000011 | 0.282503 | 151 | -6.2 | 0.4 | 1052 | 1594 | -0.98 |
| QD69#16 | 0.0102 | 0.0004 | 0.282525 | 0.000013 | 0.282524 | 151 | -5.5 | 0.5 | 1013 | 1549 | -0.99 |
| QD69#17 | 0.0434 | 0.0014 | 0.282497 | 0.000015 | 0.282493 | 151 | -6.6 | 0.5 | 1082 | 1618 | -0.96 |
| QD69#18 | 0.0369 | 0.0012 | 0.282528 | 0.000014 | 0.282524 | 151 | -5.5 | 0.5 | 1031 | 1548 | -0.96 |
| QD69#19 | 0.0424 | 0.0014 | 0.282504 | 0.000015 | 0.282500 | 151 | -6.3 | 0.5 | 1072 | 1602 | -0.96 |
| **DYS14** | | | | | | | | | | | |
| DYS14#01 | 0.0183 | 0.0007 | 0.282488 | 0.000015 | 0.282485 | 149 | -6.9 | 0.5 | 1075 | 1635 | -0.98 |

| | | | | | | | | | | | |
|---|---|---|---|---|---|---|---|---|---|---|---|
| DYS14#02 | 0.0223 | 0.0009 | 0.282497 | 0.000016 | 0.282495 | 149 | -6.5 | 0.6 | 1066 | 1615 | -0.97 |
| DYS14#03 | 0.0187 | 0.0008 | 0.282491 | 0.000018 | 0.282489 | 149 | -6.7 | 0.6 | 1071 | 1627 | -0.98 |
| DYS14#04 | 0.0199 | 0.0008 | 0.282492 | 0.000016 | 0.282489 | 149 | -6.7 | 0.6 | 1070 | 1626 | -0.98 |
| DYS14#05 | 0.0220 | 0.0009 | 0.282490 | 0.000017 | 0.282488 | 149 | -6.8 | 0.6 | 1076 | 1630 | -0.97 |
| DYS14#06 | 0.0179 | 0.0007 | 0.282510 | 0.000016 | 0.282508 | 149 | -6.1 | 0.6 | 1043 | 1585 | -0.98 |
| DYS14#07 | 0.0158 | 0.0006 | 0.282438 | 0.000017 | 0.282436 | 149 | -8.6 | 0.6 | 1141 | 1745 | -0.98 |
| DYS14#08 | 0.0210 | 0.0009 | 0.282517 | 0.000016 | 0.282515 | 149 | -5.8 | 0.6 | 1037 | 1570 | -0.97 |
| DYS14#09 | 0.0183 | 0.0007 | 0.282524 | 0.000017 | 0.282522 | 149 | -5.6 | 0.6 | 1023 | 1553 | -0.98 |
| DYS14#10 | 0.0164 | 0.0007 | 0.282490 | 0.000016 | 0.282489 | 149 | -6.8 | 0.6 | 1068 | 1628 | -0.98 |
| DYS14#11 | 0.0187 | 0.0008 | 0.282501 | 0.000016 | 0.282499 | 149 | -6.4 | 0.6 | 1057 | 1606 | -0.98 |
| DYS14#12 | 0.0567 | 0.0020 | 0.282381 | 0.000016 | 0.282350 | 819 | 3.2 | 0.6 | 1265 | 1522 | -0.94 |
| DYS14#13 | 0.0210 | 0.0008 | 0.282505 | 0.000015 | 0.282503 | 149 | -6.3 | 0.5 | 1052 | 1596 | -0.98 |
| DYS14#14 | 0.0259 | 0.0010 | 0.282475 | 0.000017 | 0.282472 | 149 | -7.3 | 0.6 | 1101 | 1665 | -0.97 |
| DYS14#15 | 0.0201 | 0.0008 | 0.282505 | 0.000016 | 0.282503 | 149 | -6.3 | 0.6 | 1053 | 1597 | -0.98 |
| DYS14#16 | 0.0204 | 0.0008 | 0.282508 | 0.000015 | 0.282506 | 149 | -6.2 | 0.5 | 1048 | 1590 | -0.98 |
| DYS14#17 | 0.0184 | 0.0008 | 0.282500 | 0.000017 | 0.282498 | 149 | -6.4 | 0.6 | 1058 | 1607 | -0.98 |
| **QD49** | | | | | | | | | | | |
| QD49#01 | 0.0120 | 0.0004 | 0.282507 | 0.000015 | 0.282506 | 132 | -6.5 | 0.5 | 1038 | 1600 | -0.99 |
| QD49#02 | 0.0196 | 0.0006 | 0.282526 | 0.000020 | 0.282525 | 132 | -5.9 | 0.7 | 1017 | 1558 | -0.98 |
| QD49#03 | 0.0262 | 0.0008 | 0.282495 | 0.000017 | 0.282493 | 132 | -7.0 | 0.6 | 1066 | 1629 | -0.98 |
| QD49#04 | 0.0089 | 0.0003 | 0.282487 | 0.000018 | 0.282486 | 132 | -7.2 | 0.6 | 1063 | 1645 | -0.99 |
| QD49#05 | 0.0223 | 0.0008 | 0.282501 | 0.000019 | 0.282499 | 132 | -6.8 | 0.7 | 1056 | 1615 | -0.98 |
| QD49#06 | 0.0078 | 0.0003 | 0.282466 | 0.000021 | 0.282466 | 132 | -7.9 | 0.7 | 1090 | 1689 | -0.99 |
| QD49#07 | 0.0167 | 0.0005 | 0.282499 | 0.000020 | 0.282498 | 132 | -6.8 | 0.7 | 1053 | 1618 | -0.98 |
| QD49#08 | 0.0124 | 0.0004 | 0.282497 | 0.000019 | 0.282496 | 132 | -6.9 | 0.7 | 1052 | 1621 | -0.99 |
| QD49#09 | 0.0186 | 0.0006 | 0.282589 | 0.000018 | 0.282587 | 132 | -3.6 | 0.7 | 930 | 1418 | -0.98 |
| QD49#10 | 0.0344 | 0.0012 | 0.282376 | 0.000020 | 0.282358 | 831 | 3.7 | 0.7 | 1244 | 1497 | -0.97 |
| QD49#11 | 0.0095 | 0.0003 | 0.282524 | 0.000020 | 0.282523 | 132 | -5.9 | 0.7 | 1013 | 1561 | -0.99 |
| QD49#12 | 0.0150 | 0.0005 | 0.282533 | 0.000020 | 0.282532 | 132 | -5.6 | 0.7 | 1004 | 1542 | -0.99 |
| QD49#13 | 0.0376 | 0.0012 | 0.282320 | 0.000024 | 0.282300 | 848 | 2.0 | 0.8 | 1325 | 1616 | -0.96 |

| | | | | | | | | | | | |
|---|---|---|---|---|---|---|---|---|---|---|---|
| QD49#14 | 0.0208 | 0.0007 | 0.282536 | 0.000020 | 0.282535 | 132 | -5.5 | 0.7 | 1005 | 1535 | -0.98 |
| QD49#15 | 0.0099 | 0.0003 | 0.282489 | 0.000025 | 0.282488 | 132 | -7.2 | 0.9 | 1062 | 1640 | -0.99 |
| QD49#16 | 0.0507 | 0.0018 | 0.282559 | 0.000020 | 0.282555 | 132 | -4.8 | 0.7 | 1001 | 1490 | -0.95 |
| QD49#17 | 0.0115 | 0.0004 | 0.282477 | 0.000021 | 0.282476 | 132 | -7.6 | 0.8 | 1079 | 1667 | -0.99 |
| QD49#18 | 0.0404 | 0.0014 | 0.282186 | 0.000032 | 0.282152 | 1246 | 5.7 | 1.1 | 1522 | 1691 | -0.96 |
| **DYS62** | | | | | | | | | | | |
| QD62#01 | 0.0512 | 0.0018 | 0.282446 | 0.000016 | 0.282442 | 127 | -8.9 | 0.6 | 1164 | 1746 | -0.95 |
| QD62#02 | 0.0184 | 0.0007 | 0.282484 | 0.000015 | 0.282482 | 127 | -7.5 | 0.5 | 1078 | 1656 | -0.98 |
| QD62#03 | 0.0581 | 0.0020 | 0.282481 | 0.000017 | 0.282476 | 127 | -7.7 | 0.6 | 1122 | 1670 | -0.94 |
| QD62#04 | 0.0078 | 0.0003 | 0.282473 | 0.000012 | 0.282472 | 127 | -7.8 | 0.4 | 1081 | 1678 | -0.99 |
| QD62#05 | 0.0457 | 0.0017 | 0.282498 | 0.000015 | 0.282494 | 127 | -7.1 | 0.5 | 1087 | 1630 | -0.95 |
| QD62#06 | 0.0513 | 0.0018 | 0.282450 | 0.000015 | 0.282446 | 127 | -8.8 | 0.5 | 1159 | 1736 | -0.95 |
| QD62#07 | 0.0452 | 0.0016 | 0.282485 | 0.000018 | 0.282481 | 127 | -7.5 | 0.6 | 1103 | 1658 | -0.95 |
| QD62#08 | 0.0412 | 0.0015 | 0.282521 | 0.000017 | 0.282517 | 127 | -6.2 | 0.6 | 1048 | 1577 | -0.96 |
| QD62#09 | 0.0121 | 0.0004 | 0.282496 | 0.000016 | 0.282495 | 127 | -7.0 | 0.6 | 1055 | 1628 | -0.99 |
| QD62#10 | 0.0124 | 0.0004 | 0.282481 | 0.000014 | 0.282480 | 127 | -7.6 | 0.5 | 1075 | 1661 | -0.99 |
| QD62#11 | 0.0119 | 0.0004 | 0.282482 | 0.000014 | 0.282481 | 127 | -7.5 | 0.5 | 1073 | 1658 | -0.99 |
| QD62#12 | 0.0215 | 0.0008 | 0.282488 | 0.000015 | 0.282486 | 127 | -7.3 | 0.5 | 1076 | 1648 | -0.98 |
| QD62#13 | 0.0501 | 0.0018 | 0.282500 | 0.000015 | 0.282496 | 127 | -7.0 | 0.5 | 1087 | 1626 | -0.95 |
| QD62#14 | 0.0381 | 0.0014 | 0.282492 | 0.000014 | 0.282489 | 127 | -7.2 | 0.5 | 1086 | 1641 | -0.96 |
| QD62#15 | 0.0260 | 0.0009 | 0.282424 | 0.000016 | 0.282422 | 127 | -9.6 | 0.6 | 1167 | 1789 | -0.97 |
| QD62#16 | 0.0382 | 0.0014 | 0.282513 | 0.000016 | 0.282510 | 127 | -6.5 | 0.6 | 1056 | 1594 | -0.96 |
| QD62#17 | 0.0204 | 0.0008 | 0.282450 | 0.000014 | 0.282448 | 127 | -8.7 | 0.5 | 1128 | 1731 | -0.98 |
| QD62#18 | 0.0171 | 0.0006 | 0.282497 | 0.000014 | 0.282495 | 127 | -7.0 | 0.5 | 1059 | 1627 | -0.98 |
| QD62#19 | 0.0383 | 0.0014 | 0.282476 | 0.000016 | 0.282473 | 127 | -7.8 | 0.6 | 1109 | 1677 | -0.96 |
| **DYS01** | | | | | | | | | | | |
| DYS01#01 | 0.0133 | 0.0005 | 0.282399 | 0.000016 | 0.282397 | 147 | -10.0 | 0.6 | 1191 | 1833 | -0.98 |
| DYS01#02 | 0.0182 | 0.0007 | 0.282442 | 0.000019 | 0.282441 | 147 | -8.5 | 0.7 | 1136 | 1736 | -0.98 |
| DYS01#03 | 0.0019 | 0.0001 | 0.282431 | 0.000015 | 0.282431 | 147 | -8.8 | 0.5 | 1133 | 1758 | -1.00 |
| DYS01#04 | 0.0175 | 0.0007 | 0.282389 | 0.000013 | 0.282387 | 147 | -10.4 | 0.5 | 1210 | 1855 | -0.98 |

| | | | | | | | | | | | |
|---|---|---|---|---|---|---|---|---|---|---|---|
| DYS01#05 | 0.0039 | 0.0001 | 0.282327 | 0.000017 | 0.282327 | 147 | -12.5 | 0.6 | 1277 | 1988 | -1.00 |
| DYS01#06 | 0.0319 | 0.0011 | 0.282380 | 0.000014 | 0.282377 | 147 | -10.7 | 0.5 | 1236 | 1877 | -0.97 |
| DYS01#07 | 0.0207 | 0.0007 | 0.282365 | 0.000014 | 0.282363 | 147 | -11.2 | 0.5 | 1244 | 1908 | -0.98 |
| DYS01#08 | 0.0190 | 0.0007 | 0.282384 | 0.000016 | 0.282382 | 147 | -10.6 | 0.6 | 1217 | 1867 | -0.98 |
| DYS01#09 | 0.0288 | 0.0010 | 0.282409 | 0.000014 | 0.282406 | 147 | -9.7 | 0.5 | 1193 | 1813 | -0.97 |
| DYS01#10 | 0.0397 | 0.0013 | 0.282392 | 0.000021 | 0.282388 | 147 | -10.3 | 0.7 | 1227 | 1852 | -0.96 |
| DYS01#11 | 0.0076 | 0.0003 | 0.282474 | 0.000018 | 0.282473 | 147 | -7.3 | 0.6 | 1080 | 1663 | -0.99 |
| DYS01#12 | 0.0450 | 0.0016 | 0.282387 | 0.000020 | 0.282362 | 836 | 3.9 | 0.7 | 1243 | 1485 | -0.95 |
| DYS01#13 | 0.0444 | 0.0016 | 0.282158 | 0.000020 | 0.282133 | 838 | -4.1 | 0.7 | 1569 | 2000 | -0.95 |
| DYS01#14 | 0.0155 | 0.0006 | 0.282424 | 0.000014 | 0.282422 | 147 | -9.1 | 0.5 | 1159 | 1777 | -0.98 |
| DYS01#15 | 0.0200 | 0.0007 | 0.282393 | 0.000018 | 0.282391 | 147 | -10.2 | 0.7 | 1206 | 1846 | -0.98 |
| DYS01#16 | 0.0493 | 0.0020 | 0.282610 | 0.000024 | 0.282579 | 839 | 11.7 | 0.9 | 934 | 989 | -0.94 |
| DYS01#17 | 0.0437 | 0.0016 | 0.282504 | 0.000018 | 0.282499 | 147 | -6.4 | 0.6 | 1078 | 1606 | -0.95 |
| DYS01#18 | 0.0159 | 0.0006 | 0.282351 | 0.000017 | 0.282350 | 147 | -11.7 | 0.6 | 1260 | 1938 | -0.98 |
| DYS01#19 | 0.0156 | 0.0006 | 0.282348 | 0.000025 | 0.282346 | 147 | -11.8 | 0.9 | 1264 | 1946 | -0.98 |
| DYS01#20 | 0.0192 | 0.0007 | 0.282365 | 0.000018 | 0.282363 | 147 | -11.2 | 0.6 | 1244 | 1908 | -0.98 |
| DYS01#21 | 0.0196 | 0.0007 | 0.282429 | 0.000014 | 0.282427 | 147 | -9.0 | 0.5 | 1155 | 1767 | -0.98 |
| **DYS03** | | | | | | | | | | | |
| DYS03#01 | 0.0142 | 0.0005 | 0.282388 | 0.000014 | 0.282386 | 146 | -10.4 | 0.5 | 1206 | 1857 | -0.99 |
| DYS03#02 | 0.0163 | 0.0005 | 0.282406 | 0.000025 | 0.282404 | 146 | -9.8 | 0.9 | 1183 | 1818 | -0.98 |
| DYS03#03 | 0.0347 | 0.0013 | 0.282462 | 0.000017 | 0.282459 | 146 | -7.9 | 0.6 | 1126 | 1696 | -0.96 |
| DYS03#04 | 0.0269 | 0.0009 | 0.282421 | 0.000025 | 0.282418 | 146 | -9.3 | 0.9 | 1172 | 1786 | -0.97 |
| DYS03#05 | 0.0377 | 0.0013 | 0.282484 | 0.000024 | 0.282480 | 146 | -7.1 | 0.9 | 1097 | 1649 | -0.96 |
| DYS03#06 | 0.0207 | 0.0007 | 0.282453 | 0.000024 | 0.282451 | 146 | -8.2 | 0.9 | 1122 | 1714 | -0.98 |
| DYS03#07 | 0.0316 | 0.0011 | 0.282454 | 0.000024 | 0.282451 | 146 | -8.1 | 0.9 | 1133 | 1713 | -0.97 |
| DYS03#08 | 0.0296 | 0.0011 | 0.282517 | 0.000029 | 0.282514 | 146 | -5.9 | 1.0 | 1042 | 1573 | -0.97 |
| DYS03#09 | 0.0115 | 0.0004 | 0.282410 | 0.000024 | 0.282409 | 146 | -9.6 | 0.8 | 1172 | 1808 | -0.99 |
| DYS03#10 | 0.0051 | 0.0002 | 0.282354 | 0.000017 | 0.282354 | 146 | -11.6 | 0.6 | 1242 | 1929 | -0.99 |
| DYS03#11 | 0.0156 | 0.0005 | 0.282384 | 0.000015 | 0.282383 | 146 | -10.6 | 0.5 | 1212 | 1865 | -0.98 |
| DYS03#12 | 0.0299 | 0.0011 | 0.282396 | 0.000016 | 0.282393 | 146 | -10.2 | 0.6 | 1213 | 1843 | -0.97 |

| | | | | | | | | | | | |
|---|---|---|---|---|---|---|---|---|---|---|---|
| DYS03#13 | 0.0252 | 0.0009 | 0.282432 | 0.000014 | 0.282430 | 146 | -8.9 | 0.5 | 1157 | 1761 | -0.97 |
| DYS03#14 | 0.0367 | 0.0014 | 0.282452 | 0.000018 | 0.282448 | 146 | -8.2 | 0.7 | 1143 | 1719 | -0.96 |
| DYS03#15 | 0.0184 | 0.0006 | 0.282396 | 0.000017 | 0.282394 | 146 | -10.2 | 0.6 | 1199 | 1840 | -0.98 |
| DYS03#16 | 0.0229 | 0.0008 | 0.282456 | 0.000015 | 0.282454 | 146 | -8.0 | 0.5 | 1120 | 1707 | -0.98 |
| DYS03#17 | 0.0255 | 0.0011 | 0.282361 | 0.000015 | 0.282358 | 146 | -11.4 | 0.5 | 1262 | 1921 | -0.97 |
| **DYS06** | | | | | | | | | | | |
| DYS06#01 | 0.0171 | 0.0006 | 0.282359 | 0.000020 | 0.282357 | 150 | -11.4 | 0.7 | 1250 | 1920 | -0.98 |
| DYS06#02 | 0.0133 | 0.0005 | 0.282342 | 0.000016 | 0.282340 | 150 | -12.0 | 0.6 | 1268 | 1957 | -0.99 |
| DYS06#03 | 0.0150 | 0.0005 | 0.282356 | 0.000014 | 0.282355 | 150 | -11.5 | 0.5 | 1249 | 1925 | -0.99 |
| DYS06#04 | 0.0193 | 0.0007 | 0.282440 | 0.000017 | 0.282439 | 150 | -8.5 | 0.6 | 1138 | 1739 | -0.98 |
| DYS06#05 | 0.0254 | 0.0009 | 0.282377 | 0.000021 | 0.282375 | 150 | -10.8 | 0.7 | 1234 | 1881 | -0.97 |
| DYS06#06 | 0.0143 | 0.0005 | 0.282375 | 0.000016 | 0.282373 | 150 | -10.8 | 0.6 | 1225 | 1884 | -0.98 |
| DYS06#07 | 0.0140 | 0.0005 | 0.282381 | 0.000018 | 0.282380 | 150 | -10.6 | 0.7 | 1215 | 1869 | -0.99 |
| DYS06#08 | 0.0126 | 0.0004 | 0.282330 | 0.000020 | 0.282329 | 150 | -12.4 | 0.7 | 1284 | 1982 | -0.99 |
| DYS06#09 | 0.0178 | 0.0006 | 0.282409 | 0.000021 | 0.282407 | 150 | -9.6 | 0.8 | 1180 | 1808 | -0.98 |
| DYS06#10 | 0.0108 | 0.0004 | 0.282376 | 0.000018 | 0.282375 | 150 | -10.8 | 0.7 | 1219 | 1881 | -0.99 |
| DYS06#11 | 0.0213 | 0.0008 | 0.282419 | 0.000018 | 0.282417 | 150 | -9.3 | 0.6 | 1171 | 1787 | -0.98 |
| DYS06#12 | 0.0140 | 0.0005 | 0.282380 | 0.000018 | 0.282379 | 150 | -10.6 | 0.6 | 1216 | 1871 | -0.99 |
| DYS06#13 | 0.0137 | 0.0005 | 0.282375 | 0.000021 | 0.282373 | 150 | -10.8 | 0.8 | 1223 | 1884 | -0.99 |
| DYS06#14 | 0.0582 | 0.0022 | 0.282421 | 0.000020 | 0.282415 | 150 | -9.3 | 0.7 | 1212 | 1791 | -0.94 |
| DYS06#15 | 0.0187 | 0.0007 | 0.282395 | 0.000021 | 0.282393 | 150 | -10.1 | 0.7 | 1202 | 1840 | -0.98 |
| DYS06#16 | 0.0123 | 0.0004 | 0.282437 | 0.000022 | 0.282436 | 150 | -8.6 | 0.8 | 1134 | 1745 | -0.99 |
| DYS06#17 | 0.0041 | 0.0001 | 0.282157 | 0.000020 | 0.282155 | 826 | -3.6 | 0.7 | 1509 | 1957 | -1.00 |
| DYS06#18 | 0.0319 | 0.0011 | 0.282396 | 0.000022 | 0.282392 | 150 | -10.1 | 0.8 | 1214 | 1842 | -0.97 |
| DYS06#19 | 0.0142 | 0.0005 | 0.282354 | 0.000024 | 0.282352 | 150 | -11.6 | 0.9 | 1254 | 1931 | -0.98 |
| DYS06#20 | 0.0138 | 0.0005 | 0.282339 | 0.000023 | 0.282338 | 150 | -12.1 | 0.8 | 1273 | 1963 | -0.99 |
| DYS06#21 | 0.0161 | 0.0006 | 0.282382 | 0.000020 | 0.282380 | 150 | -10.6 | 0.7 | 1216 | 1869 | -0.98 |
| DYS06#22 | 0.0322 | 0.0012 | 0.282416 | 0.000019 | 0.282413 | 150 | -9.4 | 0.7 | 1188 | 1796 | -0.96 |
| **DYS07** | | | | | | | | | | | |
| DYS07#01 | 0.0281 | 0.0010 | 0.282524 | 0.000013 | 0.282522 | 149 | -5.6 | 0.5 | 1029 | 1554 | -0.97 |

| | | | | | | | | | | | |
|---|---|---|---|---|---|---|---|---|---|---|---|
| DYS07#02 | 0.0269 | 0.0009 | 0.282533 | 0.000013 | 0.282530 | 149 | -5.3 | 0.5 | 1017 | 1535 | -0.97 |
| DYS07#03 | 0.0374 | 0.0014 | 0.282558 | 0.000016 | 0.282554 | 149 | -4.4 | 0.6 | 993 | 1481 | -0.96 |
| DYS07#04 | 0.0518 | 0.0018 | 0.282514 | 0.000020 | 0.282509 | 149 | -6.0 | 0.7 | 1067 | 1582 | -0.95 |
| DYS07#05 | 0.0228 | 0.0008 | 0.282533 | 0.000014 | 0.282530 | 149 | -5.3 | 0.5 | 1014 | 1534 | -0.97 |
| DYS07#06 | 0.0205 | 0.0007 | 0.282541 | 0.000013 | 0.282539 | 149 | -4.9 | 0.5 | 1000 | 1515 | -0.98 |
| DYS07#07 | 0.0085 | 0.0003 | 0.282532 | 0.000018 | 0.282531 | 149 | -5.2 | 0.6 | 1001 | 1533 | -0.99 |
| DYS07#08 | 0.0368 | 0.0013 | 0.282512 | 0.000018 | 0.282508 | 149 | -6.0 | 0.6 | 1056 | 1584 | -0.96 |
| DYS07#09 | 0.0058 | 0.0002 | 0.282486 | 0.000016 | 0.282485 | 149 | -6.9 | 0.6 | 1062 | 1636 | -0.99 |
| DYS07#10 | 0.0110 | 0.0004 | 0.282536 | 0.000020 | 0.282535 | 149 | -5.1 | 0.7 | 998 | 1524 | -0.99 |
| DYS07#11 | 0.0349 | 0.0012 | 0.282495 | 0.000018 | 0.282492 | 149 | -6.6 | 0.6 | 1077 | 1620 | -0.96 |
| DYS07#12 | 0.0523 | 0.0017 | 0.282579 | 0.000019 | 0.282574 | 149 | -3.7 | 0.7 | 972 | 1436 | -0.95 |
| DYS07#13 | 0.0350 | 0.0013 | 0.282564 | 0.000017 | 0.282560 | 149 | -4.2 | 0.6 | 983 | 1468 | -0.96 |
| DYS07#14 | 0.0377 | 0.0013 | 0.282535 | 0.000017 | 0.282532 | 149 | -5.2 | 0.6 | 1023 | 1532 | -0.96 |
| DYS07#15 | 0.0150 | 0.0006 | 0.282524 | 0.000016 | 0.282522 | 149 | -5.5 | 0.6 | 1021 | 1553 | -0.98 |
| DYS07#16 | 0.0227 | 0.0008 | 0.282509 | 0.000016 | 0.282507 | 149 | -6.1 | 0.6 | 1047 | 1587 | -0.98 |
| DYS07#17 | 0.0297 | 0.0010 | 0.282499 | 0.000014 | 0.282496 | 149 | -6.5 | 0.5 | 1067 | 1612 | -0.97 |
| DYS07#18 | 0.0050 | 0.0002 | 0.282530 | 0.000018 | 0.282529 | 149 | -5.3 | 0.7 | 1001 | 1537 | -0.99 |
| DYS07#19 | 0.0217 | 0.0008 | 0.282534 | 0.000015 | 0.282532 | 149 | -5.2 | 0.5 | 1010 | 1531 | -0.98 |
| DYS07#20 | 0.0238 | 0.0008 | 0.282558 | 0.000016 | 0.282555 | 149 | -4.4 | 0.6 | 979 | 1479 | -0.98 |
| DYS07#21 | 0.0165 | 0.0006 | 0.282547 | 0.000016 | 0.282546 | 149 | -4.7 | 0.5 | 988 | 1500 | -0.98 |